AWARD NUMBER: W81XWH-20-1-0202

TITLE: Prostate-Specific Membrane Antigen-Dependent Health Disparities in Prostate Cancer

PRINCIPAL INVESTIGATOR: Leslie A. Caromile

CONTRACTING ORGANIZATION: University of Connecticut Health Center
Farmington, CT

REPORT DATE: October 2022

TYPE OF REPORT: Annual

PREPARED FOR: U.S. Army Medical Research and Development Command
Fort Detrick, Maryland 21702-5012

REPORT DOCUMENTATION PAGE

Form Approved
OMB No. 0704-0188

1. REPORT DATE	2. REPORT TYPE	3. DATES COVERED
October 2022	Annual	30Sep2021-29Sep2022

4. TITLE AND SUBTITLE

Prostate-Specific Membrane Antigen-Dependent Health Disparities in Prostate Cancer

5a. CONTRACT NUMBER

5b. GRANT NUMBER
W81XWH-20-1-0202

5c. PROGRAM ELEMENT NUMBER

6. AUTHOR(S)
Leslie A. Caromile, PhD

E-Mail:caromile@uchc.edu

5d. PROJECT NUMBER

5e. TASK NUMBER

5f. WORK UNIT NUMBER

7. PERFORMING ORGANIZATION NAME(S) AND ADDRESS(ES)

University of Connecticut Health Center
263 Farmington Ave
Farmington CT 06030

8. PERFORMING ORGANIZATION REPORT NUMBER

9. SPONSORING / MONITORING AGENCY NAME(S) AND ADDRESS(ES)

U.S. Army Medical Research and Development Command
Fort Detrick, Maryland 21702-5012

10. SPONSOR/MONITOR'S ACRONYM(S)

11. SPONSOR/MONITOR'S REPORT NUMBER(S)

12. DISTRIBUTION / AVAILABILITY STATEMENT

Approved for Public Release; Distribution Unlimited

13. SUPPLEMENTARY NOTES

14. ABSTRACT

According to published data, African American (AA) men AA men are 1.6 times more susceptible to developing prostate cancer, and about 2 times more likely to die from this disease than men of European (EUR) descent. In fact, even when environmental factors are corrected, the disparity in mortality rate between AA and EUR men is higher for prostate cancer than that for any other malignancy, thus suggesting a molecular component. The Caromile lab is investigating if germline single nucleotide polymorphisms, or SNPs, within certain components of the PSMA signaling pathway might contribute to the increased risk of prostate cancer in AA men vs that of EUR men. Investigation into these molecular mechanisms not only has the potential to improve the outcomes of all men with lethal prostate cancer but also has the capability to reduce prostate cancer disparities by improving detection, morbidity, and mortality of lethal prostate cancer in AA and other at-risk populations through the identification of unique, tailored treatment and prevention strategies for each patient.

15. SUBJECT TERMS

Prostate cancer, prostate-specific membrane antigen (PSMA), single nucleotide polymorphism (SNP), germline, genomics, bioinformatics, health disparity

16. SECURITY CLASSIFICATION OF:			17. LIMITATION OF ABSTRACT	18. NUMBER OF PAGES	19a. NAME OF RESPONSIBLE PERSON
a. REPORT	b. ABSTRACT	c. THIS PAGE			USAMRDC
Unclassified	Unclassified	Unclassified	Unclassified	94	19b. TELEPHONE NUMBER *(include area code)*

TABLE OF CONTENTS

1. Introduction:

According to published data, African American (AA) men AA men are 1.6 times more susceptible to developing prostate cancer, and about 2 times more likely to die from this disease than men of European (EUR) descent. In fact, even when environmental factors are corrected, the disparity in mortality rate between AA and EUR men is higher for prostate cancer than that for any other malignancy, thus suggesting a molecular component. The Caromile lab is investigating if germline single nucleotide polymorphisms, or SNPs, within certain components of the PSMA signaling pathway might contribute to the increased risk of prostate cancer in AA men vs that of EUR men. Investigation into these molecular mechanisms not only has the potential to improve the outcomes of all men with lethal prostate cancer but also has the capability to reduce prostate cancer disparities by improving detection, morbidity, and mortality of lethal prostate cancer in AA and other at-risk populations through the identification of unique, tailored treatment and prevention strategies for each patient.

2. Key Words: Prostate cancer, prostate-specific membrane antigen (PSMA), single nucleotide polymorphism (SNP), germline, genomics, bioinformatics, health disparity

3. Accomplishments:

During year 2 of this grant, I was able to continue with the aims of this project. Loss of the supply chain, as well as other effects of COVID, were still affecting our workplace until well into the spring. Additionally, the Prostate Cancer Biorepository Network (PCBN) at John Hopkins recently lost its funding from the DOD and can no longer provide us with tissue samples. However, we were able to find another source of prostate cancer tissue from prostatectomies and applied for additional patient samples. Additionally, I hired a technician, hosted an undergraduate summer student (freshman) and a graduate student joined my lab and began to move the projects along. I know that everyone is in the same boat with lost research time due to the pandemic, so in this report, I will be discussing results from the parts of the project that I was able to collect as well as what I plan on doing in the future to catch up with this loss of productivity.

Major Activities: All the activities in this report were part of Aim 1 and Aim 2.

Major Goals of the project:

Below is the statement of work as presented in the grant:

Specific Aim 1(specified in the proposal)	**Timeline**	**Site 1**
Determine whether AA men have a higher risk of a known panel of SNPs vs that CA men and the effect of these SNPs on clinical metabolites.		
Genotype archived tissue of AA and CA PC patients for polygenic risk of a known panel of SNPs.	1-18	Post-Doctoral Fellow ~700 de-identified, FFPE patient samples
Statistical Analysis of MAF, Haplotype, and Risk. Associate the levels of glutamate or folate to the SNPs in the PSMA-dependent pathway	1-6	Dr. Kuo and Post-Doctoral Fellow
Whole-exome sequencing to discover additional SNPs that influence PC in EUR vs AA Men.		Dr. Caromile and Post-Doctoral Fellow
Mathematically model PSMA-dependent crosstalk and the effects of SNPs on the pathway components:	25-30	Dr. Caromile, Dr. Laubenbcaher
Milestones: Comprehensive data revealing a panel of PSMA pathway-related SNPs that correlate with PC risk. Validation of mathematical models' ability to predict outcomes of intervention; publication of peer-reviewed papers.		
Specific Aim 2 (Specified in Proposal)		
Comprehensively characterize functional effects of a known panel of SNPs on intracellular crosstalk among PSMA-dependent pathways and their effects on PC tumor growth *in vivo*.	1-18	
Generate molecular and phenotypic data from a panel of PC cell lines treated with and without pathway-specific inhibitors.	1-12	Dr. Caromile and Post-Doctoral Fellow
Evaluate molecular and phenotypic effects on PC lines engineered to express bar-coded SNPs	1-18	Dr. Caromile and Post-Doctoral Fellow
In vivo evaluation of PC cell lines engineered to express unique barcoded SNPs on tumor growth and dissemination mouse model.	6-12	Dr. Caromile and Post-Doctoral Fellow ~200 mice
Milestone: Identify SNPs, single or in combination or that have functional effects in vivo and in vitro as well as in tumor progression.		
Local IACUC Approval for proposed methods.	12	Dr. Caromile

Specific objectives and Significant Results:

Aim 1: Determine whether AA men have a higher risk of a known panel of SNPs vs than CA men and the effect of these SNPs on clinical metabolites.

a. *Obtained patient samples and stratified them by National Cancer Comprehensive Network resource stratification criteria:*

Unfortunately, the **Prostate Cancer Biorepository Network (PCBN)** at John Hopkins recently lost its funding from the DOD and can no longer provide us with tissue samples. Therefore, for most of this year, were solely dependent upon the **UCONN Health Research Biorepository**. We were able to obtain approximately 200 de-identified, formalin-fixed paraffin-embedded (FFPE) from consented AA and EUR patients who have self-identified as either European/non-Hispanic or African American/non-Hispanic, who were confirmed to have PC and have undergone radical prostatectomy at UCONN Health. Pathology reports were provided for all patient samples. Patient samples were then stratified into *highly aggressive,* where the GS sum ≥ 8, or PSA >20 ng/ml and >10% probability of pelvic lymph node involvement; *low aggressive,* where GS sum ≤ 7, or PSA ≤ 20ng/ml and < 10% probability of pelvic lymph node involvement. All our stratifications were verified by our in-house pathologist, Mary Melinda Sanders, MD. We have recently requested tissue samples from the **North Carolina-Louisiana Prostate Cancer Project,** which have samples from approximately equal numbers of African Americans and Caucasian Americans with newly diagnosed prostate cancer from Louisiana and North Carolina (2,258 total). In addition, several follow-up studies have been undertaken, which should provide us with some great additional data.

Significant Data from Section a:

Combining all of our current data from the **past 2 years**, we found that a higher number of EUR individuals who have had prostatectomies at UCONN Health had primary prostate tumors that were of a higher grade than that of AA individuals.

	EUR	AA
Average Age	66.3	62.8
Highly Aggressive (Gleason Score ≥ 8)	27	44
Low Aggressive (Gleason Score ≤ 7)	173	156

b. *PSMA verification and localization in patient tissue:*

Although PSMA is present in ~80-90% of all PC primary tumors, the presence and localization of PSMA were verified in each patient sample by the following methods:

i. *Immunohistochemistry (IHC):*

PSMA presence and localization within the PC tumor were validated on sections of FFPE tissue from each patient. A secondary antibody-only control was used to assess non-specific background staining.

Significant Data from Section i:

Our data showed that **100% of our AA samples and 82% of the EUR samples** showed varying levels of PSMA protein staining via IHC. This data aligned with published data that PSMA is present in ~80-90% of all PC primary tumors.

ii) Western blot analysis

PSMA protein expression in patient tissue samples was verified by western blot protein expression using PSMA antibody (Cell Signaling D718E), the immortalized human prostate cancer cell line LnCaP as a positive control and normalizing to a β-actin loading control (Cell Signaling D6A8).

Significant Data from Section ii:

PSMA was detectable in protein extracted from FFPE in **all our AA samples and 82% of our EUR patient samples.** This was great news for us as we knew that our proposed pathway would be perturbed (in some way) in almost all our patients.

c. SNP Verification in gDNA from Patient Tissue:

Last year I was contacted by the UCONN professional science master's program in Applied Genomics. The students in the program are required to complete a semester internship as part of their curriculum, and they were wondering if I would host a student for the Summer of 2022. I hosted a student, **Kyle Guzy**, in my lab, and he was very helpful with the sequencing of patient gDNA as well as the analysis of the sequencing and phenotype data. Additionally, I hosted a freshman URM summer student from UCONN, **Shannon Jones**, as part of an **NIH R25 program** that I run designed to increase interest, application, and matriculation of URM individuals into biomedical science doctoral programs at UConn Health or other US institutions and, eventual research career in the biological sciences. Kyle worked with the summer student and used the Applied Biosystems SeqStudio Genetic Analyzer and Data Collection Software to verify if the SNPs in the below panel were present in the genome of each patient. Using the Big Dye Kit, he ran both the PCR step and the cycle sequencing step seen below and then sent our samples to be cleaned and analyzed by the UCONN Sequencing Core.

PCR/Sanger Sequencing Primer Pairs

Gene	Coding SNP	Amino Acid Coordinate	Location	Alleles (Ancestral /MAF)	Amplicon Length (BP)	Assay ID
FOLH1	rs202676	Y75H	Chromosome 11: 49,206,018-49,206,118	A/G	274	Hs00648640_CE
FOLH1	rs202680	A111A	Chromosome 11: 49,200,283-49,200,383	T/A	274	Hs00594720_CE
FOLH1	rs182169	D244E	Chromosome 11: 49,185,713-49,185,813	A/C/G	500	Hs00329578_CE
FOLR3	rs1802609	R26W	Chromosome 11: 72,135,984-72,136,084	C/A/T	498	Hs00108820_CE
SLC7A11	rs6838248	A224A	Chromosome 4: 138,219,290-138,219,390	G/C/T	496	Hs00254036_CE
GRM1	rs6923492	S993P	Chromosome 6: 146,434,138-146,434,238	T/C	499	Hs00282287_CE
GRM5	rs61741175	T453R/M	Chromosome 11: 88,604,704-88,604,804	G/A/C	274	Hs00675325_CE

Significant Data from Section c:

Using Sequencher Software, we created a variance table that summarized all the differences between each consensus sequence and its corresponding gene reference sequence. We then validated our data by, setting our threshold to 30% and then linking each cell in our data analysis to a base call. This made it easy to find out if the SNPs in our patient panel were present. We were also able to identify novel SNPs and ones that were not in our panel. As predicted, we found that there were changes in not one, but many of the SNPs. This

data was so interesting! For example, we found that FOLH1 A111A and D224D were found exclusively in EA samples, and FOLR3 R28R was discovered exclusively in AA samples (See the below figure). Kyle used this data to write *part* of his final examination for the M.S. in Genomic Systems Analysis at UCONN. We are still adding to his data and will be publishing his results by the end of the year (I attached it here along with some of his results). I would also like to mention here that the undergraduate student from UCONN was very excited to be exposed to this type of research and technology, and she is now interested in eventually joining a Ph.D. program.

FOLH1 A111A						
Sample	AA/EA	Called (Automatic)	Primary	Secondary	Secondary as %	F/R (by ID)
4113	AA					F
4113	AA					R
3651	AA					F
3651	AA					R
4158	AA					F
4158	AA					R
3601	EA					F
3601	EA					R
3387: 130146	EA	W	T	A	71	F
3387: 130147	EA	W	T	A	65	R
3728: 130148	EA	A	A	G	7	F
3728: 130149	EA	A	A	T	5	R
4253	EA					F
4253: 134149	EA	W	A	T	97	R
4254: 134150	EA	W	T	A	61	F
4254: 134151	EA	W	T	A	85	R

Aim 2: Comprehensively characterize the functional effects of a known panel of SNPs on intracellular crosstalk among PSMA-dependent pathways and their effects on PC tumor growth *in vivo*.

a. *Prediction of biological effects of SNPs*
As shown in last year's report, we used PredictSNP1 analysis, which predicts the biological effects of one SNP at a time and saw that not all SNPs were deleterious when expressed alone. The limitation of the PredictSNP1 model is that it can only predict the consequence of **one** SNP, not multiple. We knew that some of the patient samples were positive for multiple SNPs. Therefore, using PyMol Molecular Graphics System, we used a published, high-resolution structure of PSMA (PDB ID 2OOT)[1] and constructed a model of PSMA that contained our panel of SNPs. The model showed slight structural variations between the PSMA wild type (WT) and the SNP-containing PSMA structure (See Figure). To show exactly where the SNPs affected PSMAs structure and what could be the predicted consequences; we used the publicly available PredictProtein algorithm. PredictProtein searches public sequence databases, creates alignments, and predicts aspects of protein structure and function[2]. We found that introducing all the SNPs into PSMA resulted in large changes in key protein structure and protein binding regions. Specifically, there were protein-binding changes in the apical/protease domain interface and substrate-binding region. There were also many differences in both DNA and protein-binding within the zinc-peptidase-like superfamily domain and the GCPII-like domain suggesting changes in alternative splicing and/or enhancers activity. See schematic of PSMA protein regions for

orientation Importantly, with the SNPs included, PSMAs enzymatic domain was no longer “exposed” but instead “buried”, creating an enzymatically inactive PSMA that decreased adhesion to Matrigel suggesting that the SNP has function despite the initial PredictSNP1 prediction.

b. Design and production of SNPs by site-directed mutagenesis and cloning:

We recreated all of the hPSMA SNPs in our panel above in both the hPSMA PBM-Puro Myc/His and hPSMA pQCXIP-F-Luc Myc/His plasmids by site-directed mutagenesis (GeneArt Site-Directed Mutagenesis PLUS System, Thermo Fisher, Cat# A14604). We then transduced the following cell lines with our SNPs. Information on hPSMA knockout CRISPR 22Rv1 and hPSMA knockout CRISPR C4-2B can be found in recent publications by Leslie A. Caromile. These publications are in the appendix.

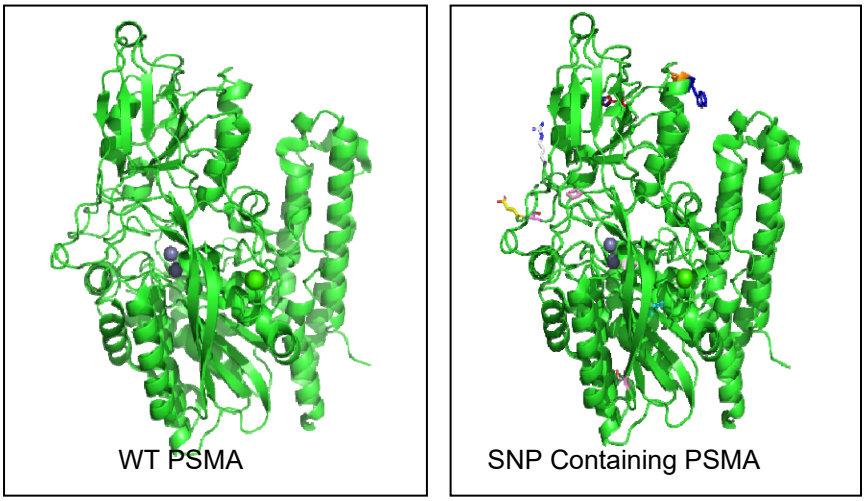

<u>Hosts:</u>
hPSMA knockout CRISPR LnCaP
hPSMA knockout CRISPR 22Rv1
hPSMA knockout CRISPR C4-2B
hPSMA knockout CRISPR MDA PCa 2b
PC-3, Du145 and RWPE1

All of these cell lines were analyzed for phenotypic and metabolic changes, and **as we hypothesized**, one base pair change made an inconsequential difference in proliferation, transmigration and metabolic assays.

c. Animal protocol and IBC:
An animal protocol and IBC were submitted for this project.

Training and professional development opportunities:

Although this project was not intended to provide training and professional development, it did so in the following ways: as an early investigator, I am now building a scientific reputation and able to start building my lab. More students know about my research and are asking to do rotations in the lab. I have been invited as reviewer for multiple health disparities journals, invited to chair the UCONN graduate school DEI committee and I have started a journal club where we discuss the need for diverse study populations as well as diverse research teams in the biomedical sciences. Additionally, I am a member of the American Society for Cell Biology Minority Affairs Committee where I have written 2 pieces discussing the need for diversity within the sciences (attached). Also, the genomic analysis that learned using PredictSNP1, Pymol and PredictProtien facilitated a collaboration with assistant professor **Teresita Padilla-Benavides, PhD** from Wesleyan University that resulted in a publication (attached). I could go on but I am happy to say that after COVID put a halt to my progress for a year and a half, I am finally seeing scientific and professional results.

How were the results disseminated to communities of interest? Nothing to report.

What do you plan to do during the next reporting period to accomplish the goals?

As mentioned throughout this section, COVID significantly impacted our ability to reach the milestones that were set in the statement of work. It caused a domino effect of lost time, work, difficulty getting supplies. There are many ways that I will be addressing this in the next funding cycle. Our statistician, Dr. Kuo, has started to assess risk associated with the SNPs and Gleason Score. I currently have 1 master’s student, Romoye Sohan, who will be working on Aim 1. Romoye is in a program called Young Innovative Investigator

Program (https://health.uconn.edu/connecticut-convergence-institute/young-innovative-investigator-program/) and her salary and supplies are covered through her program. I had an extremely difficult time finding a postdoc for this project. After 8 months of advertising through UCONN Health postdoctoral association, SACNAS, Minority Postdoc, LinkedIN, Handshake (including 19 universities), and Indeed. I offered the postdoc position to Amir Yarahmadi, and they accepted. However, he had to participate in two years of military service in his country and eventually had to withdraw their application. However, I was able to turn this into a positive experience for us both by suggesting that we write a review paper, it is attached. As previously mentioned, I hosted both Kyle Guzy and Shannon Jones for the summer of 2022 where they worked together sequencing patient gDNA and analyzing samples. I have also had a student, from the UCONN Ph.D. in the Biomedical Sciences Program, **Brenna McAllister**, just join my lab in September 2022 and she will be picking up where Kyle left off. I truly believe, with all this extra help, we will be able to make up for the lost time.

4. Impact: Nothing to report.

5. Changes and Problems:

a. Changes in approach and reasons for change

During year 2 of this grant, I was able to continue with the aims of this project. Loss of the supply chain, as well as other effects of COVID, were still felt at our workplace until well into the spring. Additionally, the Prostate Cancer Biorepository Network (PCBN) at John Hopkins recently lost its funding from the DOD and can no longer provide us with tissue samples. However, we were able to find another source of prostate cancer tissue from prostatectomies and applied for additional patient samples. Additionally, I hired a technician, and a graduate student joined my lab in April and June, respectively, and began to work move the projects along.

Significant changes in use or care of human subjects, vertebrate animals, biohazards, and/or select agents: nothing to report

6. Products: Nothing to report.

7. Participants & Other Collaborating Organizations:

Individuals that have worked on the project:

Name:	*Leslie Caromile*
Project Role:	*PI*
Researcher Identifier (e.g. ORCID ID):	0000-0003-2193-5190
Nearest person month worked:	*4.2*
Contribution to Project:	*No change*
Funding Support:	*No change*

2022 Update:

Name:	*Kyle Guzy*
Project Role:	*student*
Researcher Identifier (e.g. ORCID ID):	
Nearest person month worked:	*3*
Contribution to Project:	*No change*
Funding Support:	*No change*

7. Special Reporting Requirements: Nothing to Report

8. Appendices: See attached

References:

1 Barinka, C., Starkova, J., Konvalinka, J. & Lubkowski, J. A high-resolution structure of ligand-free human glutamate carboxypeptidase II. *Acta Crystallogr Sect F Struct Biol Cryst Commun* **63**, 150-153 (2007).

2 Rost, B., Yachdav, G. & Liu, J. The PredictProtein server. *Nucleic Acids Res* **32**, W321-326 (2004).

An Inceptive Investigation into the Potential Influence of Certain Single Nucleotide Polymorphisms and Bacterial Load on the Disproportionately-High Prostate Cancer Risks of African-American Men in Comparison to European-American Men

Kyle Guzy
Date of Submission: 8/8/2022
Date of Revision: 8/23/2022
Student ID Number: 1964035
Telephone Number: 860-986-1909
Email Address: kyle.guzy@uconn.edu

A final examination submitted
in partial fulfillment of the requirements for the
M.S. in Microbial Systems Analysis.

Committee Members
Major Advisor: Dr. Joerg Graf
Associate Advisor: Dr. Charles Giardina
Associate Advisor: Dr. Victoria Robinson

ABSTRACT

In the United States, there exists a significant disparity between men of African descent and those of European descent regarding the occurrence and lethality of prostate cancer. To investigate what may be contributing to this disparity, genes of cancerous prostate tissue from men of both races were sequenced via the Sanger method in order to find SNPs within the prostate-specific membrane antigen (PSMA) signaling pathway that may be increasing the risk for African-American men specifically. Numerous SNPs were

detected in the patient samples that potentially imply racial influence and thus merit further investigation. Additionally, cancerous prostate tissue DNA underwent qPCR targeting the bacterial 16S rRNA gene in order to explore whether a difference in bacterial load exists between the racial groups. Average starting quantities of the target sequence, 16S rRNA, indeed demonstrated a contrast.

INTRODUCTION: Overview and Rationale of Projects

American men are diagnosed with prostate cancer more than any other type of cancer[1], and the African-American subset contends with a nearly 60% higher incidence than, and over twice the mortality rate of, the Caucasian subset[2]. Clearly, this disparity must be addressed by the scientific community, and it would be beneficial for approaches to utilize an arsenal of interdisciplinary perspectives. In that spirit, our lab has advanced a pair of projects belonging to different subfields but pursuing a common goal: to understand the biological factors underlying the higher prostate cancer risk in African-American men.

The primary project concerns the study of single nucleotide polymorphisms (SNPs) in genes of men of African and men of European descent within the PSMA pathway. An SNP is a germline alteration of a single nucleotide at a particular position in the genome, thus representing an allele. The proteins encoded by the genes of interest are generally associated with the folate cycle, and some are constituents of the phosphatidylinositol-3-kinase-protein kinase B (PI3K-AKT) signaling pathway. The PI3K-AKT pathway supports prostate tumor viability by contributing to aspects of cell survival and metabolism[3,4], and is known as the most commonly-activated pathway in human cancer[5]. It is believed to be switched on by prostate-specific membrane antigen (PSMA) at the expense of the mitogen-activated protein kinase extracellular signal-regulated kinase (MAPK-ERK) pathway[6], which generally controls factors related to cell proliferation and tissue homeostasis[3,4]. PSMA, also known as glutamate carboxypeptidase II for its glutamate-cleaving behavior, is a type II transmembrane protein normally found sparingly on prostate epithelial cells, but is increasingly upregulated as prostate cancer worsens[6]. Hence, the roles PSMA and the pathways it affects play in prostate cancer merit scrutiny, and by understanding what the discovered SNPs signify and examining their frequencies between the races, a foothold can be established in addressing the disparity.

SNPs can be discovered via Sanger sequencing of cancerous prostate DNA and subsequent analysis of the base-called identity of each nucleotide in relation to the reference sequence using sequence-analyzing software such as Sequencher. Two peaks at one base position on the chromatogram suggest the presence of a heterozygote. A secondary peak indicates that the instrument has found another nucleotide at the particular position for DNA in the sample. As tumors can consist of cells with genes that are mutated and unmutated, the sequences of DNA in one sample may differ. The larger the secondary peak is in relation to the primary peak, the more confidence one can have that the sample is heterozygotic. For this paper, an SNP will be considered heterozygotic if an allele with a secondary peak percentage of 35% or greater is found on the chromatogram.

The secondary project seeks to quantitatively analyze the microflora of the cancerous prostate tissue of African-Americans and European-Americans in order to compare their bacterial loads, with the knowledge that bacteria are known to contribute to cancer elsewhere in the body. In colorectal cancer, for instance, microbes promote carcinogenesis through catalyzing inflammation and disrupting signaling pathways[7]. A study by Farhana et al. focusing on microbial presence in cancerous gastrointestinal tissue suggested that variations in bacterial taxa and overall diversity exist between the races; specifically, the authors found that African-American sufferers of colorectal cancer had higher abundance of class Bacteroidia in comparison to European-American sufferers (70.7% to 43.1%) and a lower overall microbial diversity, among other dissimilarities[8]. The hypothesis for this project is that the African-American samples will have a higher load than European-Americans.

While the cancerous prostate microbiota has not enjoyed as much attention as that of the gut, numerous studies have offered insights into the abundance and taxa of bacteria to be found in that environment. One study found that the bacterial load of high-risk African prostate tissue was 1.6-fold higher than that of Chinese and European-descent Australian patients[1] and suggested that bacteria may bear partial responsibility for severe cancer progression[9]. Miyake et al. reported that sexually-transmitted *Mycoplasma*

genitalium infected 40% of their prostate cancer cohort, but only 18% of their benign prostatic hyperplasia (BPH) cohort, and that the rate of severe progression was higher amongst infected patients (77%) than uninfected patients (44%)[10]. An earlier study even concluded that constant exposure of human BPH-1 cells to bacteria of the genus *Mycoplasma* resulted in malignant transformation, with the authors describing *Mycoplasma* protein p37 as a molecular culprit[11].

INTRODUCTION: Overview of PSMA Pathway Genes and SNPs in SNP Project

It is necessary to provide an outline of what the genes in the SNP project code for and what their functions are in order to draw a general picture of what is, for the purposes of this project, referred to as the "PSMA pathway." **FOLH1** encodes PSMA, a ~750aa integral membrane protein whose extracellular region accounts for 95% of its structure. It cleaves glutamate from folate (natural vitamin B9) and other glutamate-linked substrates, giving rise to the glutamate-induced stimulation of local class I metabotropic glutamate receptors mGluR1 and mGluR5 (encoded by **GRM1** and **GRM5**, respectively), which in turn activate the PI3K-AKT pathway[12]. **FOLR3** encodes folate receptor 3, which endocytoses extracellular folate[13]. **SLC7A11** encodes cystine/glutamate antiporter xCT and **SLC19A1** encodes reduced folate carrier protein 1, the former exporting glutamate in favor of cystine and the latter importing 5-methyltetrahydrofolate[14,15]. **MTHFD1** encodes methylenetetrahydrofolate dehydrogenase, an enzyme that catalyzes a trio of reactions, through which tetrahydrofolate is converted to cofactors for nucleotide synthesis[16]. **MTHFR** encodes methylenetetrahydrofolate reductase, an enzyme that converts the 5,10-methylenetetrahydrofolate version of folate to 5-methyltetrahydrofolate, which is used by **MTR**-encoded methionine synthase to convert homocysteine to methionine[17-18].

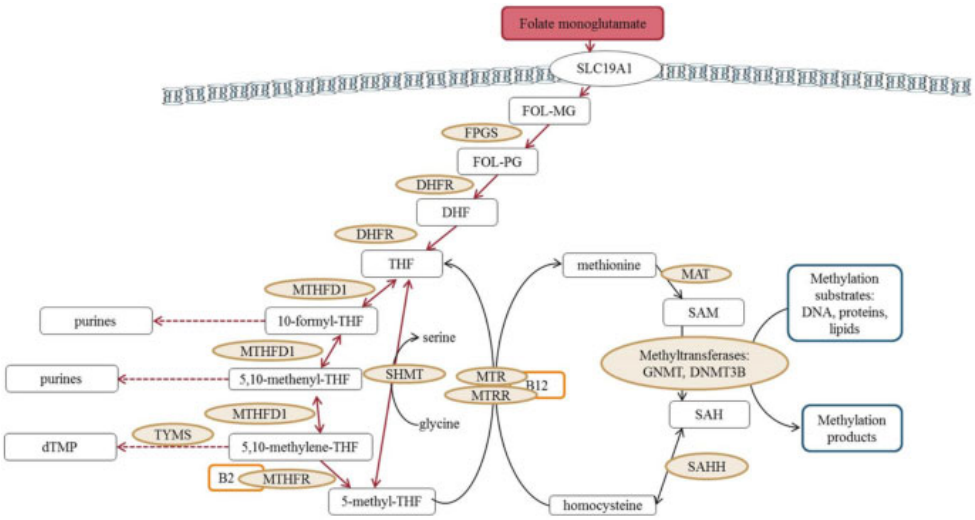

Figure 1. A diagram of folate metabolism[26], featuring some of the genes relevant to this study.

These genes contain SNPs identified by the scientific community and suspected of playing a role in prostate cancer. Information on the SNPs investigated for this project is provided below in Table 1.

Gene	SNP	Amino Acid Change	Codon Change	Orientation	rsID[2]
FOLH1	Y75H	tyrosine>histidine	**T**AT>**C**AT	minus	rs202676
	I70V	isoleucine>valine	**A**TC>**G**TC	?	?
	A111A	alanine>alanine	GC**A**>GC**T**	minus	rs202680
	D244E/D	aspartic acid>glutamic acid	D>E: GA**T**>GA**G**; D>D: GA**T**>GA**C**	minus	rs182169
FOLR3	R28R	arginine>arginine	**C**GG>**A**GG	plus	rs1802609
SLC7A11	A224A	alanine>alanine	GC**C**>GC**G**	minus	rs6838248
SLC19A1	H27R/P	histidine>arginine/proline	H>R: C**A**C>C**G**C; H>P: C**A**C>C**C**C	minus	rs1051266

[1] The authors impart the caveat that fecal contamination could not fully be ruled out.
[2] An rsID is an ID used for established SNPs.

MTHFD1	R653Q	arginine>glycine	C**G**C>C**A**G	plus	rs2236225
MTHFR	A222V	alanine>valine	G**C**C>G**T**C	minus	rs1801133
MTR	D919G	aspartic acid>glycine	G**A**C>G**G**C	plus	rs1805087
GRM1	S993P	serine>proline	**T**CC>**C**CC	plus	rs6923492
GRM5	T453R/M	threonine>arginine/methionine	T>R: A**C**G>A**G**G; T>M: A**C**G>A**T**G	minus	rs61741175
Green text signifies the amino acid change represented in the population genotype data					

Table 1. Information on the SNPs discussed in this paper.

This table can be referred to in order to understand which alleles are considered "reference" and which are considered "SNP," wherein, under "**Codon Change**," the nucleotide in bold in the first codon of the row represents the reference allele and the nucleotide in bold in the second codon represents the SNP allele.

Before analyzing the Sanger sequencing results, the frequencies of SNP genotypes as they exist naturally in African-descent and European-descent populations were examined. Genotypic data of males from both groups were extracted from Ensembl.org and compared in order to get an initial understanding of which alleles men of African heritage carry with appreciably higher frequency than do their European counterparts. Sample sizes for each SNP were about 319 individuals of African descent and about 240 individuals of European descent, gathered by the 1000 Genomes Project. These comparisons suggest that, for many of the SNPs, there do indeed exist notable differences between the two[3][4].

Population genotype frequency data for FOLH1 Y75H show that the African-descent group (henceforth "AD") have a roughly threefold-lower frequency of homozygous reference genotype AA than does the European-descent group (henceforth "ED") (19.1% to 62.1%), as well as a roughly eightfold-higher frequency of homozygous SNP genotype GG (33.2% to 4.2%). Furthermore, AD carries heterozygotic genotypes at a frequency of over ten percentage points higher than does ED (47.7% to 33.8%). These data suggest that AD is significantly more likely to carry the SNP allele of G.

Genotype (fwd strand)	Count of Genotype (fwd strand)	Ratio to Total	%
AA	61	0.191222571	19.12225705
AG	80	0.250783699	25.07836991
GA	72	0.225705329	22.57053292
GG	106	0.332288401	33.22884013
Grand Total	**319**	**1**	**100**

Genotype (fwd strand)	Count of Genotype (fwd strand)	Ratio to Total	%
AA	149	0.620833333	62.08333333
AG	48	0.2	20
GA	33	0.1375	13.75
GG	10	0.041666667	4.166666667
Grand Total	**240**	1	**100**

Table 2. AD (top) and ED (bottom) population genotype frequency tables for FOLH1 Y75H.

Data for FOLH1 A111A show that AD once again is clearly more prone to carrying genotypes homozygous or heterozygous for the SNP allele. The frequency of homozygous reference genotype TT is over threefold higher in ED than in AD (56.5% to 15.7%), and the frequency of genotypes with SNP allele A is roughly double in AD than in ED (84.3% to 43.5%). AD also has a

[3]Caveats to consider are sample size and geographic selection. These individuals are further distinguished by ethnicity. Africa is the most genetically-diverse continent on Earth, and the handful of populations sampled for these data unfortunately cannot do justice to its true diversity.

[4] Please bear in mind throughout this paper that whenever nucleotides in the population genotype frequency data table are different than those in the Sanger sequencing data table for a particular SNP (for instance, one shows A and G and the other shows T and C), it means that they are at the same location but present on complementary strands.

higher frequency of heterozygous genotypes (47.3% to 36.4%). Once again, there is a notable difference in genotype frequencies between the groups.

Genotype (fwd strand)	Count of Genotype (fwd strand)	Ratio to Total	%
AA	118	0.369905956	36.99059561
AT	74	0.231974922	23.19749216
TA	77	0.24137931	24.13793103
TT	50	0.156739812	15.67398119
Grand Total	**319**	**1**	**100**

Genotype (fwd strand)	Count of Genotype (fwd strand)	Ratio to Total	%
AA	17	0.071129707	7.112970711
AT	39	0.163179916	16.31799163
TA	48	0.20083682	20.08368201
TT	135	0.564853556	56.48535565
Grand Total	**239**	**1**	**100**

Table 3. AD (top) and ED (bottom) population genotype frequency tables for FOLH1 A111A.

Data for FOLH1 D244D similarly show an approximately threefold increase of homozygous reference genotype frequency AA in ED versus AD (56.5% to 18.1%). Heterozygote frequency is once again higher in AD (48.1% to 36.4%). The SNP allele is present in over three-quarters of AD individuals (81.9%), but not even half of ED individuals (43.5%). These data, combined with the previously-described FOLH1 data, suggest that all three FOLH1 SNPs investigated for this project are more likely to be found in men of the AD group than in men of the ED group[5].

Genotype (fwd strand)	Count of Genotype (fwd strand)	Ratio to Total	%
AA	56	0.181229773	18.12297735
AG	79	0.25566343	25.56634304
GA	70	0.226537217	22.65372168
GG	104	0.336569579	33.65695793
Grand Total	**309**	**1**	**100**

Genotype (fwd strand)	Count of Genotype (fwd strand)	Ratio to Total	%
AA	135	0.564853556	56.48535565
AG	48	0.20083682	20.08368201
GA	39	0.163179916	16.31799163
GG	17	0.071129707	7.112970711
Grand Total	**239**	**1**	**100**

Table 4. AD (top) and ED (bottom) population genotype frequency tables for FOLH1 D244D.

Data for FOLR3 R28R suggest that ED has a significantly-higher frequency of homozygous reference genotype CC (91.3% to 67.7%). Homozygous SNP genotype AA was relatively scarce in both groups at less than 3% each. Heterozygous genotypes, however, were carried by AD with a markedly-higher frequency (30.1% to 7.9%). These data suggest that the R28R allele is significantly more common in AD.

Genotype (fwd strand)	Count of Genotype (fwd strand)	Ratio to Total	%

[5] The frequency distribution of the ED Ensembl data for both A111A and D244D was confirmed to be the same four values.

AA	7	0.021943574	2.194357367
AC	30	0.094043887	9.404388715
CA	66	0.206896552	20.68965517
CC	216	0.677115987	67.71159875
Grand Total	**319**	**1**	**100**

Genotype (fwd strand)	Count of Genotype (fwd strand)	Ratio to Total	%
AA	2	0.008333333	0.833333333
AC	10	0.041666667	4.166666667
CA	9	0.0375	3.75
CC	219	0.9125	91.25
Grand Total	**240**	**1**	**100**

Table 5. AD (top) and ED (bottom) population genotype frequency tables for FOLR3 R28R.

Data for SLC7A11 A224A genotype frequency show AD more likely to carry homozygous reference genotype GG by a factor of over two (50.8% to 19.6%) and less likely to carry homozygous SNP genotype CC by a factor of around four (6.6% to 27.5%). AD was also less likely to carry heterozygous genotypes by about ten percentage points (42.6% to 52.9%). Judging by these data, there is a comparative lack of SLC7A11 SNP prevalence within AD in relation to ED.

Genotype (fwd strand)	Count of Genotype (fwd strand)	Ratio to Total	%
CC	21	0.065830721	6.5830721
CG	68	0.213166144	21.31661442
GC	68	0.213166144	21.31661442
GG	162	0.507836991	50.78369906
Grand Total	**319**	**1**	**100**

Genotype (fwd strand)	Count of Genotype (fwd strand)	Ratio to Total	%
CC	66	0.275	27.5
CG	69	0.2875	28.75
GC	58	0.241666667	24.16666667
GG	47	0.195833333	19.58333333
Grand Total	**240**	**1**	**100**

Table 6. AD (top) and ED (bottom) population genotype frequency tables for SLC7A11 A224A.

Data for SLC19A1 H27R exhibit a similar proportion of heterozygous genotypes for AD (41.7%) and ED (46.7%). However, for this variant, AD carries the homozygous reference genotype TT at about twice the frequency of ED (46.1% to 23.8%). The homozygous SNP genotype CC is nearly twice as prevalent in ED than AD (29.6% to 12.2%). For a second time, more individuals from AD carry the reference allele than those from ED.

Genotype (fwd strand)	Count of Genotype (fwd strand)	Ratio to Total	%
CC	39	0.122257053	12.22570533
CT	72	0.225705329	22.57053292
TC	61	0.191222571	19.12225705
TT	147	0.460815047	46.0815047
Grand Total	**319**	1	100

Genotype (fwd strand)	Count of Genotype (fwd	Ratio to	%

	strand)	Total	
CC	71	0.295833333	29.58333333
CT	55	0.229166667	22.91666667
TC	57	0.2375	23.75
TT	57	0.2375	23.75
Grand Total	**240**	**1**	**100**

Table 7. AD (top) and ED (bottom) population genotype frequency tables for SLC19A1 H27R.

Data for MTHFD1 R653Q present a roughly doubled frequency of homozygous reference genotype GG in AD (69.9%) versus ED (33.8%). Homozygous SNP genotype AA is much lower in AD (2.5%) than in ED (21.3%). Heterozygous genotypes are more common in ED than AD by over fifteen percentage points (45.0% to 27.6%). Once again, in the general population, a suspect SNP is showing up more in ED than in AD.

Genotype (fwd strand)	Count of Genotype (fwd strand)	Ratio to Total	%
AA	8	0.02507837	2.507836991
AG	45	0.141065831	14.10658307
GA	43	0.134796238	13.47962382
GG	223	0.699059561	69.90595611
Grand Total	**319**	**1**	**100**

Genotype (fwd strand)	Count of Genotype (fwd strand)	Ratio to Total	%
AA	51	0.2125	21.25
AG	51	0.2125	21.25
GA	57	0.2375	23.75
GG	81	0.3375	33.75
Grand Total	**240**	**1**	**100**

Table 8. AD (top) and EA (bottom) population genotype frequency tables for MTHFD1 R653Q.

Data for MTHFR A222V continue the trend of more AD men carrying the homozygous reference genotype than ED men. A sweeping majority of AD individuals (81.5%) possess GG, compared to 37.9% of ED individuals. Nearly half (47.9%) of the ED group carried a heterozygous genotype. The SNP genotype AA maintains a respectable presence within ED at 14.2%, but is almost nonexistent within AD at 1.6%.

Genotype (fwd strand)	Count of Genotype (fwd strand)	Ratio to Total	%
AA	5	0.015673981	1.567398119
AG	31	0.097178683	9.717868339
GA	23	0.072100313	7.210031348
GG	260	0.815047022	81.50470219
Grand Total	**319**	1	100

Genotype (fwd strand)	Count of Genotype (fwd strand)	Ratio to Total	%
AA	34	0.141666667	14.16666667
AG	62	0.258333333	25.83333333
GA	53	0.220833333	22.08333333
GG	91	0.379166667	37.91666667
Grand Total	**240**	1	100

Table 9. AD (top) and ED (bottom) population genotype frequency tables for MTHFR A222V.

Data for MTR D919G show that for this set of frequencies, AD and ED have similar proportions of homozygous reference, heterozygous, and homozygous SNP genotypes. ED has a higher percentage of homozygous reference genotype AA (66.3%) than does AD (52.7%) by around ten percentage points. Both groups carry homozygous SNP genotype GG at very low levels, and their heterozygous genotype frequencies are relatively close (39.5% for AD, 31.7% for ED). These data suggest no radical differences in genotype frequencies between the groups for D919G.

Genotype (fwd strand)	Count of Genotype (fwd strand)	Ratio to Total	%
AA	168	0.526645768	52.6645768
AG	57	0.178683386	17.86833856
GA	69	0.21630094	21.63009404
GG	25	0.078369906	7.836990596
Grand Total	**319**	**1**	**100**

Genotype (fwd strand)	Count of Genotype (fwd strand)	Ratio to Total	%
AA	159	0.6625	66.25
AG	31	0.129166667	12.91666667
GA	45	0.1875	18.75
GG	5	0.020833333	2.083333333
Grand Total	**240**	**1**	**100**

Table 10. AD (top) and ED (bottom) population genotype frequency tables for MTR D919G.

Data for GRM1 S993P demonstrate a preponderance in frequency of the SNP allele C over the reference allele T for both groups. In AD, homozygous SNP genotype CC is more abundant than homozygous reference genotype TT by approximately sevenfold (55.2% to 7.5%), while in ED, the difference is far less (32.1% to 22.9%). AD and ED have relatively comparable frequencies of heterozygous genotypes, with AD at 37.3% and ED at 45.0%. S993P has established a firm foothold in both populations.

Genotype (fwd strand)	Count of Genotype (fwd strand)	Ratio to Total	%
CC	176	0.551724138	55.17241379
CT	50	0.156739812	15.67398119
TC	69	0.21630094	21.63009404
TT	24	0.07523511	7.523510972
Grand Total	**319**	**1**	**100**

Genotype (fwd strand)	Count of Genotype (fwd strand)	Ratio to Total	%
CC	77	0.320833333	32.08333333
CT	52	0.216666667	21.66666667
TC	56	0.233333333	23.33333333
TT	55	0.229166667	22.91666667
Grand Total	**240**	**1**	**100**

Table 11. AD (top) and ED (bottom) population genotype frequency tables for GRM1 S993P.

Data for GRM5 T453M illustrate the dominance of the homozygous reference genotype GG in these groups. This genotype is carried by virtually all individuals within ED (99.58%), with a single heterozygous individual. Within AD, it is a slightly different story: heterozygotes comprise 13.4% of the genotypes compared to 86.0% for GG. Two AD individuals carry AA, giving the

homozygous SNP genotype a frequency of under 1%. While the reference genotype enjoys the overwhelming majority within AD, there are still forty-five individuals, a nontrivial 14.1% of the group, with at least one SNP allele.

Genotype (fwd strand)	Count of Genotype (fwd strand)	Ratio to Total	%
AA	2	0.006269592	0.626959248
AG	17	0.053291536	5.329153605
GA	26	0.081504702	8.150470219
GG	274	0.858934169	85.89341693
Grand Total	**319**	**1**	**100**

Genotype (fwd strand)	Count of Genotype (fwd strand)	Ratio to Total	%
GA	1	0.004166667	0.416666667
GG	239	0.995833333	99.58333333
Grand Total	**240**	**1**	**100**

Table 12. AD (top) and ED (bottom) population genotype frequency tables for GRM5 T453M.

RESULTS: SNP Project

Results in this section are derived from variance reports from Sequencher. The software would provide a variance report with a data table for each nucleotide position the consensus sequence generated by the software and the reference sequence disagreed on. There were numerous instances in which the consensus and reference sequences were in overall agreement for a particular SNP, but at least one sample sequence differed from them. In this case, the SNP nucleotide position in the consensus sequence was manually changed to the IUPAC code for the two most-prevalent nucleotides (e.g., S for G or C) so that the peak statistics of the SNP would be included in the variance report. Table 13 provides information on the samples used in the project[6][7]. The sequences examined in this section were not in agreement with the reference sequence on the nucleotide at the

Patient (partial OriGene ID)	AA/EUR	Age	Gleason Score	Plate and Wells
4113	AA	56	3+4	P1 A&B
3651	AA	55	3+4	P1 C&D
4158	AA	54	3+3	P1 E&F
3601	EUR	59	3+3	P1 G&H
3387	EUR	58	4+4	P2 A&B
3728	EUR	72	3+3	P2 C&D
4253 (?)	EUR	?	?	P2 E&F
4254 (?)	EUR	?	?	P2 G&H

Table 13. Information on the patients whose DNA was Sanger-sequenced. A Gleason score of 6 is low-grade prostate cancer, 7 is intermediate-grade, and 8-10 is high-grade.

position in question. Sequences with secondary peaks of less than 5% that are not homozygous for the SNP allele are not discussed, despite still showing up in the variance report tables generated by Sequencher (found in the "Supplementary Data" section). It is important to note that for virtually every gene, some sequences went unused due to Sequencher judging them as low-quality and excluding them from the contig during the trimming step, so the absence of certain sequences in the variance report tables may not

[6] Sequence labels do not indicate which plate the sequences were in. Folders signifying each plate and containing the chromatogram files for the sequences of the plate were provided by the principal investigator, and the sequences were matched up with their labeled wells on the Sanger sequencing plate diagram for identification. The information was then put into the tables.

[7] "4253" and "4254" are not the true identities of the samples due to a labeling error. While the true identities are unknown, the principal investigator confirmed that both are from men of European descent.

definitively mean that they lack the SNP of interest. Nonsynonymous substitutions resulting from SNPs were run through PredictSNP, a program that utilizes multiple tools to estimate deleteriousness of substitutions, in order to understand whether a substitution is already suspected of harmfulness before even considering possible subtleties specific to that particular protein. Synonymous substitutions resulting from SNPs were run through PredictSNP[2], which estimates deleteriousness based on alteration on a nucleotide level.

The codon of FOLH1 Y75, TAT, is present in neither the reference sequence nor the sample sequences. The stop codon TAG, however, is present for all sequences extending to that point. The nearby substitution I70V will therefore be discussed in this paper instead of Y75H. An rsID for I70V could not be located, as it may not have one because it may not be currently acknowledged as an actual SNP; nevertheless, the pervasiveness and height of the secondary peaks of non-reference allele G warrant attention. One sequence each of two African-Americans (henceforth "AA"), 4113 and 3651, and four European-Americans (henceforth "EA"), 3601, 3387, 3728, and 4253, have a secondary peak of over 5% of the primary peak of reference allele A. The average of the PredictSNP results suggests harmlessness, but with mixed opinions, with two out of six tools predicting deleteriousness and four predicting harmlessness.

Gene	SNP	**PredictSNP (%)**	MAPP (%)	PhD-SNP (%)	PolyPhen-1 (%)	PolyPhen-2 (%)	SIFT (%)	SNAP (%)
FOLH1	I70V	63	63	72	67	45	79	61
SLC19A1	H27R	74	74	72	59	79	77	67
MTHFD1	R653Q	83	74	45	67	74	75	77
MTHFR	A222V	61	57	86	67	47	79	55
MTR	D919G	83	-	72	67	87	76	61
GRM1	S993P	83	-	89	67	71	78	83
GRM5	T453R	74	75	51	67	40	73	58
GRM5	T453M	83	70	45	67	63	76	58

Table 14. PredictSNP predictions of nonsynonymous substitutions. The "PredictSNP" score is the overall score. Green signifies innocuousness, red signifies deleteriousness, and white signifies the absence of the tool's column in the results.

Gene	SNP	**PredictSNP2 (%)**	CADD (%)	DANN (%)	FATHMM (%)	FunSeq2 (%)	GWAVA (%)
FOLH1	A111A	96	94	97	72	93	53
FOLH1	D244D	96	95	97	72	93	60
FOLR3	R28R	91	89	82	89	81	65
SLC7A11	A224A	93	91	96	57	93	?

Table 15. PredictSNP[2] predictions of synonymous substitutions. The "PredictSNP2" score is the overall score. Green signifies innocuousness, red signifies deleteriousness, and blue signifies an unclear result.

FOLH1 A111A and D224D were found exclusively[8] in EA samples, in all but 3601. For A111A, reference allele A has convincingly been replaced by SNP allele T for 3387 and 4254, and the peaks are about equal for 4253, suggesting heterozygosity for all three samples. Both secondary peaks for 3387 are negligible, suggesting homozygosity for the reference allele. For D224D, with the exceptions of 3728 and 3601, all EA samples are heterozygous for the synonymous substitution. The PredictSNP[2] tools unanimously predicted that both substitutions are harmless.

FOLR3 R28R was discovered exclusively in AA samples 3651 and 4158. The primary peaks are all A, the SNP allele, and the secondary peaks are all C, the reference allele. Secondary peak percentages are all comfortably above 35%, suggesting that both patients are heterozygous for the trait. The consensus base-call by Sequencher was C, but it was manually changed to M (A or C) in order to have a table for R28R generated in the variance report. As with the two previous synonymous substitutions, the PredictSNP[2] tools all predict harmlessness.

[8] That is to say, excluding all sequences with secondary peaks below 5%.

The solute carrier SNPs are carried by numerous patients. SLC7A11 A224A was found in AA 4158 and EA 3387 and 3601. The former two patients have secondary peaks for SNP allele G of 50% and over, suggesting heterozygosity, and the latter is homozygous for it. The consensus base-call by Sequencher was C, but this was manually changed to S (G or C) in order to have a table for A224A generated in the variance report. The PredictSNP[2] consensus is that the substitution is neutral, although one prediction was negative and one was undecided. SLC19A1 H27R was discovered in AA 3651 and 4158 and EA 3601, 3387, 3728, 4253, and 4254. Reference allele A is the secondary peak in all sequences with a secondary peak over 35%, and the minuscule size (≤8%) of the secondary peaks for 3387, 4253, and 4254 indicate that all three are homozygous for SNP allele G. G is the primary peak for each, signifying that the majority of patients in this project carry it. The consensus base-call by Sequencher was A with the lowest level of confidence, but it was manually changed to R (A or G) in order to have a table for H27R generated in the variance report. The PredictSNP tools generally consider H27R to be innocuous, save for one prediction.

The SNPs within the three intracellular folate-interacting enzymes were detected by Sanger sequencing in at least one patient each. MTHFD1 R653Q was discovered in AA 4158 and EA 3601, 3387, and 3728. The reference G allele represents the primary peak for 4158 and 3601, whereas the SNP A allele is the primary peak for the other sequences. Secondary peak percentages all exceed 35%, and most exceed 75%, strongly suggesting heterozygosity. The PredictSNP tools unanimously consider this substitution to be innocuous. MTHFR A222V was located only in EA 3728. However, the allele represents the primary peak, with the reference allele, C, at over half the height. MTR D919G allele G is present in heterozygotes and one homozygote. Most sequences have reference allele A as their primary peak, with the exception of EA 3601. D919G represents either the primary peak or the secondary peak at 35% or greater for three patients: AA 3651, EA 3601, and EA 4253. All utilized PredictSNP tools indicate that D919G and R653Q are benign, but four of six indicate deleteriousness for A222V, with an overall prediction of deleteriousness.

While one metabotropic glutamate receptor SNP is abundant in the patients, the other is absent. The GRM1 S993P site was found to be strongly heterozygotic in half the total samples and homozygotic in AA 3651 and EA 3387 and 3728, as they yielded essentially no secondary peaks. Secondary peaks were mostly above 70% for these sequences. These data constitute an even split between racial groups for the trait. Neither substitution of GRM5 T453R/M was found, as the reference and sample sequences agreed on the base-call. Both substitutions were run through PredictSNP anyway in addition to S993P, and all three were found to be innocuous overall.

DISCUSSION: SNP Project

Upon first glance, it would appear that many of the investigated SNPs are not inimical. With four of the ten SNPs inducing synonymous substitutions, it may be tempting to ignore them, as there exists a widespread assumption that synonymous substitutions are benign. However, this assumption may not always be correct. A recent paper shared the startling finding that three-quarters of yeast mutants engineered to carry synonymous substitutions experienced a significant decline in fitness, and that these declines were comparable to those experienced by mutants afflicted with nonsynonymous substitutions[19]. The paper points out that synonymous substitutions have the ability to affect numerous aspects of expression, such as transcription factor binding, transcription, and pre-mRNA splicing. Ribosome processing of mRNA can also be thrown off-kilter, setting the protein on an unconventional folding pathway that can hamper its function[20-21]. Another paper suspects synonymous substitution BRCA2 L3216L of contributing to breast cancer by effectuating the bypass of an exon[22].

It is true that all synonymous SNP substitutions investigated in this project were predicted by PredictSNP[2] to be neutral. While a meaningful evaluation of the capabilities of the five tools employed by the application is well beyond the scope of this paper, it is unlikely that any can satisfactorily account for the nuanced effects of these substitutions, as strides in achieving a better understanding of synonymous substitutions, such as those mentioned above, are continuously being made, and the tools must continuously be refined to adjust for them. It is doubtful that these tools are adequately-designed for the complexities inherent in the interactions of the protein in question with other proteins sharing a pathway that may themselves carry substitutions, resulting in subtle

effects as of yet undetected. Analyzing the effect of a single substitution within one protein, without considering the substitutional status of the other proteins in the pathway it interacts with, only scratches the surface of the issue.

FOLH1 I70V appeared in most patients, and always as a secondary peak, which fluctuated greatly from patient to patient. Two sequences, one per racial group, can be considered true heterozygotes with the ≥35% criterion, which amounts to 25% of the patients. Given that this prevalence holds true for the wider population, and that two PredictSNP tools deemed it a deleterious substitution, it would seem that if this SNP truly does not yet have an rsID, then it should be given one[9]. It should be noted here that many other variants besides those searched for turned up in the variance reports, and with peaks strongly suggesting heterozygosity, but all but I70V were left out, in keeping with the current focus of the lab. The results for this SNP hint at a role potentially antagonistic to human health.

FOLH1 A111A data are worth noting for the fact that only EA patients present as true heterozygotes. 3387, 4253, and 4254 all have significant T peaks, corresponding to forward-strand A[10]. The population genotype frequency data for European men reflect that over half of them were homozygous for reference allele T (reverse-strand in Sequencher: A), whereas the plurality of AA individuals carried homozygosity for SNP allele A (reverse-strand in Sequencher: T). This suggests that most EA patients in this study are at least heterozygous for an allele far more common in men of African descent. Although the PredictSNP[2] tools undividedly judge it as harmless, there could be subtle factors at play that work to promote cancer progression. For example, perhaps an irregularity in protein folding resulting from the altered codon ultimately confers an enhancement of the glutamate-cleaving productivity of PSMA, thus setting the PI3K-AKT pathway in motion and contributing to cell survival.

FOLH1 D224D heterozygotes were discovered exclusively in EA patients, and AA patient 3651 was found to be homozygous for the SNP allele. For almost all sequences with secondary peaks ≥35%, reference allele A (reverse-strand in Sequencher: T) competed closely with SNP allele G (reverse-strand in Sequencher: C). In the population genotype data, the ED frequency of AA is the same as the ED A111A frequency of homozygosity for the reference allele at 56.5%, and the AD frequency of GG is similar to that of the homozygous SNP genotype for A111A. Once again, the Sequencher data shows that a high percentage of the EA prostate cancer samples sequenced for this study carry an allele more-closely associated with men of African descent. While the PredictSNP[2] results point to innocuousness, the conspicuous presence of the SNP allele in most EA patients may be hinting that this is not the full story.

FOLR3 R28R heterozygosity was found in AA patients 3651 and 4158. As can be observed in the population genotype frequency data for African men, homozygosity for reference allele C, while ubiquitous, is far less common than the commanding 91.3% frequency it holds in the ED group, and it follows that ED heterozygosity is extremely low, pointing to SNP allele A being relatively rare in this population. 3651 and 4158 have, respectively, intermediate and low Gleason scores, although nothing conclusive can be gleaned from this information. Given the very limited sample set of this project, it is not possible to find a real correlation between Gleason score and SNP presence; of course, even given a larger sample set, the integrity of any conclusions made from such a correlation would be dependent upon other factors, such as speed of cancer progression, that would require the vendor for the DNA, OriGene in this case, to be in possession of such details. PredictSNP[2] estimates notwithstanding, these Sanger sequencing findings show that this SNP merits further investigation within the broader context of the interactions between components of the folate pathway.

SLC7A11 A224A manifests in three of eight total patients and one of three AA patients. Given the highly-common nature of reference allele G (reverse-strand in Sequencher: C) in the wider AD population, it comes as no surprise that all AA patients are either homozygous for it or heterozygous. All three patients, AA 4158, EA 3601, and EA 3387, are within 5 years of one another in age, but the former two have low-grade Gleason scores and the latter has a high-grade score. Based on this information alone, there does not

[9] The SNP was searched for on Google Chrome using both the amino acid change, isoleucine to valine, and the nucleotide change, adenine to guanine. No pertinent results were found. This does not, however, mean it is not recognized, only that it was not found.

appear to be a correlation between cancer grade and genotype, as in that case it would be expected that EA 3387, the patient with the highest grade, would carry the homozygous C (reverse-strand in Sequencher: G) genotype. PredictSNP[2] gives A224A an overall prediction of harmlessness, with the caveat that one tool gives a negative prediction and another gives none. Thus, A224A is differentiated from the previous synonymous substitutions in that there is disharmony in the series of projections, evincing a crack in the assumption that synonymous substitutions are harmless even before the interconnectedness of this protein with others has been fully explored.

SLC19A1 H27R was found in all patients but AA 4113. The greater occurrence of SNP allele C (reverse-strand in Sequencher: G) in the EA group than in the AA group was expected due to the higher frequency in the wider population; the only homozygotes for C are found in EA patients. Given the prevalence of H27R in these patients regardless of the fact that homozygosity for the reference allele is found in nearly half of the AD population, it would seem on the surface that this SNP, while a potential contributor to prostate cancer, is not an immediate candidate for an SNP that specifically subjects men of African descent to greater risk and mortality than it does to men of European descent. H27R is another SNP for which only one PredictSNP tool issues a ruling of deleteriousness, but any such prediction should not to be ignored, with the reminder that, once more pieces of the puzzle have been put in place, the consensus could very well change.

MTHFD1 R653Q was found exclusively as a heterozygote, in one AA patient and three EA patients. The SNP has a greater presence in the EA group, which makes sense given that nearly 70% of the AD population carries the homozygous reference genotype GG. These data together suggest that R653Q would affect more men of European descent than men of African descent. The EA patients range from 6 to 8 in Gleason score, and the AA patient only had a 6, so there does not appear to be any correlation between disease severity and R653Q using the data available for this admittedly-small study and without further information on such factors as the rate of each patient's disease progression. The unanimous prediction of neutrality by the PredictSNP tools does not strengthen the case for R653Q as an SNP of interest. However, a paper on the possible relationship between a set of SNPs including rs2236225 and congenital heart defects asserted that genotypes including SNP allele A were "strongly associated" with ventricular septal defect[23], which would, on condition that a causal relationship does exist, contradict the neutral estimate by PredictSNP.

MTHFR A222V only presents in a single patient, EA 3728, with the SNP allele A (reverse-strand T in Sequencher) as the primary peak and reference allele G (reverse-strand C in Sequencher) at half the height the secondary peak. The overwhelming majority of AD individuals carrying GG fits with the lack of any AA patients carrying the SNP allele, and given the significantly-higher frequency of the latter in the ED population, it makes sense that the only case is represented by an EA patient. Given the lack of prevalence, A222V can be dismissed as a factor in the disparity between AA and EA within the confines of this study. This is the first SNP judged by PredictSNP to be deleterious on its own. While the patient's Gleason score is low, the rate of cancer progression is unknown, so the possibility exists that the prostate tissue was simply excised early-on, and the score as a snapshot in time cannot inform of the true deleteriousness of the substitution; or it could be that the substitution may have contributed to carcinogenesis in the first place. As arriving at any conclusions even remotely workable on the possible association between Gleason score, which itself is subjective, and SNP presence is prevented by the limitations of this study, it must be communicated that more work is required for a clearer picture of what kind of threat A222V poses to the prostate.

MTR D919G is present in heterozygotes for AA 3651 and EA 3601 and 4253. Although four other patients had genotypes with secondary peaks, these peaks are below 35% and are not considered true heterozygotes. Only for 3601 is SNP allele G the primary peak, with reference allele A at roughly half its height. The population genotype frequency data are basically in agreement with this outcome, as the AA genotype comprises the majority in both racial groups. While D919 was unanimously predicted to be neutral by PredictSNP, this marks another instance in which the scientific community has raised concerns about an SNP's potentially

[10] The population genotype frequency tables are in forward-strand orientation, whereas the orientation of the Sequencher data is specific to the gene and found in Table 1.

adverse impact on human health that seem to contradict the program's prediction, this time in regards to prostate cancer specifically. Zhang et al. have declared that rs1805087 "increases the risk of prostate cancer."[24] Thus, the usual caveats apply here.

GRM1 S993P is present in all patients, with sequences either heterozygotic or homozygotic for SNP allele C. The population genotype frequency data show that AD men are significantly-more likely to carry the allele than ED men (92.5% to 77.1%). The frequency of S993P homozygosity in the EA patient group (40.0%) is higher than that of the ED population (32.1%), suggesting that prostate cancer patients of European descent are more likely to carry the GRM1 genotype carried at a notably-higher frequency by the AD population (55.2%). This may hint at S993P playing a role in the risk and mortality disparity between the racial groups, despite PredictSNP giving a verdict of neutral.

RESULTS: Bacterial Abundance Project

Samples underwent qPCR amplification to measure bacterial abundance. Raw data were made available through a .csv file and a CFX Maestro .pcrd file. Although eight samples were sent, the results clearly show that the two FFPE samples, S041244A22 and S064220C17, contained virtually no target nucleic acid (i.e. the 16S rRNA gene); therefore they will be ignored. Patient information, starting quantity data, and Cq (threshold cycle) data for the OriGene samples are found in Table 16. After computing the sum of the averages of all starting quantities (SQs) per sample for AA and EA patients,

Patient	AA/EUR	Age	Gleason score	Starting Quantity (1)	Starting Quantity (2)	Starting Quantity (3)	SQ Avg	SQ St Dev	Ct Avg	Ct St Dev
4113	AA	56	3+4	1077.843	516.775	314.306	636.308	395.5544099	22.99	0.00
4158	AA	54	3+3	1333.130	602.492	447.139	794.2536667	473.1008514	22.63	0.00
3651	AA	55	3+4	1081.374	1626.380	586.524	1098.092667	520.1295613	22.10	0.00
3601	EUR	59	3+3	1733.699	887.380	495.354	1038.811	632.9084417	22.26	0.00
3514	EUR	63	3+3	749.296	924.190	444.160	705.882	242.9419309	22.71	0.00
3728	EUR	58	3+3	433.816	545.821	186.323	388.6533333	183.9550294	23.68	0.00
S041244A22	EUR	61	3+4	n/a	n/a	n/a	#DIV/0!	#DIV/0!	37.04	0.00
S064220C17	AA	54	3+4	n/a	n/a	n/a	#DIV/0!	#DIV/0!	35.53	0.00

Table 16. Patient information combined with starting quantity and Cq data. Green rows are AA and turquoise rows are EUR. The three starting quantity columns each represent a replicate.

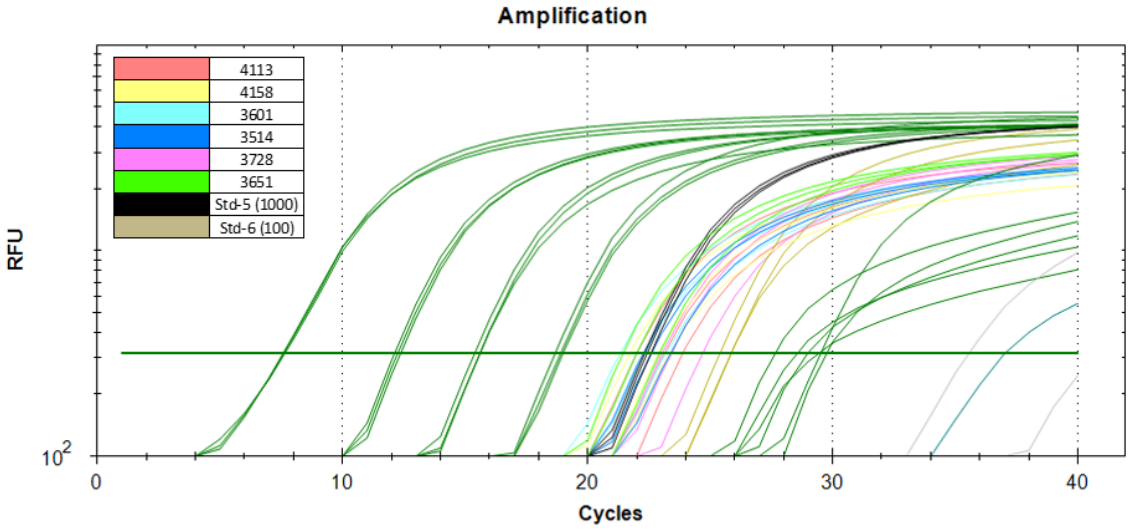

Figure 2. Amplification curves, with only OriGene samples and two standards with comparable Cq values in the legend.

it is evident that AA patients carry a higher starting quantity of microbial DNA (2,528.7) than EA patients (2,133.4). AA patient SQs also have a higher average standard deviation than EA patients, at 462.9 to 353.3. To calculate significance, an independent sample t-test (Table 17) with an Alpha level of 0.05 was done in Microsoft Excel. The p-value is above 0.05, indicating that the null hypothesis cannot be discarded. The Cq values occupy the range of 22.00 to 24.64. Standard deviation values between the Cq and Cq mean for

each replicate of each sample are zero. The OriGene DNA melt datapoints (Figure 3) each possess one clear peak, implying single products. However, two standards, Std-6 and Std-7, have two peaks.

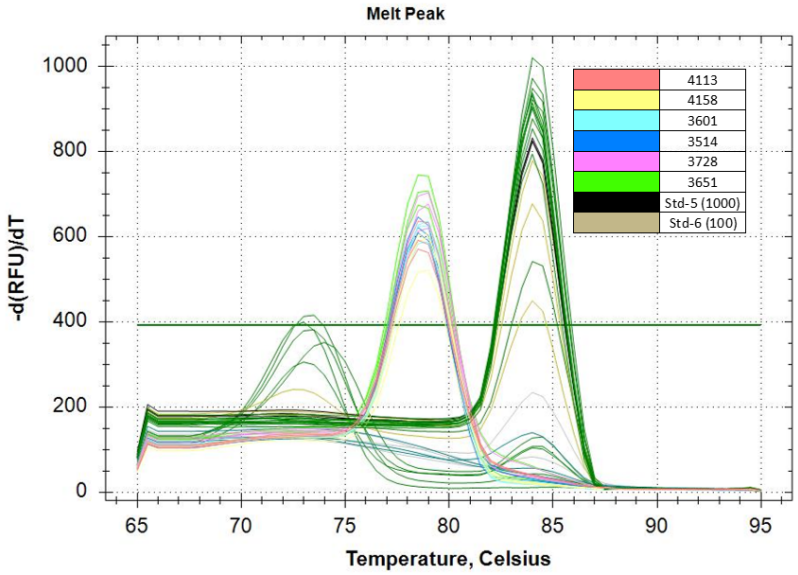

Figure 3. Melt peaks of samples. Left peaks are negative controls and Std-6 and Std-7, middle peaks are OriGene samples, and right peaks are a combination of standards (tall and medium) and FFPE samples (short).

t-Test: Two-Sample Assuming Unequal Variances

	AA	*EUR*
Mean	946.1731667	547.2676667
Variance	46159.06896	50317.01348
Observations	2	2
Hypothesized Mean Difference	0	
df	2	
t Stat	1.81624818	
P(T<=t) one-tail	0.105489855	
t Critical one-tail	2.91998558	
P(T<=t) two-tail	0.210979709	
t Critical two-tail	4.30265273	

Table 17. An independent sample t-test done on the two groups of samples.

DISCUSSION: Bacterial Abundance Project

These results translate to a quality qPCR assay. While there are two melt peaks for Std-6 and Std-7, which could indicate the presence of contaminants like primer-dimers, these are only two instances, and neither concern the OriGene samples. The lack of bacteria detected in the FFPE samples can serve here as a negative control for the OriGene samples, as well as a sign that sample purity was not compromised by exogenous DNA. While healthy prostate DNA would have been nice to include as a control, which would make possible a comparison between it and cancerous prostate DNA, procurement would not have been feasible. Threshold cycle values of all OriGene samples fall well-below 29, indicating abundant target nucleic acid. Standard deviations for Cq, the cycle during which fluorescence from the reaction between DNA and SYBR Green surpasses background fluorescence, all fall below 0.2 units, evincing the reliability of the replicates.

As mentioned above, the AA group collectively has a higher 16S rRNA gene load than the EA group. It must also be acknowledged that two of the three AA patients have intermediate-grade prostate cancer, whereas all EA patients have a score of 6. However, 4113, with a score of 7, has an average starting quantity lower than two EA patients. While the hypothesis that the AA group would have a higher bacterial load than the EA group does not hold water as far as the p-value is concerned, it must be stressed that only three samples from each group could be tested due to various constraints, and the inclusion of many more samples may have yielded different results. Even then, if the null hypothesis once again could not be rejected, it would not mean that bacteria do not bear responsibility in the disparity between the races. One disadvantage of the qPCR assay is that it cannot detect operational taxonomic units (OTUs), so that even if one of these patients were carrying less total bacterial load than others, a higher proportion of cancer-enabling bacteria would be more detrimental than a larger general load of bacteria not implicated in the disease.

CONCLUSIONS

Before settling on which SNPs still appear suspect, it must be stressed that, given an appreciably-larger sample set, outcomes could have been vastly different. In the worst-case scenario, results from this study could be misleading because many or all samples may simply represent outliers, with the absence or presence of an SNP actually having nothing to do with carcinogenicity. The multifactorial nature of cancer etiology unfortunately lends further credence to this possibility. Nevertheless, within the confines of this study, four of the SNPs remain suspect. The SNP alleles of FOLH1 A111A and D224D are much-more common in men of African descent, but a large percentage of the European-American patients possess them, so it would be a meaningful endeavor to continue studying them. The SNP allele of FOLR3 R28R was carried by two African-American patients and no one else; validation of this exclusivity by a larger study would justify further examination of the SNP. Finally, GRM1 S993P results present what may be the most-compelling case, with genotype frequency data showing that African men possess the allele at a much-higher frequency than their European counterparts, and every patient in this study carrying the allele. Additionally, this is the only nonsynonymous SNP of the four, a fact which makes it all the more deserving of further scrutiny.

The bacterial qPCR results demonstrate the existence of microbes in each sample known to contain workable DNA. The hypothesis of the African-American patients containing a higher bacterial abundance than the European-American patients could not be statistically verified, although the average starting quantity of the group was indeed larger. A recent study by Nejman et al. states that tumor microbes have not yet been fully-profiled and goes on to conclude that tumors of the breast, lung, ovary, pancreas, skin, bone, and brain each have a distinct microbial community[25]. These facts, combined with the extraordinarily-common nature of prostate cancer, support the notion that expanding scientific understanding of the prostate tumor microbiota falls deeply within the interests of humanity. More specifically, the prospect of a racial component to the composition of prostatic tumor microbiotas merits further investigation, with the goal of identifying what is causing the prostate cancer health disparity between African-Americans and European-Americans. Possible next steps include running qPCR on these samples again for taxa suspected of advancing, or even giving rise to, prostate cancer, such as *Mycoplasma genitalium*, and running next-generation sequencing on the samples to identify the prevalent OTUs of each microbiota.

METHODS

For Sanger sequencing, the BigDye® Direct Cycle Sequencing Kit was employed to read DNA samples of African-American and European-American prostate cancer patients, with forward and reverse M13 primers targeting ~250-500bp regions of the genes containing the desired SNPs. DNA was procured through OriGene Technologies of Rockville, Maryland. Sequencher software by Gene Codes Corporation was used to analyze the data. Default trim criteria were used to remove bases of low quality. A protein-coding transcript for each gene was selected based on canonicity on the Ensembl website in order to pinpoint the location of SNPs in the sample sequences, as well as run an accurate protein sequence through PredictSNP to investigate whether they were deleterious in nature (the specific identity of each transcript can be found in the “References” section). The reference sequence of each gene for

Sequencher analysis is equivalent to the nucleotide sequence of the gene available in FASTA format on its respective National Center for Biotechnology Information webpage on the National Institutes of Health government website. Genotype frequencies for the SNPs in world populations of Africans (African Caribbean in Barbados, African Ancestry in Southwestern US, Esan in Nigeria, Gambian in Western Division, The Gambia, Luhya in Webuye, Kenya, Mende in Sierra Leone, and Yoruba in Ibadan, Nigeria) and Europeans (Utah residents with Northern and Western European ancestry, Finnish in Finland, British in England and Scotland, Iberian populations in Spain, and Toscani in Italy) were determined after the data were downloaded from Ensembl, females were filtered out, and the statistics were found using Microsoft Excel tools.

For the bacterial abundance project, DNA from prostate cancer patients was obtained in two ways: through purchasing from OriGene Technologies and through extracting it in the lab from formalin-fixed, paraffin-embedded tissue samples available on-hand. Quantity and identity of samples were chosen based on what was on-hand and not required for the SNP project, as that is the main project. At least 20µL of sample with a DNA concentration of 50ng/µL was added to a 96-well plate for each sample. Most of the samples were from OriGene since the extracts from the two FFPE samples, after being run on a gel, did not yield detectable bands during the visualization step despite the NanoDrop absorbance ratios being considered passable, sparking the concern that the formalin cross-linking had degraded the DNA into pieces of unworkable size. The plate was put on ice and brought to the Engineering and Science Building on the UConn Storrs campus, where it was given to Dr. Kendra Maas of MARS for qPCR of the 16S rRNA gene. Raw data were received as a .csv file and a .pcrd file compatible with CFX Maestro, which was used to generate the figures. The Analysis ToolPak add-in in Microsoft Excel was used for the independent sample t-test.

REFERENCES: Literary sources

1. Siegel, R., DeSantis, K., et al. “Cancer treatment and survivorship statistics.” *CA Cancer J. Clin.* 62, 220-241 (2012).
2. Shenoy, D., Packianathan, S., et al. “Do African-American men need separate prostate cancer screening guidelines?” *BMC Urol.* 16:19 (2016).
3. Hellawell, G., Turner, G., et al. “Expression of the type 1 insulin-like growth factor receptor is up-regulated in primary prostate cancer and commonly persists in metastatic disease.” *Cancer Res.* 62, 2942-2950 (2002).
4. Pollak, M. “Insulin and insulin-like growth factor signalling in neoplasia.” *Nat. Rev. Cancer.* 8, 915-928 (2008).
5. Hoxhaj, G., Manning, B. “The PI3K-AKT network at the interface of oncogenic signalling and cancer metabolism.” *Nat Rev Cancer.* 20(2): 74-88 (2020).
6. Caromile, L., Dortche, K., et al. “PSMA redirects cell survival signaling from the MAPK to the PI3K-AKT pathways to promote the progression of prostate cancer.” *Sci Signal.* 10 (470) (2017).
7. Rebersek, M. “Gut microbiome and its role in colorectal cancer.” *BMC Cancer.* 21, 1325 (2021).
8. Farhana, L., Antaki, F., et al. “Gut microbiome profiling and colorectal cancer in African Americans and Caucasian Americans.” *World J Gastrointest Pathophysiol*. 9(2): 47-58 (2018).
9. Feng, Y., Jaratlerdsiri, W., et al. “Metagenomic analysis reveals a rich bacterial content in high-risk prostate tumors from African men.” *The Prostate.* 79:15 1731-1738 (2019).
10. Miyake, M., Ohnishi, K., et al. “*Mycoplasma genitalium* Infection and Chronic Inflammation in Human Prostate Cancer: Detection Using Prostatectomy and Needle Biopsy Specimens.” *Cells.* 8(3): 212 (2019).
11. Namiki, K., Goodison, S., et al. “Persistent Exposure to Mycoplasma Induces Malignant

Transformation of Human Prostate Cells." *PLoS One.* 4(9): e6872 (2009).

12. Kaittanis, C., Andreou, C., et al. "Prostate-specific membrane antigen cleavage of vitamin B9 stimulates oncogenic signaling through metabotropic glutamate receptors." *J Exp Med.* 215(1) 159-175 (2018).
13. Wibowo, A., Singh, M., et al. "Structures of human folate receptors reveal biological trafficking states and diversity in folate and antifolate recognition." *Proc Natl Acad Sci.* 110(38) 15180-15188 (2013).
14. Jyotsana, N., Ta, K., et al. "The Role of Cystine/Glutamate Antiporter SLC7A11/xCT in the Pathophysiology of Cancer." *Front. Oncol.* (2022).
15. Yee, S., Gong, L., et al. "SLC19A1 Pharmacogenomics Summary." *Pharmacogenet Genomics.* 20(11): 708-715.
16. Krajinovic, M. "*MTHFD1* gene: role in disease susceptibility and pharmacogenetics." *Pharmacogenomics*. 9(7) (2008).
17. MedlinePlus (Internet). Bethesda (MD): National Library of Medicine (US). MTHFR gene (updated October 1, 2019).
18. Datta, S., Koutmos, M., et al. "A disulfide-stabilized conformer of methionine synthase reveals an unexpected role for the histidine ligand of the cobalamin cofactor." *Proc Natl Acad of Sci.* 105(11) 4115-4120 (2008).
19. Shen, X., Song, S., et al. "Synonymous mutations in representative yeast genes are mostly strongly non-neutral." *Nature.* 606, 725-731 (2022).
20. Tsai, C., Sauna, Z., et al. "Synonymous Mutations and Ribosome Stalling Can Lead to Altered Folding Pathways and Distinct Minima." *J Mol Bio.* 383(2): 281-291 (2008).
21. Walsh, I., Bowman, M., et al. "Synonymous codon substitutions perturb cotranslational protein folding in vivo and impair cell fitness." *Proc Natl Acad Sci*. 117(7): 3528-3534 (2020).
22. Ahlborn, L., Steffensen, A., et al. "Identification of a breast cancer family double heterozygote for RAD51C and BRCA2 gene mutations." *Fam Cancer.* 14(1): 129-133 (2015).
23. Khatami, M., Ratki, F.M., et al. "Relationship of the MTHFD1 (rs2236225), eNOS (rs1799983), CBS (rs2850144) and ACE (rs4343) gene polymorphisms in a population of Iranian pediatric patients with congenital heart defects." *Kaohsiung Journal of Medical Sciences*. 33, 442-448 (2017).
24. Zhang, X., Tang, J., et al. "A single-nucleotide polymorphism (rs1805087) in the methionine synthase (METH) gene increases the risk of prostate cancer." *Aging*. 10(10): 2741-2754 (2018).
25. Nejman, D., Livyatan, I., et al. "The human tumor microbiome is composed of tumor type-specific intracellular bacteria." *Science.* 368(973-980) (2020).
26. Vidmar, M., Grželj, J., et al. "Medicines associated with folate-homocysteine-methionine pathway disruption." *Archives of Toxicology.* 93, 227-251 (2019).

REFERENCES: Transcripts used for SNP discovery and PredictSNP input (from Ensembl.org)

FOLH1: ENST00000256999.7 (FOLH-201)

FOLR3: ENST00000611028.3 (FOLR3-203)

SLC7A11: ENST00000280612.9 (SLC7A11-201)

SLC19A1: ENST00000311124.9 (SLC19A1-201)

MTHFD1: ENST00000652337.1 (MTHFD1-220)

MTHFR: ENST00000376590.9 (MTHFR-204)

MTR: ENST00000366577.10 (MTR-202)

GRM1: ENST00000282753.6 (GRM1-201)

GRM5: ENST00000305447.5 (GRM5-202)

ACKNOWLEDGEMENTS

I thank Dr. Leslie Caromile for providing a wealth of instruction in many areas, from bioinformatics with R to lab techniques to online genomics resources, as well as funding my bacterial abundance project and my attendance at a MARS workshop. I also thank Dr. Kendra Maas of MARS at UConn Storrs for her consultation regarding qPCR. Finally, I thank the members of my committee, Dr. Joerg Graf, Dr. Charles Giardina, and Dr. Victoria Robinson, for the time and effort they have spent helping me succeed, and the Department of Molecular and Cell Biology in general for accepting me into the Professional Science Master's program in Microbial Systems Analysis.

FURTHER PRIMARY AND SUPPLEMENTARY DATA

The variance report tables directly from Sequencher and their respective adapted tables are below. The adapted tables include only sequences either homozygous for the SNP allele without a registered secondary peak, or heterozygotes with secondary peaks of at least 5%. The tables directly from Sequencher were not included in the body of the paper due to the unclear nature of the sequence labels.

FOLH1 I70V:

Contig[0001]
Variant 15 of 62 • Position 2,520 A → R

Sequence	Orientation	Confidence	Base Call	Primary Peak	Secondary Peak	Secondary as % of Primary
A1_FOLH1 Y75H_F_20190425_144500	Reverse	22	A	A	G	22%
C1_FOLH1 Y75H_F_20190425_144502	Reverse	Edited	R	A	G	48%
G1_FOLH1 Y75H_F_20190425_153410	Reverse	22	A	A	G	28%
C1_FOLH1 Y75H_F_20190426_114141	Reverse	1	R	A	G	82%
B1_FOLH1 Y75H_R_20190426_114140	Forward	53	A	A	n/a	< 5%
H1_FOLH1 Y75H_R_20190425_153411	Forward	58	A	A	n/a	< 5%
B1_FOLH1 Y75H_R_20190425_144501	Forward	55	A	A	n/a	< 5%
A1_FOLH1 Y75H_F_20190426_114139	Reverse	38	A	A	G	7%
D1_FOLH1 Y75H_R_20190425_144503	Forward	58	A	A	n/a	< 5%
H1_FOLH1 Y75H_R_20190426_122144	Forward	47	A	A	n/a	< 5%
F1_FOLH1 Y75H_R_20190425_153409	Forward	58	A	A	n/a	< 5%
F1_FOLH1 Y75H_R_20190426_122142	Forward	35	A	A	C	11%

FOLH1 I70V (primers targeting Y75H region)						
Sample	AA/EA	Called (Automatic)	Primary	Secondary	Secondary as %	F/R (by ID)
4113: 144500	AA	A	A	G	22	F
4113	AA					R
3651: 144502	AA	R	A	G	48	F
3651	AA					R
4158	AA					F
4158	AA					R
3601: 153410	EA	A	A	G	28	F
3601	EA					R
3387: 114139	EA	A	A	G	7	F
3387	EA					R
3728: 114141	EA	R	A	G	82	F

3728	EA					R
4253	EA					F
4253: 122142	EA	A	A	C	11	R
4254	EA					F
4254	EA					R

FOLH1 A111A:

Contig[0001]
Variant 37 of 62 • Position 8,270 A → T

Sequence	Orientation	Confidence	Base Call	Primary Peak	Secondary Peak	Secondary as % of Primary
G2_FOLH1 A11A_F_20190426_134150	Reverse	4	W	T	A	61%
C2_FOLH1 A11A_F_20190426_130148	Reverse	44	A	A	G	7%
G2_FOLH1 A11A_F_20190425_165420	Reverse	43	A	A	n/a	< 5%
A2_FOLH1 A11A_F_20190425_161412	Reverse	54	A	A	n/a	< 5%
E2_FOLH1 A11A_F_20190425_165418	Reverse	54	A	A	n/a	< 5%
A2_FOLH1 A11A_F_20190426_130146	Reverse	14	W	T	A	71%
H2_FOLH1 A11A_R_20190425_165421	Forward	53	A	A	n/a	< 5%
B2_FOLH1 A11A_R_20190425_161413	Forward	43	A	A	n/a	< 5%
F2_FOLH1 A11A_R_20190425_165419	Forward	38	A	A	n/a	< 5%
D2_FOLH1 A11A_R_20190425_161415	Forward	54	T	T	n/a	< 5%
D2_FOLH1 A11A_R_20190426_130149	Forward	28	A	A	T	5%
H2_FOLH1 A11A_R_20190426_134151	Forward	4	W	T	A	85%
B2_FOLH1 A11A_R_20190426_130147	Forward	1	W	T	A	65%
F2_FOLH1 A11A_R_20190426_134149	Forward	6	W	A	T	97%
C2_FOLH1 A11A_F_20190425_161414	Reverse	58	T	T	n/a	< 5%

FOLH1 A111A						
Sample	AA/EA	Called (Automatic)	Primary	Secondary	Secondary as %	F/R (by ID)
4113	AA					F
4113	AA					R
3651	AA					F
3651	AA					R
4158	AA					F
4158	AA					R
3601	EA					F
3601	EA					R
3387: 130146	EA	W	T	A	71	F
3387: 130147	EA	W	T	A	65	R
3728: 130148	EA	A	A	G	7	F
3728: 130149	EA	A	A	T	5	R
4253	EA					F
4253: 134149	EA	W	A	T	97	R
4254: 134150	EA	W	T	A	61	F
4254: 134151	EA	W	T	A	85	R

FOLH1 D244D:

Contig[0001]
Variant 57 of 62 • Position 22,840 T → H

Sequence	Orientation	Confidence	Base Call	Primary Peak	Secondary Peak	Secondary as % of Primary
F3_FOLH1 D244E_R_4158	Forward	54	T	T	n/a	< 5%
D3_FOLH1 D244E_R_3651	Forward	55	C	C	n/a	< 5%
B3_FOLH1 D244E_R_4113	Forward	54	T	T	n/a	< 5%
A3_FOLH1 D244E_F_4113	Reverse	54	T	T	n/a	< 5%
H3_FOLH1 D244E_R_3601	Forward	46	T	T	n/a	< 5%
H3_FOLH1 D244E_R_20190426_150154	Forward	5	Y	C	T	63%
C3_FOLH1 D244E_F_3651	Reverse	54	C	C	n/a	< 5%
B3_FOLH1 D244E_R_20190426_142152	Forward	10	Y	C	T	51%
A3_FOLH1 D244E_F_20190426_142151	Reverse	4	Y	C	T	90%
E3_FOLH1 D244E_F_4158	Reverse	54	T	T	n/a	< 5%
E3_FOLH1 D244E_F_20190426_150151	Reverse	9	Y	C	T	55%
C3_FOLH1 D244E_F_20190426_142153	Reverse	33	T	T	n/a	< 5%
G3_FOLH1 D244E_F_20190426_150153	Reverse	Edited	H	C	T	86%
D3_FOLH1 D244E_R_20190426_142154	Forward	36	T	T	G	6%
F3_FOLH1 D244E_R_20190426_150152	Forward	1	Y	T	C	43%
G3_FOLH1 D244E_F_3601	Reverse	54	T	T	n/a	< 5%

FOLH1 D244D						
Sample	AA/EA	Called (Automatic)	Primary	Secondary	Secondary as %	F/R (by ID)
4113	AA					F
4113	AA					R
3651	AA	C	C	n/a	<5%	F
3651	AA	C	C	n/a	<5%	R
4158	AA					F
4158	AA					R
3601	EA					F
3601	EA					R
3387: 142151	EA	Y	C	T	90	F
3387: 142152	EA	Y	C	T	51	R
3728	EA					F
3728: 142154	EA	T	T	G	6	R
4253: 150151	EA	Y	C	T	55	F
4253: 150152	EA	Y	T	C	43	R
4254: 150153	EA	H	C	T	86	F
4254: 150154	EA	Y	C	T	63	R

FOLR3 R28R:

Contig[0001]
Variant 36 of 40 • Position 310 C → M

Sequence	Orientation	Confidence	Base Call	Primary Peak	Secondary Peak	Secondary as % of Primary
G4_FOLH3 R26W_F_20190425_193505	Forward	Edited	M	C	n/a	< 5%
A4_FOLH3 R26W_F_20190426_154152	Forward	Edited	M	C	n/a	< 5%
A4_FOLH3 R26W_F_20190425_185455	Forward	Edited	M	C	n/a	< 5%
E4_FOLH3 R26W_F_20190425_193503	Forward	3	M	A	C	67%
C4_FOLH3 R26W_F_20190425_185457	Forward	3	M	A	C	85%
B4_FOLH3 R26W_R_20190425_185456	Reverse	Edited	M	C	G	6%
H4_FOLH3 R26W_R_20190425_193506	Reverse	Edited	M	C	G	6%
D4_FOLH3 R26W_R_20190425_185458	Reverse	1	M	A	C	96%
B4_FOLH3 R26W_R_20190426_154153	Reverse	Edited	M	C	G	12%
F4_FOLH3 R26W_R_20190425_193504	Reverse	5	M	A	C	75%

FOLR3 R28R						
Sample	AA/CA	Called (Manual)	Primary	Secondary	Secondary as %	F/R (by ID)
4113	AA					F
4113: 185456	AA	M	C	G	6	R
3651: 185457	AA	M	A	C	85	F
3651: 185458	AA	M	A	C	96	R

4158: 193503	AA	M	A	C	67	F
4158: 193504	AA	M	A	C	75	R
3601	CA					F
3601: 193506	CA	M	C	G	6	R
3387	CA					F
3387: 154153	CA	M	C	G	12	R
3728	CA					F
3728	CA					R
4253	CA					F
4253	CA					R
4254	CA					F
4254	CA					R

SLC7A11 A224A:

Contig[0001]
Variant 1 of 1 • Position 93,332 C → S

Sequence	Orientation	Confidence	Base Call	Primary Peak	Secondary Peak	Secondary as % of Primary
D5_SLC7A11 A224A_R_20190425_201536 (1)	Forward	Edited	S	C	n/a	< 5%
B5_SLC7A11 A224A_R_20190426_170150	Forward	8	S	C	G	75%
F5_SLC7A11 A224A_R_20190425_205557 (1)	Forward	13	S	C	G	67%
B5_SLC7A11 A224A_R_20190425_201534 (1)	Forward	Edited	S	C	n/a	< 5%
H5_SLC7A11 A224A_R_20190425_205559 (1)	Forward	Edited	S	G	n/a	< 5%
F5_SLC7A11 A224A_R_20190426_174152	Forward	Edited	S	C	n/a	< 5%
D5_SLC7A11 A224A_R_20190426_170152	Forward	Edited	S	C	G	5%
H5_SLC7A11 A224A_R_20190426_174154	Forward	Edited	S	C	n/a	< 5%
C5_SLC7A11 A224A_F_20190425_201535 (1)	Reverse	Edited	S	C	n/a	< 5%
E5_SLC7A11 A224A_F_20190425_205556 (1)	Reverse	17	S	C	G	54%
C5_SLC7A11 A224A_F_20190426_170151 (1)	Reverse	Edited	S	C	n/a	< 5%
A5_SLC7A11 A22_K14_E_E14_J21_20190426_170149	Reverse	17	S	C	G	50%
G5_SLC7A11 A224A_F_20190425_205558 (1)	Reverse	Edited	S	G	n/a	< 5%
A5_SLC7A11 A22_K14_E_E14_J21_20190425_201533	Reverse	Edited	S	C	n/a	< 5%
G5_SLC7A11 A224A_F_20190426_174153	Reverse	Edited	S	C	A	5%

SLC7A11 A224A						
Sample	AA/CA	Called (Manual)	Primary	Secondary	Secondary as %	F/R (by ID)
4113	AA					F
4113	AA					R
3651	AA					F
3651	AA					R
4158: 205556	AA	S	C	G	54	F
4158: 205557	AA	S	C	G	67	R
3601: 205558	CA	S	G	n/a	<5	F
3601: 205559	CA	S	G	n/a	<5	R
3387: 170149	CA	S	C	G	50	F
3387: 170150	CA	S	C	G	75	R
3728	CA					F
3728: 170152	CA	S	C	G	5	R
4253	CA					F
4253	CA					R
4254: 174153	CA	S	C	A	5	F
4254	CA					R

SLC19A1 H27R:

Contig[0001]
Variant 11 of 51 • Position 25,146 A → R

Sequence	Orientation	Confidence	Base Call	Primary Peak	Secondary Peak	Secondary as % of Primary
D6_SLC19A1 R27C_R_20190426_182150	Forward	5	R	G	A	36%
H6_SLC19A1 R27C_R_20190425_221635	Forward	5	R	G	A	70%
B6_SLC19A1 R27C_R_20190425_213628	Forward	Edited	R	A	n/a	< 5%
D6_SLC19A1 R27C_R_20190425_213630	Forward	3	R	G	A	46%
F6_SLC19A1 R27C_R_20190425_221633	Forward	9	R	G	A	72%
B6_SLC19A1 R27C_R_20190426_182148	Forward	Edited	R	G	T	8%
F6_SLC19A1 R27C_R_20190426_190149	Forward	Edited	R	G	n/a	< 5%
H6_SLC19A1 R27C_R_20190426_190151	Forward	Edited	R	G	C	5%

SLC19A1 H27R/P						
Sample	AA/CA	Called (Manual)	Primary	Secondary	Secondary as %	F/R (by ID)
4113	AA					F
4113	AA					R
3651	AA					F
3651: 213630	AA	R	G	A	46	R
4158	AA					F
4158: 221633	AA	R	G	A	72	R
3601	CA					F
3601: 221635	CA	R	G	A	70	R
3387	CA					F
3387: 182148	CA	R	G	T	8	R
3728	CA					F
3728: 182150	CA	R	G	A	36	R
4253	CA					F
4253: 190149	CA	R	G	n/a	<5	R
4254	CA					F
4254: 190151	CA	R	G	C	5	R

MTHFD1 R653Q:

Contig[0001]
Variant 2 of 7 • Position 53,775 G → R

Sequence	Orientation	Confidence	Base Call	Primary Peak	Secondary Peak	Secondary as % of Primary
G7_MTHFD1 G1958A_F_20190425_233704	Forward	14	R	G	A	42%
E7_MTHFD1 G1958A_F_20190425_233702	Forward	17	R	G	A	89%
A7_MTHFD1 G1958A_F_20190425_225652	Forward	58	G	G	n/a	< 5%
F7_MTHFD1 G1958A_R_20190425_233703	Reverse	13	R	A	G	86%
F7_MTHFD1 G1958A_R_20190426_202149	Reverse	56	G	G	n/a	< 5%
B7_MTHFD1 G1958A_R_20190425_225653	Reverse	52	G	G	n/a	< 5%
B7_MTHFD1 G1958A_R_20190426_194151	Reverse	11	R	A	G	79%
D7_MTHFD1 G1958A_R_20190425_225655	Reverse	53	G	G	n/a	< 5%
H7_MTHFD1 G1958A_R_20190425_233705	Reverse	15	R	A	G	87%
C7_MTHFD1 G1958A_F_20190426_194152	Forward	Edited	R	A	G	38%

MTHFD1 R653Q						
Sample	AA/CA	Called (Automatic)	Primary	Secondary	Secondary as %	F/R (by ID)
4113	AA					F
4113	AA					R
3651	AA					F
3651	AA					R
4158: 233702	AA	R	G	A	89	F
4158: 233703	AA	R	A	G	86	R
3601: 233704	CA	R	G	A	42	F
3601: 233705	CA	R	A	G	87	R
3387	CA					F

3387: 194151	CA	R	A	G	79	R
3728: 194152	CA	R	A	G	38	F
3728	CA					R
4253	CA					F
4253	CA					R
4254	CA					F
4254	CA					R

MTHFR A222V:

Contig[0001]
Variant 3 of 4 • Position 9,644 C → Y

Sequence	Orientation	Confidence	Base Call	Primary Peak	Secondary Peak	Secondary as % of Primary
H8_MTHFR C177T_R_20190426_005725	Forward	Edited	Y	C	n/a	< 5%
F8_MTHFR C177T_R_20190426_005723	Forward	Edited	Y	C	n/a	< 5%
B8_MTHFR C177T_R_20190426_001717	Forward	Edited	Y	C	n/a	< 5%
H8_MTHFR C177T_R_20190426_214150	Forward	Edited	Y	C	n/a	< 5%
G8_MTHFR C177T_F_20190426_005724	Reverse	Edited	Y	C	n/a	< 5%
E8_MTHFR C177T_F_20190426_214147	Reverse	Edited	Y	C	n/a	< 5%
C8_MTHFR C177T_F_20190426_210148	Reverse	9	Y	T	C	51%
G8_MTHFR C177T_F_20190426_214149	Reverse	Edited	Y	C	A	6%
E8_MTHFR C177T_F_20190426_005722	Reverse	Edited	Y	C	n/a	< 5%
C8_MTHFR C177T_F_20190426_001718	Reverse	Edited	Y	C	n/a	< 5%
A8_MTHFR C177T_F_20190426_001716	Reverse	Edited	Y	C	n/a	< 5%

MTHFR A222V						
Sample	AA/CA	Called (Manual)	Primary	Secondary	Secondary as %	F/R (by ID)
4113	AA					F
4113	AA					R
3651	AA					F
3651	AA					R
4158	AA					F
4158	AA					R
3601	CA					F
3601	CA					R
3387	CA					F
3387	CA					R
3728: 210148	CA	Y	T	C	51	F
3728	CA					R
4253	CA					F
4253	CA					R
4254: 214149	CA	Y	C	A	6	F
4254	CA					R

MTR D919G:

Contig[0001]
Variant 3 of 22 • Position 89,920 A → R

Sequence	Orientation	Confidence	Base Call	Primary Peak	Secondary Peak	Secondary as % of Primary
A9_MTR A798C_F_20190426_222145	Forward	52	A	A	n/a	< 5%
E9_MTR A798C_F_20190426_021747	Forward	35	A	A	T	11%
B9_MTR A798C_R_20190426_222146	Reverse	22	A	A	G	10%
C9_MTR A798C_F_20190426_222147	Forward	33	A	A	T	7%
G9_MTR A798C_F_20190426_230155	Forward	36	A	A	G	11%
F9_MTR A798C_R_20190426_021748	Reverse	21	A	A	G	10%
A9_MTR A798C_F_20190426_013742	Forward	44	A	A	n/a	< 5%
C9_MTR A798C_F_20190426_013744	Forward	52	A	A	n/a	< 5%
H9_MTR A798C_R_20190426_021750	Reverse	1	R	G	A	49%
D9_MTR A798C_R_20190426_013745	Reverse	Edited	R	A	G	37%
H9_MTR A798C_R_20190426_230156	Reverse	16	A	A	G	20%
F9_MTR A798C_R_20190426_230154	Reverse	1	R	A	G	55%

MTR D919G						
Sample	AA/CA	Called (Automatic)	Primary	Secondary	Secondary as %	F/R (by ID)
4113	AA					F
4113	AA					R
3651	AA					F
3651: 013745	AA	R	A	G	37	R
4158: 021747	AA	A	A	T	11	F
4158: 021748	AA	A	A	G	10	R
3601	CA					F
3601: 021750	CA	R	G	A	49	R
3387	CA					F
3387: 222146	CA	A	A	G	10	R
3728: 222147	CA	A	A	T	7	F
3728	CA					R
4253	CA					F
4253: 230154	CA	R	A	G	55	R
4254: 230155	CA	A	A	G	11	F
4254: 230156	CA	A	A	G	20	R

GRM1 S993P:

Contig[0001]
Variant 3 of 5 • Position 406,482 T → C

Sequence	Orientation	Confidence	Base Call	Primary Peak	Secondary Peak	Secondary as % of Primary
E10_GRM1 S933P_F_20190426_033803	Forward	1	Y	C	T	43%
A10_GRM1 S933P_F_20190426_025755	Forward	1	Y	C	T	79%
G10_GRM1 S933P_F_20190426_033805	Forward	1	Y	C	T	70%
G10_GRM1 S933P_F_20190427_002200	Forward	22	C	C	T	27%
C10_GRM1 S933P_F_20190426_234204	Forward	28	C	C	n/a	< 5%
C10_GRM1 S933P_F_20190426_025757	Forward	19	C	C	n/a	< 5%
B10_GRM1 S933P_R_20190426_234203	Reverse	32	C	C	n/a	< 5%
B10_GRM1 S933P_R_20190426_025756	Reverse	2	Y	T	C	73%
F10_GRM1 S933P_R_20190426_033804	Reverse	2	Y	T	C	90%
H10_GRM1 S933P_R_20190426_033806	Reverse	2	Y	T	C	74%
D10_GRM1 S933P_R_20190426_025758	Reverse	52	C	C	n/a	< 5%
F10_GRM1 S933P_R_20190427_002159	Reverse	3	Y	C	T	81%

GRM1 S993P						
Sample	AA/CA	Called (Automatic)	Primary	Secondary	Secondary as %	F/R (by ID)
4113: 025755	AA	Y	C	T	79	F
4113: 025756	AA	Y	T	C	73	R
3651: 025757	AA	C	C	n/a	<5	F
3651	AA					R
4158: 033803	AA	Y	C	T	43	F
4158: 033804	AA	Y	T	C	90	R
3601: 033805	CA	Y	C	T	70	F
3601: 033806	CA	Y	T	C	74	R
3387	CA					F
3387: 234203	CA	C	C	n/a	<5	R
3728: 234204	CA	C	C	n/a	<5	F
3728	CA					R
4253	CA					F
4253: 002159	CA	Y	C	T	81	R
4254: 002200	CA	C	C	T	27	F
4254	CA					R

Screenshots of aligned sequences in Sequencher are below.

FOLH1 Y75H:

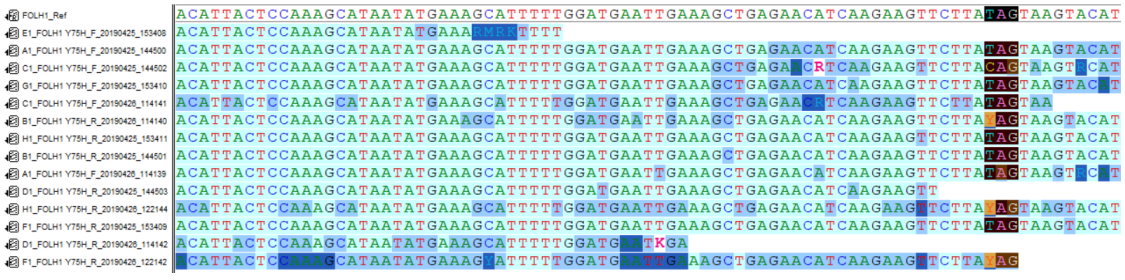

GRM5 T453R/M:

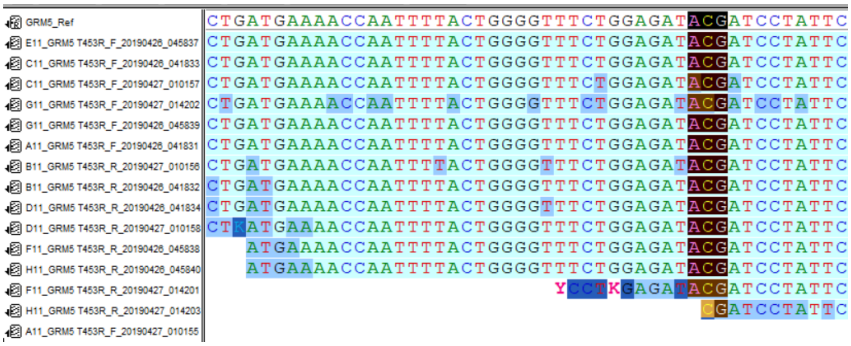
GRM5_Ref
E11_GRM5 T453R_F_20190426_045837
C11_GRM5 T453R_F_20190426_041833
C11_GRM5 T453R_F_20190427_010157
G11_GRM5 T453R_F_20190427_014202
G11_GRM5 T453R_F_20190426_045839
A11_GRM5 T453R_F_20190426_041831
B11_GRM5 T453R_R_20190427_010156
B11_GRM5 T453R_R_20190426_041832
D11_GRM5 T453R_R_20190426_041834
D11_GRM5 T453R_R_20190427_010158
F11_GRM5 T453R_R_20190426_045838
H11_GRM5 T453R_R_20190426_045840
F11_GRM5 T453R_R_20190427_014201
H11_GRM5 T453R_R_20190427_014203
A11_GRM5 T453R_F_20190427_010155

Caromile, Leslie A. “Be more like Harry: Creating inclusive spaces in STEM”. American Society for Cell Biology Newsletter. Diversity Matters August 2022. https://www.ascb.org/publications-columns/diversity-matters/be-more-like-harry-creating-inclusive-spaces-in-stem/.

The creation of a fair environment where everyone from all races, ethnicities, and genders should have the same chance and the same opportunities to excel is a critical part of the commitment to equitable and meritocratic treatment. However, in a recent article published in *Science Advances* and reviewed in *Nature*, author Erin Cech concluded that this is not the case. In this paper, Cech skillfully applied the concept of intersectionality to determine if white, able-bodied, heterosexual men (WAHM) in STEM experience more equitable and inclusive treatment, more professional respect, increased monetary compensation, and more job satisfaction when compared with members of 32 other intersectional gender, race, sexual identity, and disability status categories. Using a survey of 25,324 US STEM professionals, Cech concluded that WAHM are uniquely privileged in STEM. Statistical analysis showed that these privileges were not confounded by human capital, work effort/attitudes, job characteristics, background characteristics, or family responsibilities. Instead, many of these advantages remained as “premiums” attached to WAHM status itself[1,2].

To many of us, this is not a surprise but another example of the devastating effects that institutional and structural racism can have on professional-level STEM-based diversity recruitment and retention efforts. Unfortunately, many organizations have created diversity initiatives as a marketing/recruiting tool but do not understand the difference between diversity and inclusion in the workspace. Put simply, diversity efforts are concerned with representation and who is included. Diversity efforts should not be confused with the *creation* of an inclusive environment. An inclusive environment does not simply mean that people from various groups are included; it is concerned with what their inclusion in that organization or environment means. Just because diversity exists within a particular space, it does not mean that everyone is being included and treated fairly.

Sadly, this is a common mistake. Some organizations opt for easy solutions like unconscious bias training and resource groups, hoping that this training will reduce unconscious bias in attitudes and behaviors in both hiring and promotion decisions as well as in interactions with colleagues. These are a good start but these are not long-term solutions as simply increasing awareness is not enough. Instead, it is important to teach people to manage their biases, change their behavior, and track their progress. This type of training provides information that contradicts stereotypes and allows learners to connect with people whose experiences are different from theirs. And it’s not just a one-time education session; it entails a long journey. This might be exactly what was missing in the environments of some of the STEM professionals whose surveyed responses were analyzed for this study. So, rather than providing unconscious bias training as a check-the-box exercise, organizations should take an altruistic approach and make a real, long-term commitment to diversity, equity and inclusion because they think it is worthy and essential.

Those who are most effective in the STEM diversity, equity, and inclusion space are those who have done deep personal work around their privileged and marginalized identities, examined their wounds, and built their emotional intelligence. They are curious thinkers, deep listeners, and excellent communicators. For example, Jane makes a suggestion at her organization’s meeting, Everyone ignores it. Ten minutes later, Joe makes the same suggestion. People say “Wow Joe! What a great idea!” Jane thinks, what just happened? If she brings it up to a colleague, they are likely to say, “Don’t make a mountain out of a molehill”. Being ignored in a meeting is a molehill, but molehills matter because advantage accumulates via molehills. Jane’s colleague Harry is an emotionally intelligent individual who is self-aware and self-reflective. If Harry was attending this meeting, he would have said, “Jane made a suggestion that I think we should discuss” and then repeat Janes’s suggestion. Now, he would not necessarily say that it was a good suggestion nor would he chastise his colleagues for ignoring Jane. His aim is to ensure that everyone is heard. Be like Harry.

Many people from all races, ethnicities, and gender are doing impactful work in the STEM diversity, equity, and inclusion space, while others are open to creating more equitable and inclusive STEM environments for everyone but are unsure how to go about it. Well, you need to look no further than The American Society of Cell Biology (ASCB). Not only is ASCB planning to develop programs to educate and equip members (and the larger scientific community) about how to be inclusive and equity-minded (look at the ASCB diversity, equity, and inclusion strategic plan). But ASCB realizes that this cannot be simply a top-down approach. Therefore, they also have many different types of diversity initiatives and committees for the individual to get involved in (https://www.ascb.org/about-ascb/diversity-equity-and-inclusion/). For example, the Minority Affairs Committee (MAC) and other ASCB committees and groups, like WICB and LGBTQ+, are always looking for volunteers to step out of their various identities to participate in their committee's initiatives to not only institute a collective change but to connect with diverse people who are scientists just like you. As mentioned earlier, individual change involves some deep soul searching but by making a concerted effort to listen to and include all voices and also holding people accountable when they do not; you are on your way to being more like Harry.

1 Cech, E. A. The intersectional privilege of white able-bodied heterosexual men in STEM. *Sci Adv* **8**, eabo1558 (2022). https://doi.org:10.1126/sciadv.abo1558

2 doi: https://doi.org/10.1038/d41586-022-01851-4

Caromile, Leslie A. “Why do we still use the word “minority?”. American Society for Cell Biology Newsletter, Diversity Matters, June 2022. https://www.ascb.org/publications-columns/diversity-matters/why-do-we-still-use-the-word-minority/.

Why do we still use the word “minority”?

This term no longer makes sense in the United States, where historically excluded peoples are the majority in many cities. In fact, according to the Pew Research Center, by 2055, the United States “will have no racial or ethnic majority group.” When used correctly, the word “minority” is not problematic. However, the term “minority” is often used to refer to a group that is smaller, nonwhite, or “other,” rarely specifying race, background, or sexual orientation. Many recklessly use “minority” to group African Americans, Asian Americans, Indigenous peoples, Hispanics, Latinos, and immigrants together. The people considered part of “minority groups” are diverse and deserve proper recognition. The worst thing about the word “minority” is that it implies oppression and discrimination, and if too often utilized, will continue to minimize excluded peoples, and promote structural racism.

The word “minority” is pervasive throughout the biomedical sciences and commonly refers to ethnic and racial groups that are underrepresented within the biomedical science workforce. However, this concept is non-congruent. For example, most biomedical Ph.D. students nationwide are women and thus are not a numerical “minority”. However, they are still subject to interpersonal and systemic sexism. On the other side, there are questions about the appropriateness of using “minority” for groups that are numerical minorities in the general population but well represented in the biomedical sciences. Additionally, within the biomedical sciences, “minority” is not only a word of othering but is often attached to accomplishments. Many excluded scientists at all levels worry about the diminished impact their accomplishments might have, such as achieving a milestone, earning a scholarship, being nominated for an award, or receiving a grant, if prefaced with the word “minority”. Does this mean their hard-earned accomplishments are somehow less?

The ASCB and the Minority Affairs Committee (MAC) are working hard to change this culture and remove this outdated and harmful word from the Societies lexicon. The ASCB and MAC believe that many benefits flow from a diverse scientific workforce. Research shows that diverse teams working together and capitalizing on innovative ideas and distinct perspectives outperform homogenous teams. Scientists and trainees from diverse backgrounds and life experiences that truly represent the national population bring different perspectives, creativity, and individual enterprise to address complex scientific problems. However, for this to happen, one must feel comfortable working in an environment in which they feel seen, heard, fairly supported, and welcomed - not separate. A preference for people we perceive to be like us is a factor limiting inclusion that, in turn, undermines not only the ability to achieve diversity in the workforce but in the professional networking setting as well. For example, a preference for homophily can affect who talks to whom in a department or University or at meetings; who chooses to work with whom; who invites whom to give a talk or to be on a thesis committee. Unfortunately, despite successful outreach, excluded people are leaving the sciences early in their careers not because of education, ability, or interest but lack of inclusion(*1*). Those who experience a lack of inclusion are more likely to report burnout as well as adverse psychological, neural, physiological, and medical outcomes than those who have not.

Therefore, as communities become more diverse, we must evolve our terminology to promote inclusivity rather than inadvertently marginalizing groups that have much to offer in terms of scholarship, and perspective and ensuring that the national population is properly represented.

The ASCB believes that it is essential for all members of our community and beyond to feel secure and welcome within the Society, and for *all* voices to be respected and heard. The Society’s Diversity, Equity, and Inclusion Strategic Plan thoughtfully outline a set of recommendations that, if successful, can lead to a more diverse and inclusive environment. The strategic plan is expansive and provides recommendations that focus on increasing the diversity, equity, inclusion, and recognition of speakers, awards recipients, authors/editors, Society governance, and policy-makers at the Annual Meeting, in membership, partners, and volunteers(*2*). Interestingly, within the Diversity, Equity, and Inclusion Strategic Plan, the word “minority” is only found in one place: when referencing the

Minorities Affairs Committee (MAC). When the MAC officially became an ASCB committee in the mid-1980s, we centered our efforts on increasing the recruitment and participation of “racial and ethnic minorities” in the ASCB. However, in 2022, the word “minority” has become outdated, inaccurate, and potentially harmful. Therefore, the MAC will be removing and replacing the word “minority” in the Committee’s official name. Just because the MAC will be changing its name, it does not mean that it will be changing its focus. The MAC will continue to focus on increasing the recruitment and participation of excluded peoples from racial and ethnic groups to the ASCB and science as a whole by using all the innovative approaches that we currently do, while still collaborating and standing in solidarity with other ASCB committees and groups, like WICB and LGBTQ+.

While a new committee name has not been decided upon yet, the MAC welcomes any suggestions that you might have to help us and the ASCB create a more inclusive culture and scrub the use of the word “minority” from our vocabulary. Please visit the ASCB Community Online group titled “Suggestions for a new name for the Minority Affairs Committee (MAC)” to make your suggestions.

References

1. D. J. Asai, Race Matters. *Cell* **181**, 754-757 (2020).
2. ASCB. (2022).

UCONN
SCHOOL OF MEDICINE

Position: **Student Position in Prostate Cancer Health Disparities**
Employer: **University of Connecticut Health Center (UConn Health)**
Department: **Center for Vascular Biology, Department of Cell Biology**
Location: **Farmington, CT USA**

This position is available in the laboratory of Dr. Leslie Caromile, Ph.D.

Description:

Independently conduct laboratory experiments and techniques on DOD-funded prostate cancer research projects that are investigating the role of Prostate Specific Membrane Antigen (PSMA) in health disparities.

Qualifications:

The successful applicant should have a BS in a STEM field and be currently enrolled in a professional MS program in genomics. The applicant should have detailed knowledge of molecular, biochemical, cellular, genomic, and bioinformatic approaches to functionally annotate and assess the risk of previously identified germline coding SNPs within oncogenic signaling pathways. Experience or knowledge of genomic data analysis, cell culture procedures, and maintenance of stable cell lines; recombinant DNA techniques (such as molecular cloning and characterization of recombinant molecules), sequencing, and RT-PCR are highly desired. The applicant should have excellent communication skills, both oral and written; the ability to multitask be self-motivated; have the ability to acquire, arrange, interpret, analyze, evaluate and present data. Participation in laboratory maintenance and related duties as required.

UCONN
SCHOOL OF MEDICINE

Position: Special Payroll Position in Prostate Cancer Health Disparities

Employer: University of Connecticut Health Center (UConn Health)

Department: Center for Vascular Biology, Department of Cell Biology

Location: Farmington, CT USA

This special payroll position is available in the laboratory of Dr. Leslie Caromile, Ph.D.

Position Description: Special payroll. Full-time employment conducting laboratory experiments and techniques on a DOD-funded prostate cancer research project that examines the molecular underpinnings of prostate cancer health disparities in metastasis. Participate in laboratory management, maintenance, and related duties as required.

Qualifications: Successful candidates should have a minimum of a Bachelor of Science within the STEM field, such as biology, molecular biology, or biochemistry, from an accredited university. Applicant must have knowledge of molecular cloning, RT-PCR, and PCR. Additional highly desired techniques relevant to this project include knowledge of immunohistochemistry and fluorescence microscopy, gene editing, and site-directed mutagenesis. The applicant should have excellent communication skills, both oral and written; the ability to multitask and be self-motivated.

Salary will be commensurate with research experience.

frontiers | Frontiers in Cell and Developmental Biology

ORIGINAL RESEARCH
published: 11 July 2022
doi: 10.3389/fcell.2022.895433

ZIP11 Regulates Nuclear Zinc Homeostasis in HeLa Cells and Is Required for Proliferation and Establishment of the Carcinogenic Phenotype

*Monserrat Olea-Flores[1,2], Julia Kan[1], Alyssa Carlson[1†], Sabriya A. Syed[2], Cat McCann[1], Varsha Mondal[1], Cecily Szady[3], Heather M. Ricker[3], Amy McQueen[1], Juan G. Navea[3], Leslie A. Caromile[4] and Teresita Padilla-Benavides[1]**

[1]Department of Molecular Biology and Biochemistry, Wesleyan University, Middletown, CT, United States, [2]Department of Biochemistry and Molecular Biotechnology, University of Massachusetts Chan Medical School, Worcester, MA, United States, [3]Department of Chemistry, Skidmore College, Saratoga Springs, NY, United States, [4]Department of Cell Biology, Center for Vascular Biology, UCONN Health-Center, Farmington, CT, United States

OPEN ACCESS

Edited by:
Peter-Leon Hagedoorn,
Delft University of Technology,
Netherlands

Reviewed by:
Jian Hu,
Michigan State University,
United States
Sangyong Choi,
University of Connecticut,
United States
Kourosh Honarmand Ebrahimi,
King's College London,
United Kingdom

***Correspondence:**
Teresita Padilla-Benavides
tpadillabena@wesleyan.edu

†Present address:
Alyssa Carlson,
Tisch Multiple Sclerosis Research Center of New York, New York, NY, United States

Specialty section:
This article was submitted to Cellular Biochemistry, a section of the journal Frontiers in Cell and Developmental Biology

Received: 13 March 2022
Accepted: 13 June 2022
Published: 11 July 2022

Citation:
Olea-Flores M, Kan J, Carlson A, Syed SA, McCann C, Mondal V, Szady C, Ricker HM, McQueen A, Navea JG, Caromile LA and Padilla-Benavides T (2022) ZIP11 Regulates Nuclear Zinc Homeostasis in HeLa Cells and Is Required for Proliferation and Establishment of the Carcinogenic Phenotype. Front. Cell Dev. Biol. 10:895433. doi: 10.3389/fcell.2022.895433

Zinc (Zn) is an essential trace element that plays a key role in several biological processes, including transcription, signaling, and catalysis. A subcellular network of transporters ensures adequate distribution of Zn to facilitate homeostasis. Among these are a family of importers, the Zrt/Irt-like proteins (ZIP), which consists of 14 members (ZIP1-ZIP14) that mobilize Zn from the extracellular domain and organelles into the cytosol. Expression of these transporters varies among tissues and during developmental stages, and their distribution at various cellular locations is essential for defining the net cellular Zn transport. Normally, the ion is bound to proteins or sequestered in organelles and vesicles. However, though research has focused on Zn internalization in mammalian cells, little is known about Zn mobilization within organelles, including within the nuclei under both normal and pathological conditions. Analyses from stomach and colon tissues isolated from mouse suggested that ZIP11 is the only ZIP transporter localized to the nucleus of mammalian cells, yet no clear cellular role has been attributed to this protein. We hypothesized that ZIP11 is essential to maintaining nuclear Zn homeostasis in mammalian cells. To test this, we utilized HeLa cells, as research in humans correlated elevated expression of ZIP11 with poor prognosis in cervical cancer patients. We stably knocked down ZIP11 in HeLa cancer cells and investigated the effect of Zn dysregulation *in vitro*. Our data show that ZIP11 knockdown (KD) reduced HeLa cells proliferation due to nuclear accumulation of Zn. RNA-seq analyses revealed that genes related to angiogenesis, apoptosis, mRNA metabolism, and signaling pathways are dysregulated. Although the KD cells undergoing nuclear Zn stress can activate the homeostasis response by MTF1 and MT1, the RNA-seq analyses showed that only ZIP14 (an importer expressed on the plasma membrane and endocytic vesicles) is mildly induced, which may explain the sensitivity to elevated levels of extracellular Zn. Consequently, ZIP11 KD HeLa cells have impaired migration, invasive properties and decreased mitochondrial potential. Furthermore, KD of ZIP11 delayed cell

cycle progression and rendered an enhanced senescent state in HeLa cells, pointing to a novel mechanism whereby maintenance of nuclear Zn homeostasis is essential for cancer progression.

Keywords: ZIP11, zinc transport, cell cycle, senescence, gene expression, MTF1, cervical cancer cells

INTRODUCTION

Zinc (Zn) is among the most abundant trace elements essential for life. As a micronutrient, Zn is involved in many biological processes, such as cell signaling, transcriptional modulation, and as a catalytic cofactor and structural component of several proteins (Reviewed by (Wu and Wu, 1987; Kambe et al., 2015)). Under physiological conditions, Zn is present in a non-redox active form as a divalent cation (Zn^{2+}). Zn homeostasis plays a key role in human health, as Zn deficiencies have been identified as leading causes of diverse diseases. Patients lacking this ion may present skin abnormalities, hypogonadism, anemia, growth delays, alopecia, chronic inflammation, as well as deficiencies in immune, hepatic, and mental functions (Vallee and Falchuk, 1993; Hambidge, 2000; Maret and Sandstead, 2006; Devirgiliis et al., 2007; Takeda and Tamano, 2009; Sandstead, 2013). On the other hand, excess Zn is toxic and may disrupt the cellular acquisition of other micronutrients, such as copper (Cu) (Ogiso et al., 1979; Fischer et al., 1981; Broun et al., 1990). Total cellular Zn concentrations are typically in or below the micromolar range (Palmiter and Findley, 1995; Krezel and Maret, 2006; Colvin et al., 2008; Paskavitz et al., 2018; Gordon et al., 2019a; Gordon et al., 2019b; Tavera-Montañez et al., 2019). In general, 50% of subcellular Zn is located in the cytoplasm, 30–40% in the nucleus, and approximately 10% in the plasma membrane (Thiers and Vallee, 1957; Haase and Rink, 2014). However, Zn distribution may change depending on the developmental stage of the cells in a lineage-specific manner (Gordon et al., 2019a). The levels of labile, or "free," Zn in the cytosol are low, ranging from picomolar and low nanomolar concentrations, as it is normally bound to proteins and sequestered into organelles and vesicles (Tavera-Montañez et al., 2019; Gordon et al., 2019a; Gordon et al., 2019b; Outten and O'Halloran, 2001; Qin et al., 2011; Vinkenborg et al., 2009; Sensi et al., 1997). To maintain low levels and adequate subcellular distribution of the ion, cells have developed complex systems to maintain Zn homeostasis.

Two families of Zn transporters mobilize Zn between the extracellular milieu, the cytoplasm, and the organelles (Dufner-Beattie et al., 2003a; Eide, 2006; Kambe et al., 2014; Kambe et al., 2015). The Zn transporter family (also named ZnT, solute-linked carrier 30, or SLC30) mediates cellular Zn export, while the Zrt- and Irt-like proteins (also named ZIP, solute-linked carrier 39, or SLC39) mediate cellular Zn import. ZnTs and ZIPs are transmembrane proteins with six or eight predicted transmembrane (TM) domains, respectively (Dufner-Beattie et al., 2003a; Kambe et al., 2015). Mammalian cells express nine ZnT (1–8, 10) exporters and 14 ZIP importers (1–14), but their contributions to Zn physiology continue to be largely understudied. These transporters maintain cytosolic Zn pools by mobilizing the ion from the extracellular space and intracellular compartments, as they are differentially distributed based on the cellular demands for Zn and stage of life (Lichten and Cousins, 2009; Jeong and Eide, 2013). The majority of ZIP transporters have a dynamic localization to the cell membrane, as their expression, internalization, and degradation is dependent on the levels of the ion (Chowanadisai et al., 2013; Weaver et al., 2007; Hojyo et al., 2011; Dufner-Beattie et al., 2003b; Kelleher and Lönnerdal, 2003; Liuzzi et al., 2004; Liu et al., 2008; Lichten et al., 2011; Gaither and Eide, 2000; Wang et al., 2004; Huang and Kirschke, 2007; Mao et al., 2007; Taylor et al., 2005). Though they mainly mobilize Zn, ZIP importers can also transport iron (Fe) (Liuzzi et al., 2006; Gao et al., 2008; Jenkitkasemwong et al., 2015), manganese (Mn), and cadmium (Cd) (Girijashanker et al., 2008; Fujishiro et al., 2012; Jenkitkasemwong et al., 2012; Gordon et al., 2019b).

To date, the only crystal structure available for a ZIP transporter is from the bacteria *Bordetella bronchiseptica* (BbZIP), which was obtained in the presence of Cd^{2+} (Zhang et al., 2017). BbZIP structure shows eight TM helices that are proposed to form a tight bundle. TM2, TM4, TM5, and TM7 constitute an inner bundle surrounded by the remaining TMs (Zhang et al., 2017). The BbZIP TM2 contains a 36 amino acid-long domain with a kink associated with a conserved proline (P110) (Zhang et al., 2017). TM4 and TM5 are also bent due to the presence of two proline residues in the metal-binding sites (MBS (Zhang et al., 2017)). BbZIP was found to have a novel symmetric structure. The first three TMs, TM1-TM3, are symmetrically related with the last three, TM6-TM8, by a pseudo-two-fold axis, which was defined to be almost parallel to the proposed membrane plane. Further, TM4 and TM5 also seem to be symmetrically related by the same axis, however these two segments appear to be fitted-in by the other two named 3-TM repeats (Zhang et al., 2017). This previously unrecognized architecture was defined as an unusual 3+2+3TM structure (Zhang et al., 2017). Crystallization of BbZIP in the presence of $CdCl_2$ allowed for the identification of four Cd^{2+}-binding sites and revealed that the amino- and carboxy-termini both face the extracellular domain (Zhang et al., 2017). This novel structural data support previous hydrophobicity plot predictions that suggested that ZIP transporters have eight TM helices with extracellular amino- and carboxy-terminal domains (Lichten and Cousins, 2009; Jeong and Eide, 2013).

To transport Zn, ZIP importers are proposed to form homodimers (Lin et al., 2010; Bin et al., 2011). Biochemical characterization and overexpression analyses have demonstrated that the apparent K_m ranges from hundreds of nM to approximately 20 μM (Gaither and Eide, 2000; Gaither and Eide, 2001a; Dufner-Beattie et al., 2003a; Wang et al., 2004; Liu

et al., 2008; Pinilla-Tenas et al., 2011; Antala and Dempski, 2012; Dempski, 2012). Although the mechanism of Zn transport is not fully understood, early biochemical analyses of BbZIP suggested that Zn transport occurs in a channel-like, non-saturable electrogenic manner (Lin et al., 2010), and that phosphorylation by casein kinase 2 may also activate transport (Taylor et al., 2012). BbZIP crystallization points to a putative mechanism of Zn transport that may apply to other members of the ZIP family. Essentially, two conserved metal-binding residues, D113 and D305, seem to be necessary to recruit the metal to the transporter (Zhang et al., 2017). A conserved serine (S106) located at the bottom of the entrance cavity seems to be required to guide the ion into the transport pathway, while A102 was proposed to be a pore-lining residue at the extracellular side (Zhang et al., 2017). An inward-open conformation of the transporter can be stabilized by substrate binding at the binuclear metal center, which is in the middle of the transport pathway. Then the ion may be released to the cytoplasm through a "chain" of metal-binding residues (H177, E276, H275, and D144) and a histidine-rich loop that connects TM3 and TM4 (Zhang et al., 2017). These weak Zn-binding sites are located at the exit cavity and were named as a "metal sink," proposed to facilitate metal release from the binuclear metal center (Zhang et al., 2017). Zn release is thought to occur due to the effect of repulsive electrostatic forces between the MBS and/or the removal of geometric constraints in the rearrangement of the TMs to form an open channel at the extracellular side of the membrane which may be blocked by conserved hydrophobic residues (M99 and A102 on TM2, L200 and I204 on TM5, and M269 on TM7) as the transporter opens to the cytosol (Zhang et al., 2017).

ZIP transporters are classified into subfamilies I, II, LIV-1, and GufA according to their sequence similarities (Taylor, 2000; Gaither and Eide, 2001b; Taylor and Nicholson, 2003; Yu et al., 2013; Hu, 2021). These transporters localize to specific cellular compartments and are regulated depending on cellular needs and stage of development or disease (Reviewed by (Kambe et al., 2015)). However, there is still a gap in our knowledge on the specific functions of some members of the family, such as ZIP11. This transporter was classified as a member of the GufA subfamily of ZIP proteins. The *ZIP11* gene contains several metal responsive elements (MRE), which are targets of the classic Metal Regulatory Transcription Factor 1 (MTF1) that enable *ZIP11* expression to respond to metal levels (Martin et al., 2013; Yu et al., 2013). However, it seems that this transporter is not largely induced by MTF1 upon increase in Zn levels, as are other transporters. In mice, a modest increase in *Zip11* mRNA expression was detected in the intestine and other organs (e.g. spleen) of animals exposed to acute oral Zn exposure (Yu et al., 2013). Thus, it was proposed that ZIP11 is not required to maintain the net quota of cellular Zn, and rather instead helps to maintain appropriate subcellular distribution of the ion. Gene expression analyses showed that the murine *Zip11* (*mZip11*) is highly expressed in the testes, stomach, ileum, and cecum, with a lower level of expression detected in the liver, duodenum, jejunum, and colon (Martin et al., 2013; Yu et al., 2013). Martin and coworkers (Martin et al., 2013) showed that within the murine gastrointestinal tract, ZIP11 is modestly downregulated by Zn deficiency in the stomach. This data showed that Zn deficiency may trigger the absorption of Z from the colon by ZIP4 rather than by ZIP11 (Martin et al., 2013).

Overexpression analyses determined that HEK cells expressing *mZip11-Flag* had elevated Zn content compared to controls. Moreover, incubation of cells expressing *mZip11-Flag* in the presence of Zn led to cell death after 2 days, while supplementation with the chelator N,N,N′N′-tetrakis (−) [2-pyridylmethyl]-ethylenediamine (TPEN) favored cell growth (Yu et al., 2013). Knockdown (KD) experiments in Raw264.7 cells consistently showed a decrease in cellular Zn levels, strengthening the hypothesis that mZip11 is a Zn importer (Yu et al., 2013). However, experiments using MDCK cells expressing the *mZip11-Flag* construct determined that the transporter may also mobilize Cu (Yu et al., 2013). Murine models have demonstrated that *Zip11* expression in different tissues have differential responses to Zn acquired from the diet (Martin et al., 2013; Yu et al., 2013). At the cellular level, ZIP11 is proposed to be localized to the nucleus and Golgi apparatus (Kelleher et al., 2012; Martin et al., 2013). Despite this evidence, the physiological and cellular functions of ZIP11 have not been established.

Emerging evidence has shown that ZIP transporters are associated with the development of various types of cancer. In the particular case of ZIP11, early gene association analyses using genome-wide association study (GWAS) datasets coupled with analyses of tumors for somatic change of *ZIP11* gene variants, and patient survival from data in The Cancer Genome Atlas (TCGA) showed that the variant (rs8081059) was significantly associated with increased risk of renal cell carcinoma, while four other variants (rs11871756, rs11077654, rs9913017, and rs4969054) were significantly associated with bladder cancer risk. These variants were located within predicted transcribed or enhancer regions. Moreover, out of 253 bladder cancer patients reported in TCGA, two had tumors that contained deleterious missense mutations in *ZIP11*. These data led to the identification of *ZIP11* as a contributor to bladder cancer (Wu et al., 2015). A recent study of patients with pancreatic adenocarcinoma (PAAD) showed that patients present with decreased serum Zn levels. Analysis of TCGA and the Genotype-Tissue Expression (GTEx) databases showed a correlation between high expression of *ZIP11* and poor prognosis in PAAD patients (Zhu et al., 2021). Gene expression analyses showed that *ZIP11* is upregulated in PAAD tumors compared to normal pancreatic controls (Zhu et al., 2021). KD of *ZIP11* in Capan-1 pancreatic cancer cells impaired cell proliferation associated with a decreased activation of ERK1/2 pathway (Zhu et al., 2021). A transcriptome analysis focused on colorectal cancer (CRC) and breast cancer samples showed that *ZIP11* is also upregulated in these patients (Barresi et al., 2018). Conversely, a negative correlation between *ZIP11* expression and glioma grades was described. A study involving 74 glioma tissue samples showed that low expression of *ZIP11* in gliomas correlated with grades III and IV tumors, while higher expression of the transporter correlated with grade I and II tumors (Kang et al., 2015). In this context, the data suggest that ZIP11 is a potential contributor

to the development of "low grade" tumors that do not spread out of the brain, but instead grow into the normal brain tissue. However, despite this evidence, there is no information on the mechanism or detailed biological function of ZIP11 in the onset and progression of brain or other types of cancer.

In this study, we characterized the contributions of ZIP11 in maintaining cell proliferation *via* regulating Zn levels in the nuclei of HeLa cells. We reduced the expression of *ZIP11* in HeLa cells using two short hairpin RNA (shRNA) against the *SLC39A11* gene and then assessed the proliferation capabilities and Zn accumulation in whole, cytosolic, and nuclear fractions. We then treated with increasing concentrations of $ZnSO_4$ and tested for metal resistance. Our data show that decreased ZIP11 expression impaired growth under normal culture conditions and increased the sensitivity of the cells due to Zn accumulation in the nuclei. RNA-seq analyses showed that the Notch pathway is downregulated in cells lacking *ZIP11*. RNA-seq and qPCR analyses revealed that the expression of cell cycle related genes was altered. For instance, we found that genes related to cell growth, such as Cyclin Dependent Kinase 20 (*CDK20*), is downregulated. On the other hand, genes implicated in the negative control of cell growth and division, such as Cyclin Dependent Kinase Inhibitor 2C (*CDKN2C*) and the Protein Phosphatase 2 Catalytic Subunit Alpha (*PPP2CA*), are induced. These analyses also showed that some DNA repair and senescence associated genes, as well as some apoptotic and genes related to epithelial mesenchymal transition (EMT), are downregulated, suggesting that the impaired growth may be due to the induction of a senescent state in the cells. Expression of exogenous wild type (WT) ZIP11 rescues the proliferation defect, restores nuclear Zn levels, and ameliorates the metal resistance phenotype observed in *ZIP11* KD HeLa cells. Interestingly, overexpression of ZIP11 in WT HeLa cells enhanced cell growth and resistance to higher levels of Zn in the media, while maintaining similar levels of the metal in cytosol and nuclei, compared to controls. Functional analyses of cancer cell migration and invasion phenotypes demonstrated that ZIP11 KD decreases the mobility and invasive capabilities of HeLa cells. As expected, ZIP11 reconstitution experiments restored these metastasis-associated properties, while overexpression of ZIP11 enhanced these phenotypes. Finally, ZIP11 KD cells have a significant decrease in mitochondrial potential and elevated β-galactosidase activity, which may also be a reflection of the dormant, or senescent, state (Chapman et al., 2019) and other metabolic deficiencies. We conclude that ZIP11 is required to maintain nuclear levels of Zn to enable proper gene expression and proliferation in HeLa cells by impairing the machinery associated with DNA damage and maintaining the cells in a senescent state. This nuclear Zn dyshomeostasis is reflected in defective metastatic properties, making ZIP11 a new potential target for further investigation using *in vivo* models and anti-cancer drug development.

MATERIALS AND METHODS

Database Searches

We queried the publicly available database cBioPortal for Cancer Genomics, (https://www.cbioportal.org/), for SNPs within the coding region of *ZIP11* in patients with either cervical or ovarian cancer. To determine if the ZIP11 coding SNPs A234P and P243S had individual biological consequences, we queried the publicly available consensus classifier PredictSNP1 (https://loschmidt.chemi.muni.cz/predictsnp1/ (Bendl et al., 2014)). To evaluate the effects of A234P and P243S (alone or in combination) on the ZIP11 protein structure, we incorporated the SNPs into a published model of ZIP11 (AF-Q8N1S5-F1) using the PyMol Molecular Graphics System version 2.4.1 (https://pymol.org; Schrödinger, LLC). To investigate the predicted consequences that A234P and P243S might have on ZIP11s protein structure, we queried the publicly available PredictProtein algorithm (https://predictprotein.org/ (Rost et al., 2004)). To verify if the HeLa cell line was appropriate for our studies, we queried the interactive HeLa Spatial Proteome Database (http://mapofthecell.biochem.mpg.de/index.html) (Itzhak et al., 2016). To determine if wild type HeLa cells contained either the A234P or the P243S mutation within the ZIP11 gene within of its genome, we queried the Broad Institutes DEPMAP Portal (https://depmap.org/portal/cell_line/HELA_CERVIX?tab=mutation). The https://www.ncbi.nlm.nih.gov/gene?Db=gene&Cmd=DetailsSearch&Term=201266 website was used to identify the number of ZIP11 isoforms that may be present in cells.

Cell Culture

HeLa and HEK293T cells were obtained from American Type Culture Collection (ATCC, Manassas, VA, United States) and cultured in DMEM media (Sigma-Aldrich, St Louis, MO, United States) supplemented with 10% fetal bovine serum (FBS) and 1% antibiotics (penicillin G/Streptomycin, Gibco, Waltham, MA, United States) in a humidified atmosphere containing 5% CO_2 at 37°C.

Plasmids and Lentivirus Production

Mission plasmids encoding for two different shRNA against human *ZIP11* and the control scrambled (Scr) construct with a puromycin resistance cassette were obtained from Sigma (**Supplementary Table S1**). The mammalian gene expression lentiviral vector pLV[Exp]-EGFP/Neo-EF1A encoding hSLC39A11 or empty vectors with a neomycin resistance cassette were purchased from Vector Builder. Plasmids were isolated with the ZymoPURE™ II maxiprep plasmid system (Zymo Research, Irvine, CA, United States) following the manufacturer's instructions. shRNA (15 μg) and the packing vectors pLP1 (15 μg), pLP2 (6 μg), pSVGV (3 μg) were transfected using lipofectamine 2000 (Thermo Fisher, Waltham, MA, United States) into HEK293T cells for lentiviral production. After 24 and 48 h, the supernatant containing viral particles were collected and filtered using a 0.22 μm syringe filter (Millipore Sigma, Burlington, MA, United States). HeLa cells were transduced with lentivirus in the presence of 8 mg/ml polybrene and selected with 4 μg/ml puromycin (Invitrogen, Waltham, MA, United States) or 2 mg/ml geneticin. After selection, the cells were maintained with 1 μg/ml of puromycin or 200 μg/ml of geneticin as needed.

Antibodies

The rabbit anti-ZIP11 (PA5-20679), antibody was from Thermo Fisher. The mouse anti-lamin A/C (SC376248) and anti-tubulin (TU-02; SC8035) were from Santa Cruz Biotechnologies (Dallas, TX, United States). The rabbit anti-GAPDH (A19056) and anti-MTF1 (custom made against the residues 520–630 from the human protein) were from Abclonal Technologies (Woburn, MA, United States). The rabbit anti-Caspase-3 antibody was from Cell Signaling Technologies (9662). The mouse anti-Golgin-97 (A21270) and the secondary HRP-conjugated anti-mouse and anti-rabbit antibodies were from Invitrogen (31,430 and 31,460, respectively). The fluorescent goat anti-rabbit Alexa-488 secondary antibody was from Thermo Fisher (A-11008).

Western Blot Analyses

Protein samples from HeLa cells (WT, Scr control, *ZIP11*-KD, and cells transduced with the empty or ZIP11-containing pLV [Exp]-EGFP/Neo-EF1A vectors) were solubilized with RIPA buffer (10 mM piperazine-N,N-bis(2-ethanesulfonic acid), pH 7.4, 150 mM NaCl, 2 mM ethylenediamine-tetraacetic acid (EDTA), 1% Triton X-100, 0.5% sodium deoxycholate and 10% glycerol) supplemented with protease inhibitor cocktail (Thermo Fisher). Protein content was quantified by Bradford assay (Bradford, 1976). Samples (20 μg) were separated by SDS-PAGE and electrotransferred to PVDF membranes (Millipore Sigma). The proteins of interest were detected using the primary antibodies anti-ZIP11 and anti-GAPDH as a loading control. The membranes were then incubated with species-specific secondary antibodies coupled to horseradish peroxidase. Chemiluminescent detection was performed using high sensitivity Tanon reagents (Abclonal Technologies).

Confocal Microscopy

Monolayers of HeLa cells were fixed overnight in 10% formalin-PBS at 4°C. Samples were washed with PBS, permeabilized with 0.2% Triton X-100 in PBS for 15 min, incubated for 1 h at RT in blocking solution (PBS, 0.2% Triton X-100, 3% FBS), and incubated overnight with anti-ZIP11 and anti-Golgin 97 antibodies in blocking buffer at 4°C. The next day, the cells were incubated for 3 h with fluorescent goat anti-rabbit Alexa-594 and anti-mouse Alexa-633 secondary antibodies in blocking solution for at RT and 30 min with DAPI. Microscopy and image processing were performed using a Leica SP8 Confocal Microscope and the Leica Application Suite X (Leica Microsystems Inc., Buffalo Grove, IL, United States).

Cell Proliferation Assays

HeLa and HeK293T cells were seeded at 1×10^4 cells/cm^2 and samples were collected 24, 48, 72, and 96 h after plating. Increasing concentrations of $ZnSO_4$ (0–200 μM) were added to the cell cultures as indicated in the figures and figure legends. The cells were trypsinized, washed three times with PBS, and counted using a Cellometer Spectrum (Nexcelcom Biosciences, Lawrence, MA, United States). To determine cell viability, HeLa cells were collected at 72 h after plating and stained with 0.4% Trypan Blue (Sigma) diluted in PBS for 5 min at RT. Cell number and viability were determined using the Cellometer Spectrum, and data were analyzed with FCS Express 7 software (*De Novo* Software).

Metal Content Analysis

Three independent biological replicates of HeLa cells stably expressing the shRNA or the pLV[Exp]-EGFP/Neo-EF1A encoding hSLC39A11 or empty vectors were seeded at 1×10^4 cells/cm^2 and allowed to proliferate for 48 h. Then the cells were rinsed three times with ice-cold PBS without Ca^{2+} and Mg^{2+} (Gibco). Subcellular fractionation was performed following the Rapid, Efficient, and Practical nuclear and cytoplasmic separation method (Suzuki et al., 2010; Gordon et al., 2019a; Tavera-Montañez et al., 2019). Briefly, cells were scraped and transferred to a 1.5-ml microcentrifuge tube. Cells were centrifuged for 10 s at 13,000 × *g* and the supernatant was discarded. The samples were resuspended in 400 ml of ice-cold PBS containing 0.1% NP40 (Sigma-Aldrich) and 50 μl of the cell suspension were collected as the whole cell fraction. The remaining 350 μl were used to obtain nuclear and cytosolic fractions by disrupting the cells by pipetting using a 1-ml pipette tip. Cell suspension was centrifuged for another 10 s and the supernatant was collected as the cytosolic fraction. The nuclear pellet was washed twice in 1 ml of ice-cold PBS containing 0.1% NP40 and centrifuged for additional 10 s. The supernatant was removed, and the pellet was resuspended in 100 μl of PBS. Nuclear integrity was verified by light microscopy. All samples were sonicated at medium intensity for 5 min in 30 s on 30 s off cycles. Protein was quantified by the Bradford method (Bradford, 1976). Purity of cytosolic and nuclear fractions used to determine metal levels was verified by western blot using an anti-Tubulin and anti-Lamin A/C antibodies.

The comparative analysis of ultra-trace (<1 ppm) Zn concentrations from each sample was determined using a method adapted from previously described protocols (Paskavitz et al., 2018; Gordon et al., 2019a; Tavera-Montañez et al., 2019). Here, Zn measurements were carried out using a PerkinElmer AAnalyst 800 atomic absorption spectrometer (AAS) with a zinc hollow cathode lamp as the radiation source. The AAS was equipped with a graphite furnace (GF-AAS) with UltraClean THGA® graphite tubes (PerkinElmer, Waltham, MA, United States). This technique allowed accurate ultra-trace zinc analysis in low volume samples, where dilution was limited by the low initial concentration of Zn in the samples (Paskavitz et al., 2018; Gordon et al., 2019a). In a typical analysis, a known mass of the sample was digested in concentrated nitric acid using single-stage digestion (Paskavitz et al., 2018; Gordon et al., 2019a; Tavera-Montañez et al., 2019). The resulting solution was analyzed for Zn *via* AAS with measurements carried out at least in triplicates. Contamination was avoided by using analytical grade reagents and 18 MΩ purified water. All analytical glassware was acid washed overnight in 10% (v/v) hydrochloric acid and rinsed with 18 MΩ purified water before use (Paskavitz et al., 2018; Gordon et al., 2019a; Tavera-Montañez et al., 2019; Kim et al., 2020). Zn standard solutions were prepared from 1000 mg/L (Sigma-Aldrich) to determine the limits of detection and obtain a calibration curve for the method. The limit of detection for Zn, calculated as three times the standard deviation of the intercept (3σ), was 0.05 ppb, with a limit of linearity at 2.5 ppb. Zn content on each sample was normalized to the initial protein content in each sample.

RNA-Seq and Data Analysis

Total RNA from HeLa cells transduced with Scr or one of two shRNA against *ZIP11* was isolated using TRIzol and frozen at −80°C until analysis. Independent replicates for each sample were evaluated for quality and concentration at the Molecular Biology Core Lab at the University of Massachusetts Chan Medical School. Quality Control-approved samples were submitted to BGI Genomics for library preparation and sequencing. Libraries were sequenced using the BGISEQ-500 platform and reads were filtered to remove adaptor-polluted, low quality and high content of unknown base reads. About 99% of the raw reads were identified as clean reads (~65 M). The resulting reads were mapped onto the reference human genome (hg38) using HISAT (Kim et al., 2015). Transcripts were reconstructed using StringTie (Pertea et al., 2015), and novel transcripts were identified using Cufflinks (Trapnell et al., 2010) and combined and mapped to the hg38 reference transcriptome using Bowtie2 (Langmead and Salzberg, 2012). Gene expression levels were calculated using RSEM (Li and Dewey, 2011). DEseq2 (Love et al., 2014) and PoissonDis (Audic and Claverie, 1997) algorithms were used to identify differentially expressed genes (DEG). Gene Ontology (GO) analysis was performed on DEGs to cluster genes into function-based categories.

RT-qPCR Gene Expression Analysis

RNA was purified from three independent biological replicates of proliferating HeLa cells (Scr control and KDs) with TRIzol (Invitrogen) following the manufacturer's instructions. cDNA synthesis was performed with 500 ng of RNA as template, random primers, and SuperScript III reverse transcriptase (Invitrogen) following the manufacturer's protocol. Quantitative RT-PCR was performed with Fast SYBR green master mix on the ABI StepOne Plus Sequence Detection System (Applied Biosystems) using the primers listed in **Supplementary Table S2**, and the delta threshold cycle value (ΔC_T) (Livak and Schmittgen, 2001) was calculated for each gene and represented the difference between the C_T value of the gene of interest and that of the control gene, *GAPDH*.

Wound Healing Assay

Cells were grown until confluence on 24 well plates in DMEM supplemented with 10% FBS and antibiotics. Cells were starved for 24 h in DMEM without FBS and cell proliferation was inhibited by treating the cells with Cytosine β-D-Arabinofuranoside (AraC) for 2 h. The monolayers were then scratch-wounded using a sterile 200 µl pipette tip and suspended cells were washed away with PBS twice. The progress of cell migration into the wound was monitored every 24 h until wound closure using the ×10 objective of an Echo Rebel Microscope as previously described (Lacombe et al., 2021). The bottom of the plate was marked for reference, and the same field of the monolayers was photographed immediately after performing the wound (time = 0 h) and at different time points after performing the scratch, as indicated in the figures. Area migrated by the cells was quantified using FIJI software, version 1.44p (Schindelin et al., 2012).

Matrigel Invasion Assay

Matrigel invasion assay was performed following the Transwell chamber method as described (Olea-Flores et al., 2019). Briefly, BioCoat® Matrigel® Invasion Chambers with 8.0 µm PET membrane placed in 6-well Plates were used to seed cells that were previously treated for 2 h with 10 µM AraC to inhibit cell proliferation. The cells were plated at 1.25×10^5 cells/ml in 2 ml of serum-free medium on the top chamber, as recommended by the manufacturer. The lower chamber of the Transwell contained 2.5 ml of advanced DMEM supplemented with 10% FCS. Cells were incubated for 24 h at 37°C in a 5% CO_2 atmosphere. Following incubation, cells and Matrigel on the upper surface of the Transwell membrane were gently removed with cotton swabs. Invading cells on the lower surface of the membrane were washed and fixed with methanol for 5 min and stained with 0.1% crystal violet diluted in PBS. Images from 10 fields of three independent biological replicates were taken and used for cell quantification using FIJI software, version 1.44p (Schindelin et al., 2012). The invasion index was calculated as the ratio between number of cells of *ZIP11* KD cells, KDs reconstituted with EV or *ZIP11*, or WT overexpressing the EV or *ZIP11* and the number of WT control cells.

Cell Cycle Analyses

HeLa cells (1×10^6 cells) were arrested in mitosis with 50 ng/ml nocodazole (Kaida et al., 2011) for 16 h and released by washing with PBS and cultured with medium with 10% FBS for an additional 24 h. Timepoints were collected as indicated in the figure legend. Cell cycle analysis was performed using a standard propidium iodide (PI)-based cell cycle assay. Briefly, cells were trypsinized, washed three times with PBS, and fixed by slowly adding 200 µl of ice-cold 70% ethanol and incubated overnight at 4°C. Cells were washed with PBS, and the pellet was resuspended in 50 µl PBS containing 100 µg/ml RNAse A and 0.1% Triton X-100 and incubated at 37°C for 30 min. Finally, the cells were incubated with 40 µg/ml PI staining solution at 37°C for 40 min and analyzed in a Cellometer Spectrum instrument. Data were analyzed with FCS Express 7 software.

Senescence Assay

We used CellEvent™ Senescence Green Flow Cytometry Assay Kit following manufacturer's instructions (Thermo Fisher). Briefly, HeLa cells (WT, Scr control, *ZIP11* KD, and cells transduced with the empty or *ZIP11*-containing pLV[Exp]-EGFP/Neo-EF1A vectors) were seeded at 1×10^6 cells/cm^2 and maintained on DMEM media supplemented with 10% FBS for 48 h. We treated wild type HeLa cells with 5 mM Palbociclib (Sigma-Aldrich) as a positive control for senescence, as suggested by the manufacturer. HeLa cells were trypsinized, washed and resuspended in PBS and fixed in 4% paraformaldehyde for 10 min at room temperature. The cells suspension was stained with the CellEvent™ Senescence Green Probe (1/500) in CellEvent™ Senescence Buffer for 90 min in a 37°C incubator with no CO_2. Cells were washed in PBS containing 1% BSA, and finally resuspended in PBS. Fluorescence intensity of β-gal was measured by Spectrum Cellometer (Nexcelom Biosciences) by setting the filter excitation at 530/30 nm filter. Data was analyzed with FCS Express 7 (*De Novo* Software).

Mitochondrial Membrane Potential

Changes in mitochondrial membrane potential produced by *ZIP11* KD in HeLa cells were determined with the tetramethylrhodamine ethyl ester (TMRE)-Mitochondrial Membrane Potential Assay Kit (Abcam, Cambridge, MA, United States) following the manufacturer's protocol. Briefly, proliferating cells were supplemented with 200 nM TMRE and incubated in the dark for 10 min at 37°C. The cells were then trypsinized and washed three times with PBS. Fluorescence intensity of TMRE was measured by Spectrum Cellometer (Nexcelom Biosciences, Lawrence, MA, United States) by setting the filter excitation at 502 nm and emission at 595 nm, as previously reported (Angireddy et al., 2020; Chowdhury et al., 2020; Lacombe et al., 2021). Data was analyzed with FCS Express 7 (*De Novo* Software).

Statistical Analysis

Statistical analyses were performed using Kaleidagraph (Version 4.1). Statistical significance was determined using *t*-test where $p < 0.05$ was considered to be statistically significant.

RESULTS

ZIP11 Plays a Role in the Progression of Cervical and Ovarian Cancer

A closer look to the TCGA database showed that of 1321 cases reported in the TCGA database for *ZIP11* (SLC39A11) mutations, 61% have been found in females and 39% in males. The higher incidence of mutations for *ZIP11* gene occurs in patients presenting uterine corpus endometrial carcinoma (**Supplementary Figure S1A**). In terms of loss of function or decrease expression of the *ZIP11* gene esophageal cancer patients represent the most affected population (8% of the patients), while for gain of function or increased expression of *ZIP11*, impacts primarily ovarian cysteous adenocarcinoma (almost 30% of the patients), followed by breast invasive carcinoma (approximately 22% of the individual; **Supplementary Figure S1B**). Between 10 and 15% of the patients presenting lung squamous cell carcinoma, bladder urothelial carcinoma, esophageal carcinoma, uterine corpus endometrial and cervical squamous cell and endocervical carcinomas are also among the groups presenting increased expression of *ZIP11* (**Supplementary Figure S1C**).

Patients of cervical and ovarian cancers represent the groups with larger numbers in *ZIP11* mutations, however mutations on this gene are not considered to be a prognostic marker of the disease (**Figure 1** and **Supplementary Figure S1** and **Supplementary Table S3**). Therefore, we looked closely into genotypes and phenotypes observed in these populations. Analysis of 2344 samples from 2330 patients found in seven publicly available cervical and ovarian cancer studies (https://www.cbioportal.org/) confirmed that *ZIP11* had an alteration frequency of 2–3%, within the genome, with the majority of the genes being amplified or mutated rather than deleted (**Figure 1A**). Further structural analysis of these datasets revealed two unique missense mutations within the *ZIP11* coding region, A26S and A234P, while another two mutations, P243S and A89V, correlated with the two known coding SNPs rs763797008 and rs202154945 (**Figure 1B**). Although the effect of an individual SNP is generally minor, some variants do affect gene expression or the function of the translated proteins (Risch and Merikangas, 1996; Collins et al., 1997). Therefore, the effect of combinations of functionally relevant SNPs may synergistically contribute to increased disease progression. Compared to individual SNPs, multiple SNPs can be either more or less deleterious. Multiple SNPs on the same gene have been found to contribute or be linked to various genetic diseases (Rafi et al., 2003; Kamphans et al., 2013). To determine if these SNPs had biological consequences, we used PredictSNP (Bendl et al., 2014), a publicly available consensus classifier for disease related amino acid mutations. Results showed that both A234P and P243S had deleterious biological consequences (**Figure 1C**). The limitation of the PredictSNP model is that it can only predict the consequence of one SNP, not multiple. We knew that some of the patients in these data sets were positive for both A234P and P243S mutations. Therefore, using PyMol Molecular Graphics System, we used the predicted structure of ZIP11 (PDB AF-Q8N1S5-F1) to construct a model that contained the two deleterious SNPs and compared this to the wild type structure. The model indicated SNP induced structural variations within the substrate binding region that possibly could affect the function of the protein (**Figures 1D,E**). To show exactly where the SNPs affected ZIP11 structure and what could be the predicted consequences; we used the publicly available PredictProtein algorithm. PredictProtein searches public sequence databases, creates alignments, and predicts aspects of protein structure and function (Rost et al., 2004). These *in silico* analyses suggested that substitutions in A234P and P243S may result in an increase in substrate accessibility (**Figure 1F**). Since these residues are facing away from the transmembrane metal binding site, these mutations may potentially affect the interactions between surrounding transmembrane helices. However, further biochemical characterization is needed to clarify this point. Finally, using the Human Protein Atlas (https://www.proteinatlas.org/) we constructed a Kaplan-Meier survival curve using a cervical cancer data set containing 291 patients. The survival curve demonstrated that patients with high *ZIP11* RNA expression within their cervical cancer tumors had a 63% chance of surviving over 5 years, while those with low *ZIP11* RNA had a 72% survival rate (**Figure 1G** and **Supplementary Table S3**). This trend in survival suggests that ZIP11 expression may correlate with the progression of cervical cancer, although the information provided by the database does not specify whether these patients harbor the indicated SNPs.

ZIP11 has been proposed to be a transporter that mobilizes Zn from the nucleus and Golgi into the cytosol (Kambe et al., 2015). However, overexpression studies in early characterization of RAW264.7 cells, which are monocyte/macrophage-like cells suggested a potential role mobilizing extracellular Zn into the cytosol (Yu et al., 2013). To verify if the HeLa cell line was an appropriate model for our studies of ZIP11 in the context of nuclear transport, we used the interactive HeLa Spatial Proteome Database (http://mapofthecell.biochem.mpg.de/index.html) to

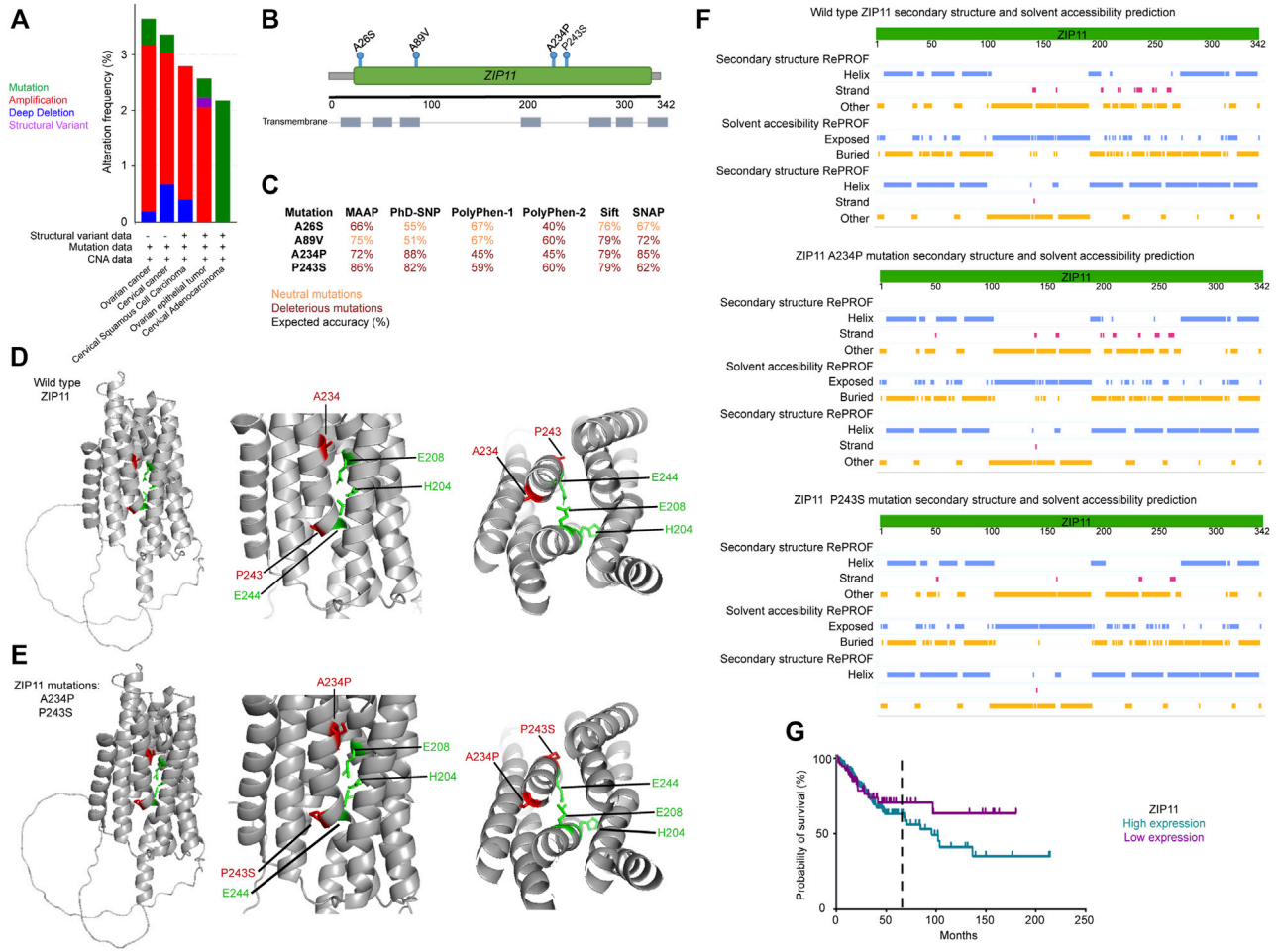

FIGURE 1 | ZIP11 role in the progression of cervical and ovarian cancer. **(A)** Analysis of 2344 samples from 2330 patients found in seven publicly available cervical and ovarian cancer studies (https://www.cbioportal.org/) confirmed that ZIP11 had an alteration frequency of 2–3%, within the genome. **(B)** Schematic of ZIP11 and SNP locations (green) within the ZIP11 protein and transmembrane domains (gray). **(C)** PredictSNP analysis of *ZIP11* SNPs in cervical and ovarian cancer (red = deleterious; orange = neutral mutations). Representative model of wild type ZIP11 **(D)** and ZIP11 containing two deleterious SNPs (A234P and P243S, **(E)** within the substrate binging region. **(F)** *In silico* modeling with PredictProtein calculated that ZIP11 may have increased substrate accessibility when the two deleterious SNPs (A234P and P243S) are introduced. **(G)** Kaplan-Meier survival curve using a cervical cancer data set containing 291 patients. Five-year survival indicated by black, vertical, dashed line. The statistical information for the comparison of survival curves can be found in **Supplementary Table S3**.

understand the cellular localization of ZIP11. The HeLa Spatial Proteome Database provides subcellular localization information for 8,700 proteins from HeLa cells. It indicates how a queried protein is distributed over the nucleus, cytosol, and organelles of the HeLa cells using a cross-validation of a 1,000-member organelle marker set resulting in a median prediction accuracy of >94% (Itzhak et al., 2016). Principal components analysis of six Dynamic Organellar Maps of ZIP11 generated by the HeLa Spatial Proteome interactive (**Supplementary Figures S2A–F**) database revealed that ZIP11 is present in both the nucleus and some organelle compartments of HeLa cells in roughly equal numbers and is also present in the cytosol (p = 0.0269 when comparing nucleus to cytosol; (**Supplementary Figure S2G**). Finally, using the DEPMAP portal, we confirmed that the wild type HeLa cell line does not harbor either the A234P or the P243S mutation in the ZIP11 gene within its genome (https://depmap.org/portal/cell_line/HELA_CERVIX?tab=mutation). Taken together, the HeLa cell line was determined to be an appropriate model for our studies of ZIP11 in the context of nuclear transport.

ZIP11 Expression Is Required for Proliferation in HeLa Cells

Considering that cervical cancer patients are amongst the higher incident population of individuals with mutations in *ZIP11*, we chose HeLa cervical carcinoma cells as a model to investigate the contributions of this transporter to the cancer phenotype. ZIP11 has been proposed to localize in the nuclei and Golgi, and confocal microscopy analyses of WT cells shows that ZIP11 is primarily located in the perinuclear/nuclear region of the cells and partially colocalized with the Golgi marker Golgin-97 vesicles

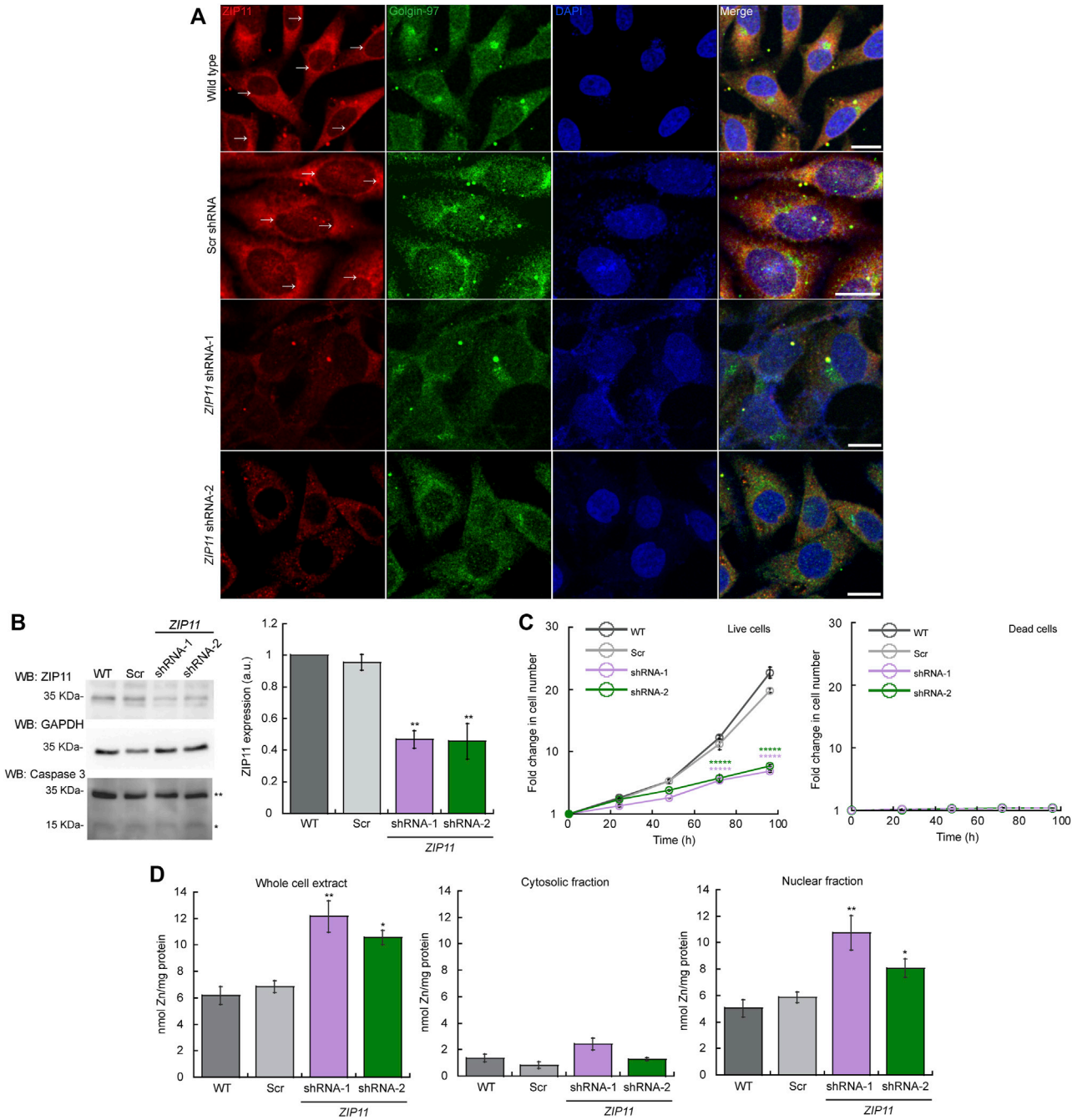

FIGURE 2 | ZIP11 is required for proliferation of HeLa cells and regulates nuclear levels of Zn. **(A)** Representative confocal images showing a perinuclear and cytosolic punctuated pattern of expression of ZIP11 (red) in wild type and scramble (Scr) shRNA transduced HeLa cells. Confocal images of HeLa cells transduced with *ZIP11* shRNA-1 and shRNA-2 show a decrease in the staining around the nucleus and vesicles. shRNA1 and shRNA2 targets the CDS and UTR regions of *ZIP11*, respectively. The anti-Golgi-97 antibody (green) was used as a marker of Golgi apparatus and nuclei was stained with DAPI (blue). Bar = 10 μm. **(B)** Representative immunoblot (left) and quantification (right) of *ZIP11* levels of the 35 KDa (isoform 1) in HeLa proliferating cells for 72 h. *See* **Supplementary Figure S3** for the data of the rest of isoforms. Immunoblots against GAPDH were used as loading controls. Samples were compared to the corresponding wild type sample. An anti-caspase 3 antibody was used to detect cell death in HeLa cells proliferating for 72 h; single asterisk (*) indicate cleaved caspase 3 and double asterisks (**) indicate the full inactive pro-caspase 3 form. **(C)** Cell counting assay of proliferating WT, and cells transduced with scrambled shRNA (shRNA Scr), or *ZIP11* shRNAs. Data represent the fold change in number of live and dead cells as determined by Trypan blue assay. **(D)** Zn levels in proliferating HeLa cells. Wild type and cells stably expressing Scr, shRNA-1 or shRNA-2 against *ZIP11* were allowed to grow for 48 h and subcellular fractions were obtained using the REAP protocol. Whole cell (left) cytosolic (middle) and nuclear (right) Zn content determined by AAS (Suzuki et al., 2010; Gordon et al., 2019a; Tavera-Montañez et al., 2019). For all samples, data are the mean ± SE of three independent biological replicates. *$p < 0.05$; **$p < 0.01$; *****$p < 0.00001$.

(**Figure 2A**). Furthermore, we performed confocal microscopy analyses of ZIP11 and the endoplasmic reticulum (ER) marker calnexin and detected minimal colocalization between these proteins, suggesting no strong association of ZIP11 with the ER on HeLa cells (**Supplementary Figure S3**).

To test the biological role of ZIP11 in the proliferation of HeLa cells, we reduced the expression of the transporter using two different shRNA clones, one which targeted the coding sequence (sh-1) and the other the UTR region (sh-2). Confocal microscopy (**Figure 2A**), and western blot and densitometric analyses of three independent biological replicates (**Figure 2B**) showed the decreased expression of *ZIP11* following this strategy and confirms the specificity of the ZIP11 antibody. According to the https://www.ncbi.nlm.nih.gov/gene?Db=gene&Cmd=DetailsSearch&Term=201266 website, there are 16 known isoforms of the ZIP11 protein expressed in human cells that range from 20 to 36 KDa (**Supplementary Figure S3**). Analyses of the complete membrane showed that the selected antibody likely recognize some of these variants of ZIP11 (**Supplementary Figure S3**). The specific roles of these isoforms are beyond the scope of this work; however we can detect a reduction on their expression with the two shRNAs used in this study. Two higher MW bands are present on the gel. We believe these are non-specific targets in western blot analyses, as quantification of the individual bands/clusters of bands indicates these species are not reduced by the ZIP11 shRNAs whereas the ZIP11 isoforms are reduced by the shRNAs. We focused on the 35 KDa isoform (X1) for our study as it is one of the most common forms expressed in human cells.

Upon reduction of the expression of ZIP11, we detected a significant decrease in the proliferation rate of KD cells (**Figure 2C** left panel). Trypan blue analyses determined that there is no increase in cell death in *ZIP11* KD cells during the experiment (**Figure 2C** right panel), which was verified by western blot analyses against caspase 3 of proliferating HeLa cells at a representative time point of 72 h (**Figure 2B**). We also tested the effect of *ZIP11* KD in the non-carcinogenic cell line HEK273T, isolated from human embryonic kidneys. We observed that upon KD of the transporter there are no significant changes in the proliferation of these cells (**Supplementary Figure S2**). The contrasting results of the effect of *ZIP11* KD on the proliferation rate observed between HeLa and HEK cells suggest that the biological role of the transporter may be dependent on the cellular context and may be a distinctive feature across cell types and tissues.

Therefore, we focused our studies in HeLa cells, as we observed the most dramatic phenotype associated to *ZIP11* KD in this cell line. Considering the location of the transporter, we evaluated the effect of ZIP11 KD on metal accumulation in whole cell extract, cytosolic and nuclear fractions of HeLa cells (**Figure 2D** left, middle and right panels, respectively). ZIP11 has been implicated in nuclear transport of Zn because its expression is dependent on Zn levels; however, *ZIP11* does not exhibit drastic changes upon cellular exposure to this metal, as other metalloprotective genes (Martin et al., 2013; Yu et al., 2013). Therefore, to understand how partial loss of ZIP11 affects accumulation of Zn, we used AAS to measure total metal levels in proliferating HeLa cells (**Figure 2D**). WT and cells transfected with scrambled (Scr) shRNA showed similar content of Zn in whole cell extracts, with Zn mainly located in the nucleus. Importantly, a significant increase in whole cell levels of Zn was observed in the two *ZIP11* KD cell lines with the metal accumulated primarily in the nuclei (**Figure 2D**), suggesting that reduced expression of this transporter impairs the mobilization of the ion from the nucleus to the cytosol. **Supplementary Figure S6** shows a representative western blot of the purity of the cytosolic and nuclear fractions used in the metal content analyses. Tubulin was used as a marker of cytosol and Lamin A/C was used as marker of the nuclear fractions.

We then analyzed the effect of Zn stress on the growth of HeLa cells KD for ZIP11 (**Figure 3**). To this end, cells were cultured in the presence of increasing concentrations of $ZnSO_4$, and counting assays were performed over 5 days. We found that the KD cells had a decrease in proliferation at 75 μM $ZnSO_4$ (**Figure 3C**) compared to non-treated KD and control cells, which were sensitive to higher concentrations of the metal (200 μM; **Figures 3D,E**). These data suggest that ZIP11 may be a regulator of proliferation in HeLa cells by mediating nuclear Zn homeostasis, by potentially mediating appropriate gene expression. However, we cannot overrule alternative mechanisms that lead to a different pathway where *ZIP11* KD also influences the levels of Zn in Golgi and potentially other subcellular organelles which have not been isolated yet, to produce this deleterious effect.

Effect of *ZIP11* KD in HeLa Cells Transcriptome

We performed RNA-seq to investigate global changes in gene expression in proliferating HeLa cells transduced with either the Scr or the two different *ZIP11* shRNAs. The sequenced libraries from the samples had approximately 92M total reads, where the average mapping ratio with the gene is 85.28%. The unique matched reads are shown in **Supplementary Table S4**. Reads were mapped to the human genome (GRCh38/hg38) and gene expression levels were determined. Differentially expressed genes that were significant in both replicates for each shRNA were considered for analysis (log_2FoldChange>1 and <−1). Replicate samples for scramble and *ZIP11* shRNA resulted in Pearson coefficients of >0.94 for each comparison of replicates (**Supplementary Table S4**). Each *ZIP11* KD affected the expression of a similar number of genes, however, there are noticeable differences (**Figures 4A–C**). shRNA-1 affected a total of 4433 genes, of which 2136 were upregulated and 2297 were downregulated (**Figure 4A**), and shRNA-2 affected 5121 genes in total, with 2645 genes upregulated and 2476 downregulated (**Figure 4B**). Both shRNAs shared 2292 differentially expressed genes (DEG) compared to gene expression in the control cells (**Supplementary Table S4** and **Figure 4C**). To identify function-based categories, we performed gene ontology (GO) analysis on DEG that were significant in both replicates for both shRNAs. The complete results are listed in **Supplementary Table S4**. The top 10 significant categories of down-regulated and up-regulated genes shared by both KD cells are shown in **Figures 4D,E**. The top ranked categories of down-regulated genes included regulation of cell migration involved in angiogenesis, metabolism of dicarboxylic acid, regulation of smooth muscle proliferation, and Notch signaling pathway (**Figure 4D** and **Supplementary Table S4**). RNA processing

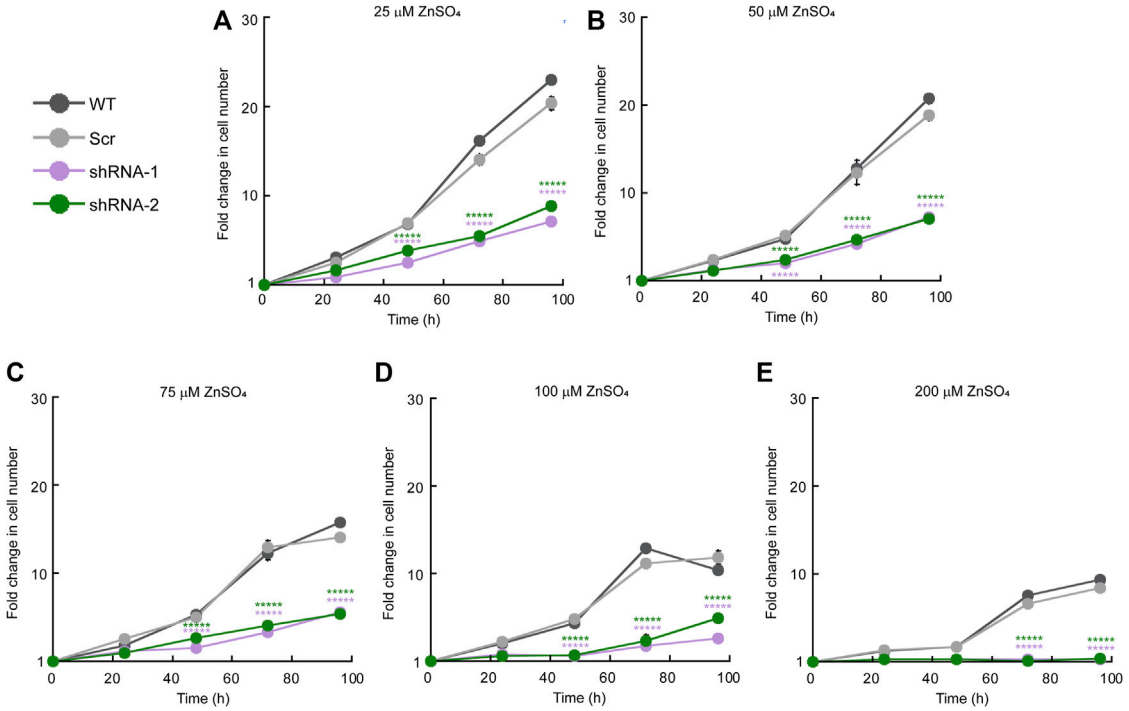

FIGURE 3 | *ZIP11* knockdown results in elevated sensitivity to Zn in HeLa cells. Cell counting assay of proliferating WT, and cells transduced with scrambled shRNA (shRNA Scr), or *ZIP11* shRNAs cultured for 96 h with increasing concentrations of $ZnSO_4$. **(A)** 25 μM. **(B)** 50 μM. **(C)** 75 μM. **(D)** 100 μM. **(E)** 200 μM. Cells were seeded at 1×10^4 cells/cm^2 and the growth for each clone and timepoint was normalized to the seeding density. The data represents the mean ± SE for three independent experiments. *****$p < 0.00001$.

and metabolism were the most remarkable up-regulated categories followed by regulation of cell cycle, but genes involved in the regulation of DNA transcription and termination were also upregulated (**Figure 4E** and **Supplementary Table S4**). A close analysis of genes related to cell growth, DNA repair, senescence, apoptosis, and EMT suggested important changes that may explain the impaired proliferation phenotype and different shapes observed in both KD strains. Some of these genes were validated by qPCR analyses. For instance, the expression of the cell cycle regulatory gene *CDK20* is decreased (**Figure 4F** and **Supplementary Table S4**), and genes related to EMT (*LOXL3* and *FUZ*; **Supplementary Table S4**) are downregulated as well. Interestingly, we found changes in the expression of senescence associated genes, however, these behaved slightly different in both shRNA KD strains. In addition, genes implicated in the negative control of cell growth and division, such as *CDKN2C* and *PPP2CA*, were upregulated (**Figure 4F**). Genes implicated in senescence (*CDKNA* (*p21*) (Pospelova et al., 2009; Noren Hooten and Evans, 2017)) were also upregulated in both cell lines partially depleted for *ZIP11* (**Supplementary Figure S7A** and **Supplementary Table S4**). Additional senescence genes (i.e. *CXCL1*, *CXCL2*, *CSF2*, and *ANKRD1*) presented a small increase in HeLa cells transduced with shRNA2, with minor changes in shRNA1 cells (**Supplementary Table S4**).

Changes were also detected in the expression of the metalloprotective transcription factor, MTF1, and the target gene *METALLOTHIONEIN*, *MT1A* (**Supplementary Figures S7B,C** and **Supplementary Table S4**). However, the RNA-seq analyses showed that the members of the network of Zn exporters and importers, *ZnTs1-8,10* and *ZIPs1-13*, do not present any significant changes in their expression (**Supplementary Table S4**). Only the gene encoding *ZIP14* has a significant and consistent decrease in its expression in both KD HeLa cells. The data suggest that the cells are unable to cope with the nuclear Zn stress produced by the KD of ZIP11, and potentially the impaired growth may be due to a senescent state and decrease in cell cycle progression rate induced by nuclear Zn dysregulation. Distinctive GO categories between shRNA-1 and shRNA-2 are shown in **Supplementary Figure S8**.

Expression of Exogenous ZIP11 Rescues the Proliferation Defect, Restores Nuclear Zn Levels, and Confers Resistance to Elevated Levels of the Metal

To determine whether the lack of ZIP11 and increase in nuclear Zn levels are responsible for the growth defect observed in KD cells, we reintroduced the *ZIP11* gene using a standard protocol of viral transduction and generated clones stably expressing the protein

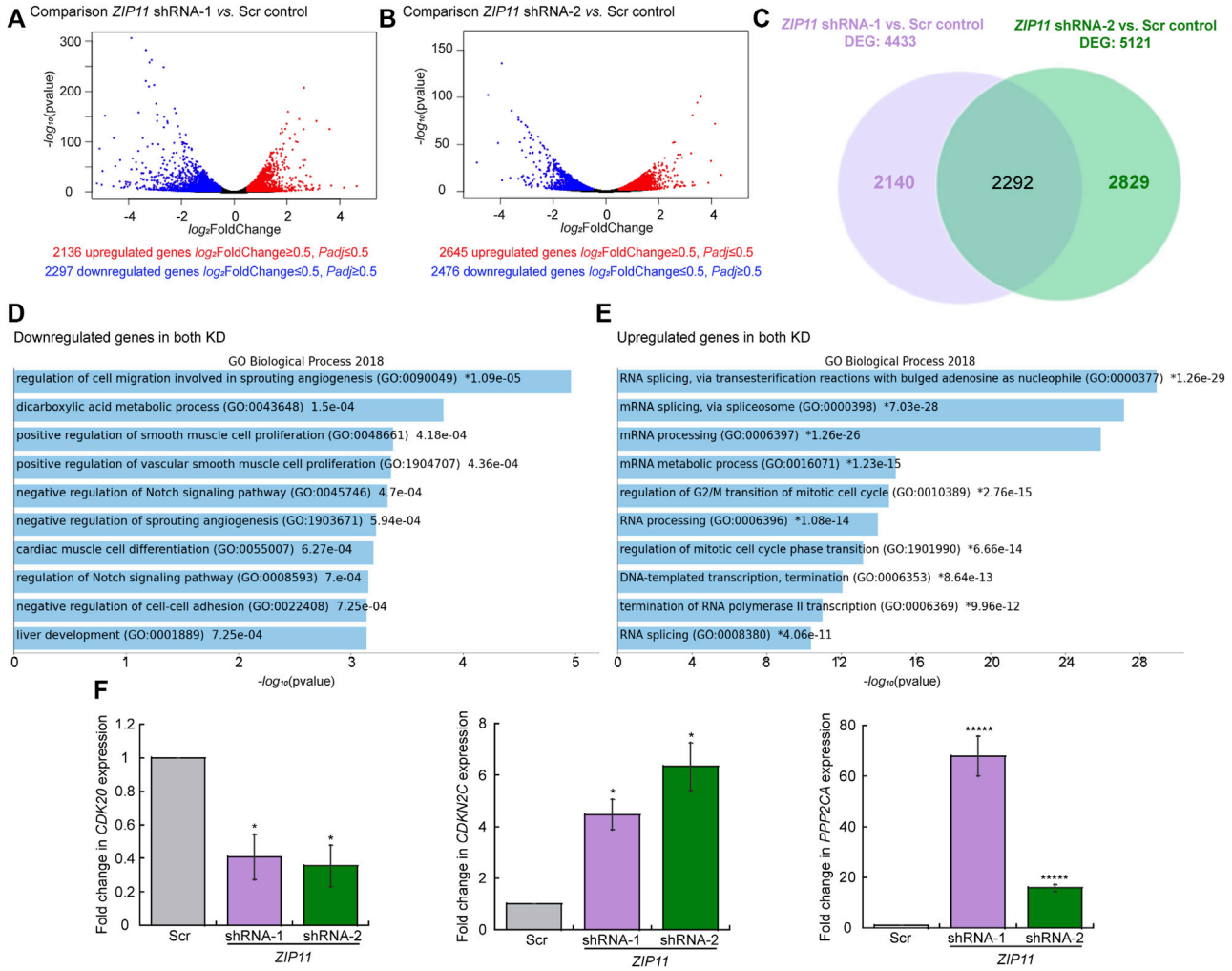

FIGURE 4 | Changes in gene expression dependent on *ZIP11* knockdown in HeLa cells. Volcano plots displaying differentially expressed genes between Scr control and *ZIP11* KD with shRNA1 **(A)** or*shRNA2* **(B)** in HeLa cells. The *y*-axis corresponds to the mean log10 expression levels (*p* values). The red and blue dots represent the up- and down-regulated transcripts in *ZIP11* KD (false-discovery rate [FDR] of <0.05), respectively. The gray dots represent the expression levels of transcripts that did not reach statistical significance (FDR of >0.05). **(C)** Venn diagram showing the overlapping DEG between the two shRNAs used to KD *ZIP11*. GO term analysis of down-regulated **(D)** or up-regulate **(E)** genes consistent in both KD of *ZIP11* in HeLa cells. Cut-off was set at 2.0 of the –log(adjusted *p* value). *See* **Supplementary Table S4** for the complete list of genes and individual GO terms detected for each shRNA using Panther. **(F)** Steady state mRNA levels determined by qRT-PCR of representative downregulated (*CDK20*) and up-regulated (*CDKN2C* and *PPP2CA*) genes selected from the RNA-seq analyses which are associated to cell cycle progression and apoptosis. Data are the mean ± SE for three independent experiments. *$p < 0.05$, *****$p < 0.00001$.

(**Figure 5**). Cells transduced with an empty vector (EV) were used as controls. For the reconstitution experiments, we used cells expressing the shRNA-2 for *ZIP11* KD, as this shRNA recognizes the UTR of the transporter gene. Expression of exogenous ZIP11 was confirmed by immunoblot (**Figure 5A**). Consistent with our RNA-Seq and gene expression profiles, under normal metal conditions, the expression of MTF1 protein was elevated in cells KD for ZIP11 and restored to basal levels in cells expressing exogenous *ZIP11* gene (**Figure 5A**). The proliferation defect detected in *ZIP11* KD cells was rescued upon expression of WT ZIP11 as shown by cell counting assays (**Figure 5B**). Confocal microscopy analyses showed an increase in the staining of ZIP11 in a perinuclear and cytosolic punctuated pattern upon reintroducing the gene to the KD cells (**Figure 5C**). Importantly, the cells expressing ZIP11 also presented a concentration of nuclear Zn similar to the levels of control cells (**Figure 5D** By contrast, the cells transduced with the EV maintained the proliferation defect, reduced levels of the protein in the perinuclear area and maintained elevated levels of the metal in the nucleus (**Figures 5B–D**). We then asked whether reintroduction of the gene would also restore cell resistance to extracellular Zn stress. The cells were grown under increasing concentrations of $ZnSO_4$ and proliferation was determined by cell counting assays. **Figures 5E–I** show that cells expressing the recombinant transporter are less sensitive to Zn stress and can grow at a rate similar to control cells. As expected, the cells transduced with EV were sensitive to extracellular Zn

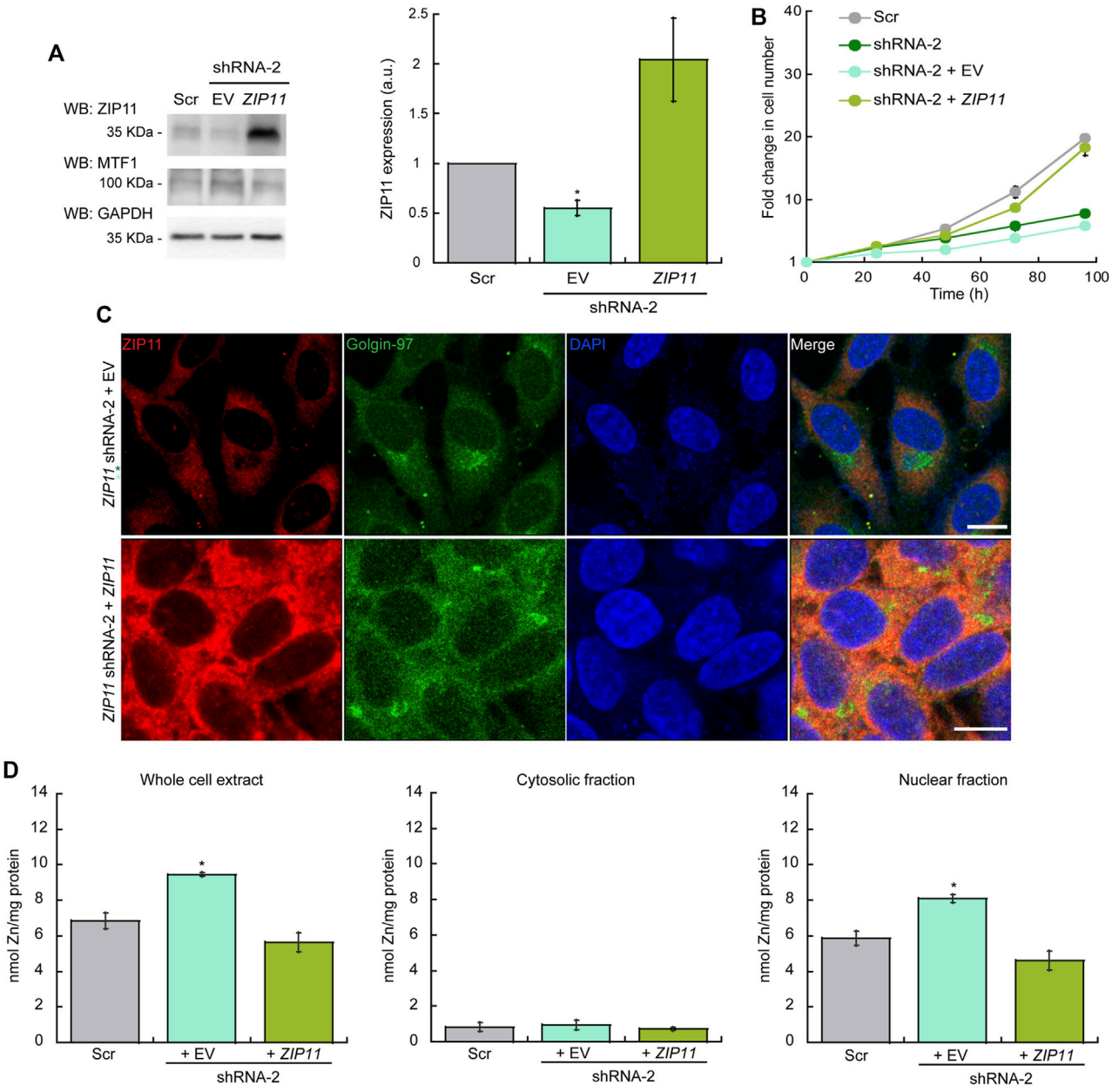

FIGURE 5 | (Continued).

stress as non-transduced cells. Thus, the data supports a role for ZIP11 in maintaining nuclear Zn homeostasis.

Overexpression of Exogenous ZIP11 Exacerbates the Growth of HeLa Cells and Provides Elevated Resistance to External Zn Stress

To further understand the effect of ZIP11 in the proliferation and metal resistance of HeLa cells, we performed overexpression experiments where WT cells were transduced with and stably expressed either the *ZIP11* gene or the EV as a control (**Figure 6**). Evaluation of ZIP11 by western blot shows that cells transduced with the vector encoding the *ZIP11* gene expressed a significantly larger amount of the transporter compared to non-transduced EV-infected control cells (**Figure 6A**). In this case, the levels of MTF1 protein remained constant in the three cell lines tested (**Figure 6A**). Cell proliferation assays revealed that overexpression of *ZIP11* in WT cells enhanced proliferation (**Figure 6B**). Confocal microscopy analyses showed an increased perinuclear and cytosolic punctuated staining for ZIP11 (**Figure 6C**), similar to the observed pattern of reconstitution experiments (**Figure 5C**), though the total, cytosolic, and nuclear

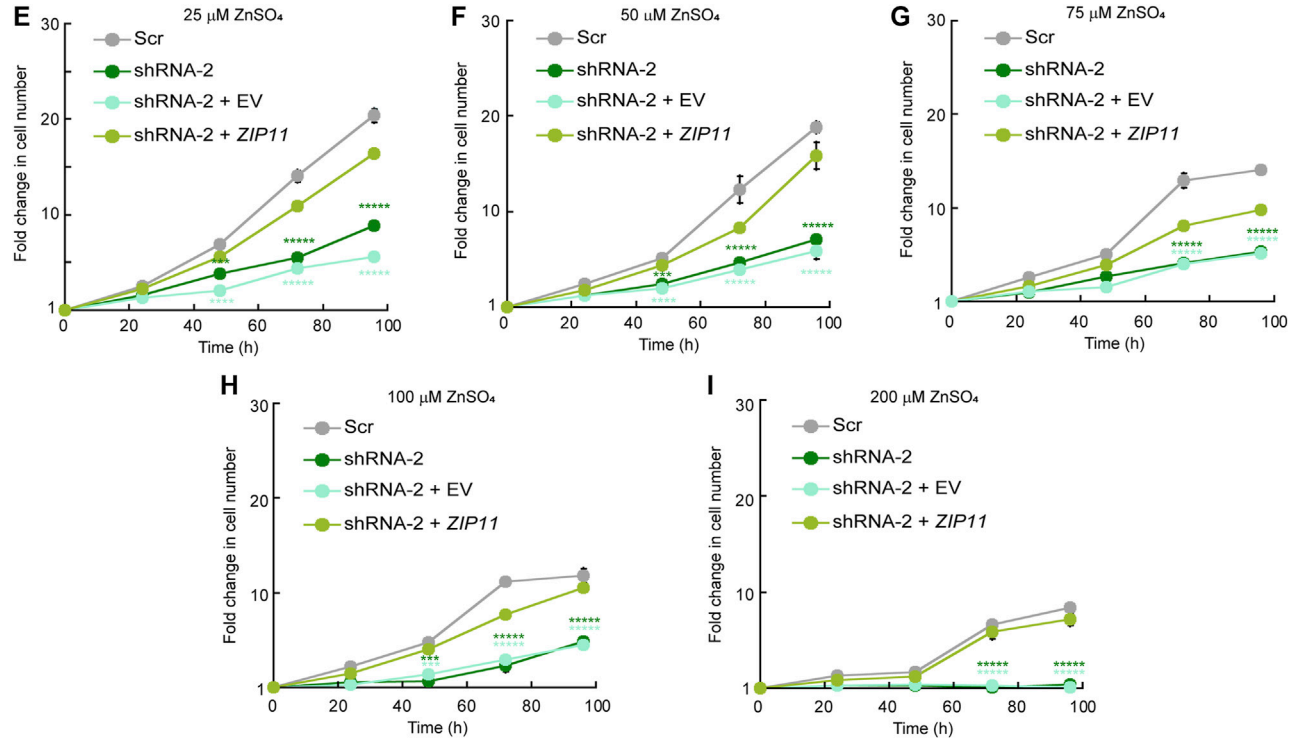

FIGURE 5 | Reintroducing *ZIP11* in HeLa cells restores growth, nuclear Zn levels and resistance to elevated levels of Zn. **(A)** Representative immunoblot (left) and quantification (right) of *ZIP11* levels in HeLa proliferating cells. The cells expressing the shRNA2 against *ZIP11* targeting the UTR region of *ZIP11* were used for reconstitution of phenotypes experiments. Immunoblots against MTF1 shows increased expression of its metalloprotective transcription factor in ZIP11 KD cells. GAPDH was used as loading controls. **(B)** Cell counting assay of proliferating cells transduced with scrambled shRNA (shRNA Scr), or *ZIP11* shRNA-2 expressing exogenous ZIP11 or empty vector (EV). **(C)** Representative confocal micrographies of ZIP11 (red) and Golgin-97 (green) showing the enhanced expression and perinuclear and vesicular distribution of ZIP11 in HeLa cells KD for *ZIP11* (shRNA-2) and stably expressing ZIP11 or the empty vector (EV). Nuclei was stained with DAPI. Bar = 10 μm. **(D)** Distribution of the Zn levels in proliferating HeLa cells. Cells stably expressing Scr, and shRNA-2 against ZIP11 reconstituted with ZIP11 or the empty vector were allowed to grow for 48 h and subcellular fractions were obtained using the REAP protocol. Whole cell (left) cytosolic (middle) and nuclear (right) Zn content determined by AAS (Itzhak et al., 2016; Gordon et al., 2019a; Tavera-Montañez et al., 2019). **(E–I)** Analyses of Zn resistance upon reintroduction of the *ZIP11* gene. Cell counting assay of proliferating cells transduced with scrambled shRNA (shRNA Scr), *ZIP11* shRNA2 expressing the transporter gene or an empty vector, cultured for 96 h with increasing concentrations of ZnSO4. **(E)** 25 μM. **(F)** 50 μM. **(G)** 75 μM. **(H)** 100 μM. **(I)** 200 μM. The data represents the mean ± SE for three independent experiments. *****$p < 0.00001$.For all samples, data are the mean ± SE of three independent biological replicates. *$p < 0.05$; **$p < 0.01$; *****$p < 0.00001$.

levels of Zn remained stable and similar to control cells (**Figure 6C**). Importantly, the cells overexpressing ZIP11 were significantly more resistant to elevated levels of Zn (up to 200 μM) supplemented in the culture media than control cells (**Figures 6D–H**). The data corroborates a function for ZIP11 in maintaining nuclear Zn homeostasis to enable appropriate gene regulation and cell growth.

ZIP11 KD Impairs the Migration and Invasive Properties of HeLa Cells

Cancer cells have several hallmarks and biological functions that promote EMT and metastasis. Thus far, we have evidence showing that ZIP11 is required for the growth of HeLa cells. Therefore, we utilized two functional assays to assess the contributions of ZIP11 to the carcinogenic phenotype of these cells. First, we performed a wound-healing assay, wherein a confluent cell monolayer is scratched and the time and extent of cell migration to close the wound was determined. **Figure 7** shows a time course of representative light microscopy images of the wound-healing assay for WT HeLa cells, cells transduced with Scr, shRNA-1, and shRNA-2, and cells reconstituted and overexpressing *ZIP11* and the EV. Time 0 h indicates the moment when the wound is performed, and subsequent pictures are representative of subsequent time points (taken every 24 h) where the cells were monitored to determine the time needed for the wound to close (**Figure 7A**). Quantification of the area migrated over time showed that the rate of migration of *ZIP11* KD cells into the wound was reduced compared to Scr controls (**Figure 7B**). This deficient migration phenotype was reverted by reintroducing the exogenous *ZIP11* gene into the KD cells (**Figure 7C**), and was enhanced in WT cells overexpressing ZIP11, as these cells fully covered the wound 1 day earlier than the rest of the cells (**Figure 7D**). Thus, directional migration induced by a wound closure is impaired with ZIP11 KD and conversely enhanced by ZIP11 overexpression.

To further investigate the functional consequences of decreasing the expression of ZIP11 in HeLa cells, we also studied their invasive

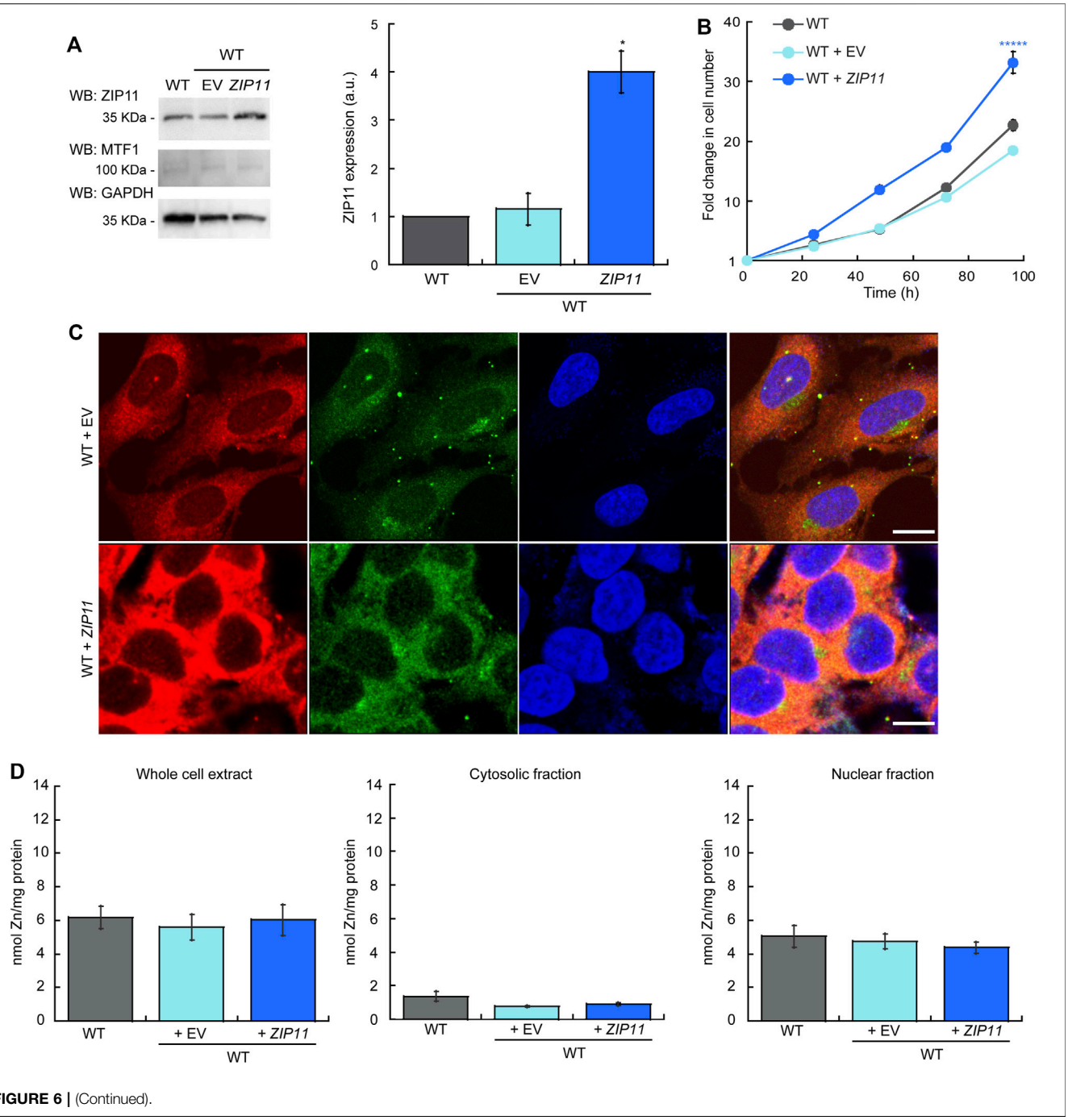

FIGURE 6 | (Continued).

properties through Matrigel, a basement membrane extract. In this experiment, cells were seeded on the top of a polycarbonate membrane with 8 µm pores covered with Matrigel. This model allows invasive cells to cross and invade the opposite side of the membrane, which are then fixed and stained (**Figure 8**). To prevent cell proliferation, the cells were pre-treated with AraC before performing the invasion assays (Olea-Flores et al., 2019; Lacombe et al., 2021). Consistent with the migration results, we found that after 24 h of culture the *ZIP11* KD cells were unable to cross the matrix and the membrane, while control cells could colonize the other side of the membrane (**Figure 8A**). As expected, reconstitution of *ZIP11* gene in the shRNA-2 KD cells recovered the invasive phenotype (**Figure 8B**), and overexpression of the transporter in WT cells exacerbated the effect (**Figure 8C**). On average, the cells overexpressing *ZIP11* had a 3.5-fold increase in number of cells migrating across the Matrigel and the membrane

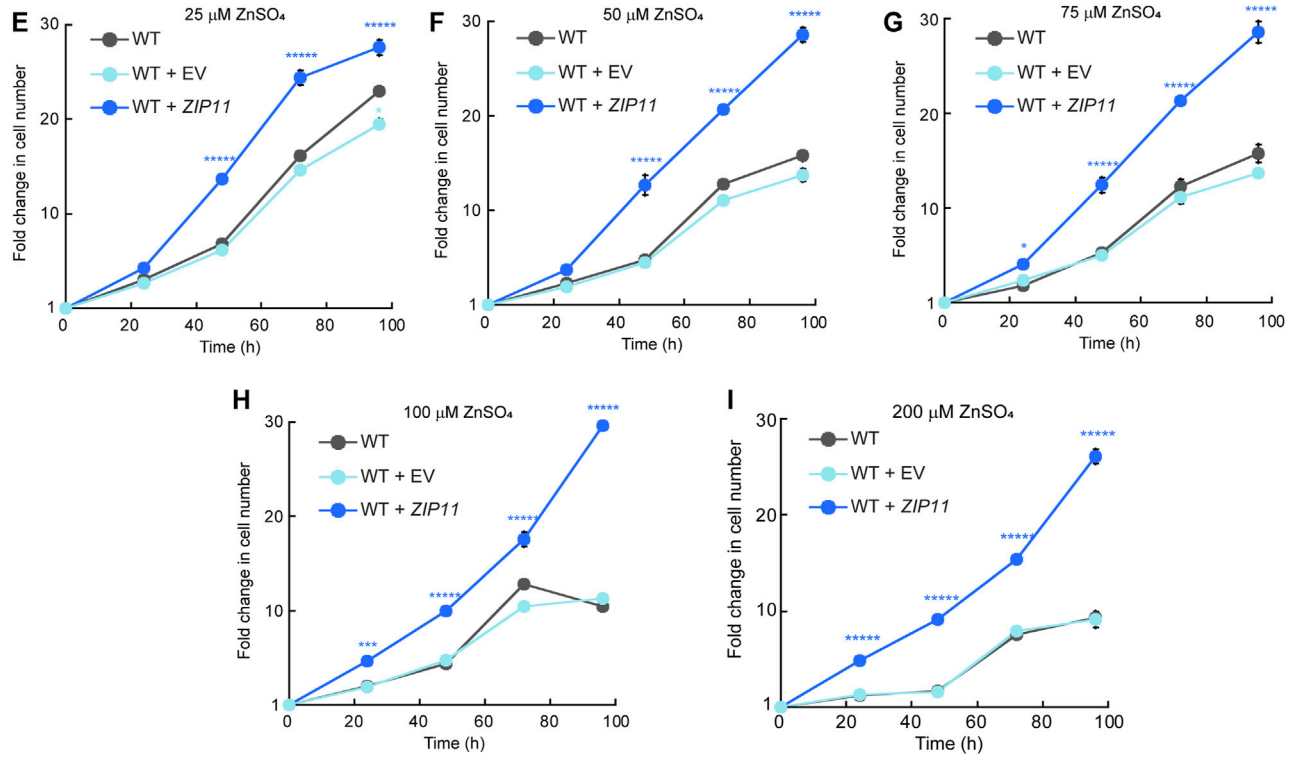

FIGURE 6 | Overexpression of *ZIP11* in WT HeLa enhances growth and resistance to elevated levels of Zn. **(A)** Representative immunoblot (left) and quantification (right) of *ZIP11* levels in HeLa proliferating cells. WT cells were transduced with a plasmid encoding the ZIP11 gene or the empty vector as control. Immunoblots against MTF1 shows no changes in the expression of the metalloprotective transcription factor in WT HeLa cells overexpressing ZIP11. Immunoblot against GAPDH was used as loading control. **(B)** Cell counting assay of proliferating cells WT HeLa cells expressing exogenous ZIP11 or empty vectors. **(C)** Representative confocal micrographies of ZIP11 (red) and Golgin-97 (green) showing the enhanced expression and perinuclear and vesicular distribution of ZIP11 in wild type HeLa cells stably expressing ZIP11 or the empty vector (EV). Nuclei was stained with DAPI. Bar = 10 μm. **(D)** Wild type cells stably expressing ZIP11 or the empty vector were allowed to grow for 48 h and subcellular fractions were obtained using the REAP protocol. Whole cell (left) cytosolic (middle) and nuclear (right) Zn content determined by AAS (Itzhak et al., 2016; Gordon et al., 2019a; Tavera-Montañez et al., 2019). **(E–I)** Analyses of Zn resistance in cells overexpression of the *ZIP11* gene. Cell counting assay of proliferating cells transduced with the *ZIP11* gene or an empty vector, cultured for 96 h with increasing concentrations of ZnSO4. **(E)** 25 μM. **(F)** 50 μM. **(G)** 75 μM. **(H)** 100 μM. **(I)** 200 μM. The data represents the mean ± SE for three independent experiments. For all samples, data are the mean ± SE of three independent biological replicates. $^{*}p < 0.05$; $^{*****}p < 0.00001$.

pores compared to the control cells. Together, these data indicate that the transporter, and potentially nuclear Zn homeostasis, are important players in the development of the migratory and invasive phenotype in cancer cells. The fact that *ZIP11* KD cells have impaired migration and invasion of the Matrigel supports the idea of a potential dormancy or senescent state triggered by nuclear Zn dysregulation. Conversely, the increase in migration and invasion through Matrigel when ZIP11 is overexpressed supports the idea of a role for this transporter in promoting aggressive cancer phenotypes observed in cervical cancer patients (**Figure 1** and **Supplementary Figure S1**).

Alterations in Cell Cycle Progression and in Functional Senescence Markers Reflect a Potential Senescent State of the Cells KD for *ZIP11*

Increasing evidence points to a correlation between DNA damage, cellular senescence, and mitochondrial dysfunction as hallmarks of aging and the onset of various age-related pathologies, such as cancer (Reviewed by (Chapman et al., 2019; Gudmundsrud et al., 2021)). To better understand the growth defect and decreased mobility and invasion properties of HeLa cells KD for *ZIP11,* we tested for changes in cell cycle progression and metabolic changes of the senescence marker β-galactosidase and mitochondrial membrane potential. Our data show that ZIP11 contributes to proliferation and to re-entry into the cell cycle following release from a nocodazole-induced mitotic block, as KD HeLa cells present a delayed progression of the cycle and accumulate in sub G0 after 24 h of arrest (**Figure 9A**). The arrest in sub G0 phase was rescued by reintroduction of exogenous *ZIP11* into the KD cells. Consistent with the enhanced proliferation effect observed in wild type HeLa cells overexpressing the transporter, we detected a small but significant increase of cells in S phase compared to control cells that were largely in G0/G1 stage (**Figure 9B**). This data suggests that ZIP11 contributes, at least in part, to successful transition through cell cycle, which is also

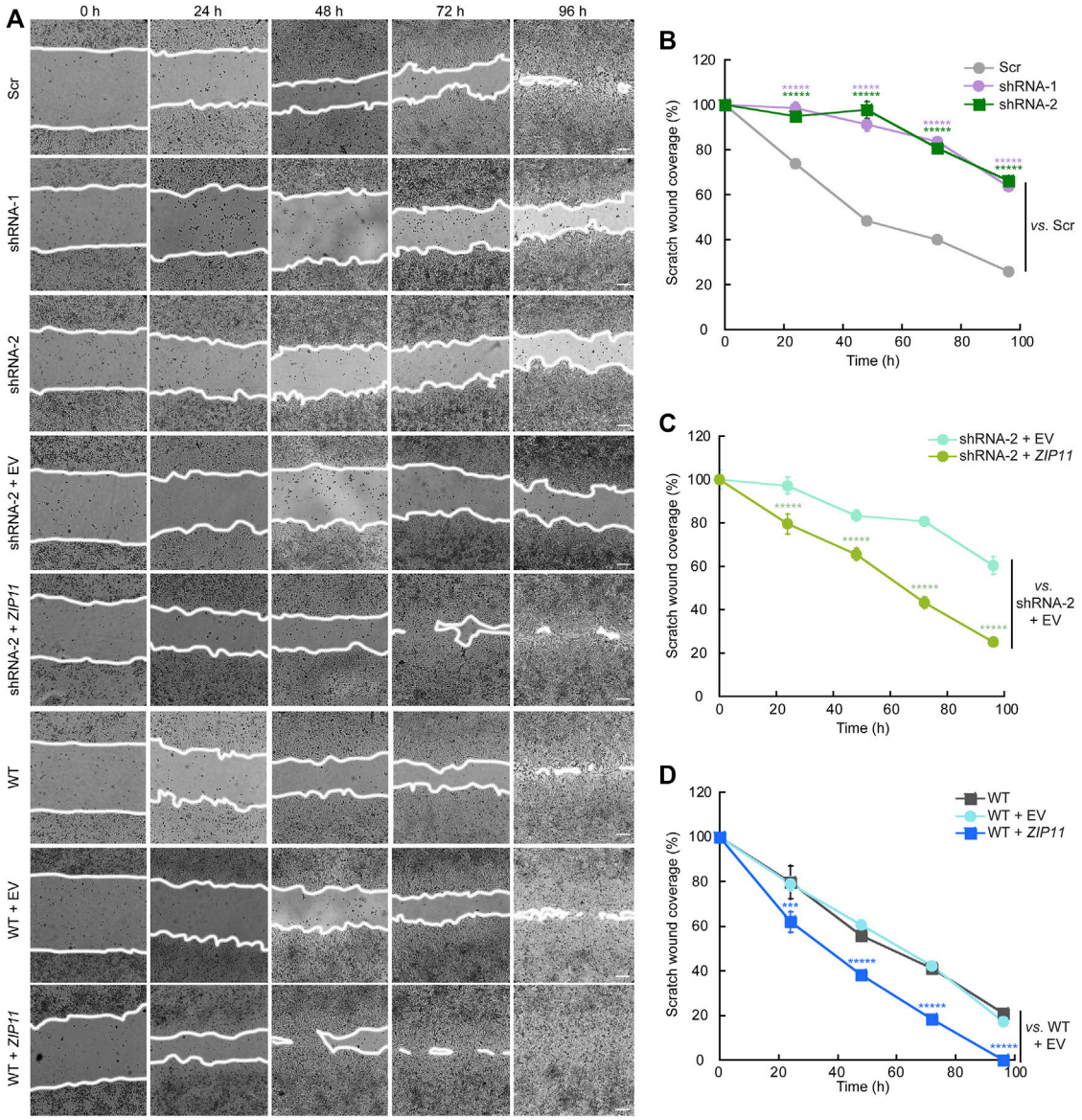

FIGURE 7 | *ZIP11* is required for directional migration of HeLA cells. **(A)** Representative light microscopy images of the wound healing assay of HeLA cells in which *ZIP11* was KD or overexpressed. Time 0 represents confluent monolayer wounds at 0 h and wounds were monitored until the monolayers of WT cells overexpressing *ZIP11* became fully closed 96 h after scratching the monolayer. Images are representative of three independent biological replicates. Scale bar: 100 μm. **(B–D)** Quantification of the area of migration over time shown in **(A)**. **(B)** HeLa cells expressing Scr and both shRNAs against *ZIP11*. **(C)** Data for the reconstitution of phenotype of *ZIP11* KD cells. **(D)** Migration data of non-transduced WT HeLa cells and those overexpressing ZIP11 or the empty vector (EV). Data represents the means ± SE of three independent biological replicates imaged. *****$p < 0.00001$ relative to the samples indicated in the plot.

consistent with the gene expression changes shown in our RNA-seq analyses.

To further provide insight into whether *ZIP11* KD induces a dormant or senescent state in the cells, we performed a classic functional assay of β-galactosidase activity to evaluate senescence in cells. The CellEvent Senescence Green assay relies on a fluorescent probe that contains two galactoside fractions which are targets for β-galactosidase (β-gal), a marker for senescent cells. The activation of the hydrolase activity of β-gal occurs in lysosomes under acidic pH and converts β-galactosides into monosaccharides which remains in the cell and emit a fluorescent signal. **Figure 10A** shows that *ZIP11* KD cells present an increase in the activation of β-gal which is similar to senescent control cells, which was reverted by reintroducing the transporter. Interestingly, a small but not significant decrease in β-gal activity was detected for wild type HeLa cells overexpressing ZIP11 (**Figure 10B**). Finally, we investigated the mitochondrial potential of HeLa cells KD and overexpressing ZIP11 using a TMRE assay as a proxy measure of their metabolic state. TMRE is a positively-charged,

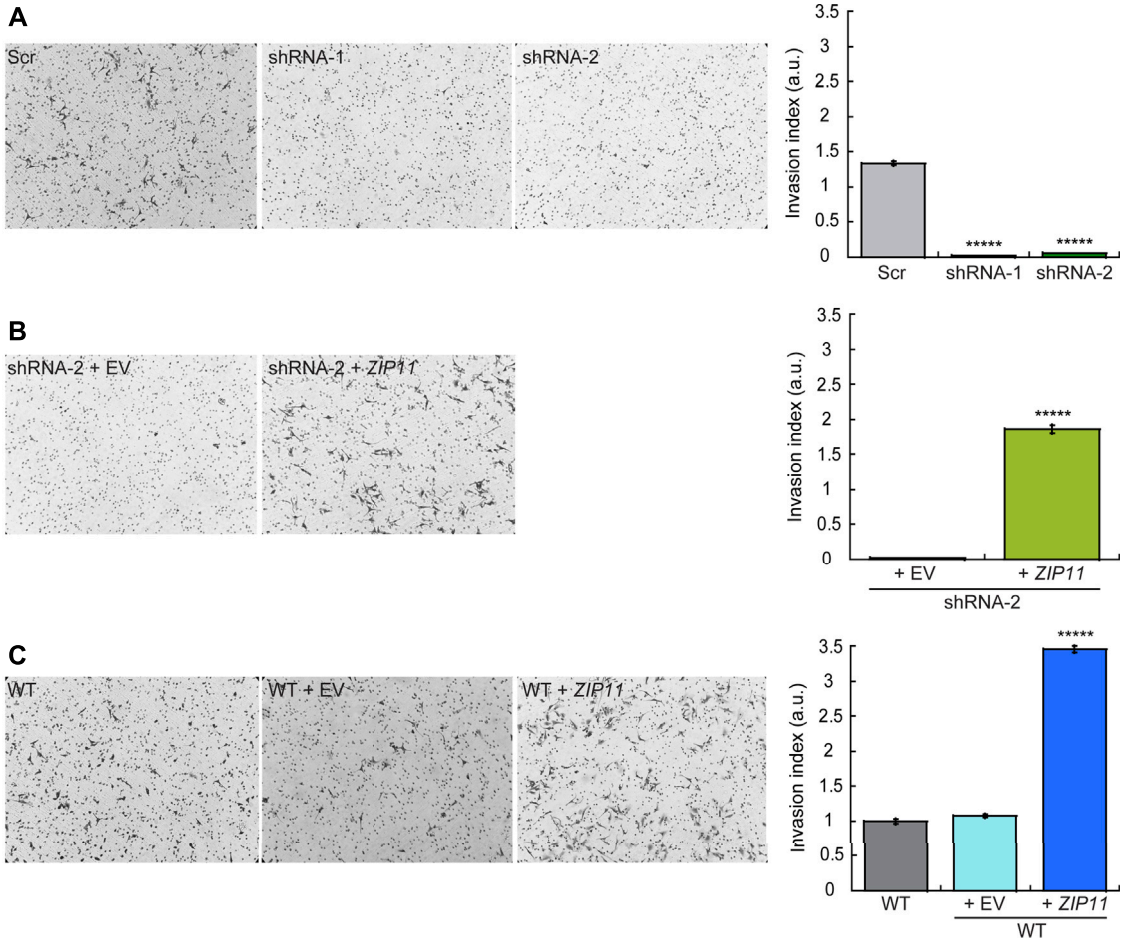

FIGURE 8 | ZIP11 is required for HeLa cells invasion through Matrigel. Representative light microscopy images (left panels) and quantification (right panels) of Matrigel invasion assay at 24 h for HeLa cells in which ZIP11 was KD **(A)**, reconstituted in the shRNA2 strain **(B),** or overexpressed in WT cells **(C)**. The data show the means ± SE of three independent biological replicates imaged and are expressed as the percentage of invading cells compared to the control shown in the plots. *****$p < 0.00001$.

permeable dye that enters the cells and accumulates in active mitochondria, as this organelle presents a relatively high negative charge. When cells have depolarized or their mitochondria are inactive, a decrease in mitochondrial membrane potential consequently impairs the internalization of the TMRE dye. The data show that HeLa cells partially depleted of ZIP11 have a significant decrease in the incorporation of TMRE into the mitochondria compared to control cells, as indicated by a decrease in the intensity of the fluorescent signal of TMRE (**Figure 10C**). This decrease in mitochondrial function and potential can be restored upon reintroduction of the *ZIP11* gene, but not when the cells are transduced with the EV plasmid (**Figure 10C**). No significant changes were detected in TMRE incorporation into the mitochondria of WT cells overexpressing the ZIP11 transporter (**Figure 10D**). Together, the data suggest that nuclear control of Zn homeostasis by ZIP11 contributes to cell cycle progression and establishment of carcinogenic properties in HeLa cells.

DISCUSSION

Cancer development and progression encompasses metabolic changes that rely on the bioavailability of transition metals, like Zn, to promote cell growth and development of metastatic properties. In this work, we provide evidence that ZIP11 is a Zn transporter is located in the perinuclear area and in small vesicles partially associated to Golgi that may contribute to the maintenance of metal homeostasis in the nuclei. We determined the functional significance of ZIP11 expression by decreasing the levels of this transporter using a stable shRNA KD strategy in proliferating HeLa cells. We found that dysregulation of nuclear Zn levels produced by the ZIP11 KD resulted in a delay in cell cycle progression and a potential senescent state in the cells that may be related to DNA damage, as suggested by the alterations in expression of cell cycle and some senescence genes (Pospelova et al., 2009). RNA-Seq analyses also showed that angiogenic, EMT-related, and apoptotic genes were dysregulated. In terms of expression of additional Zn

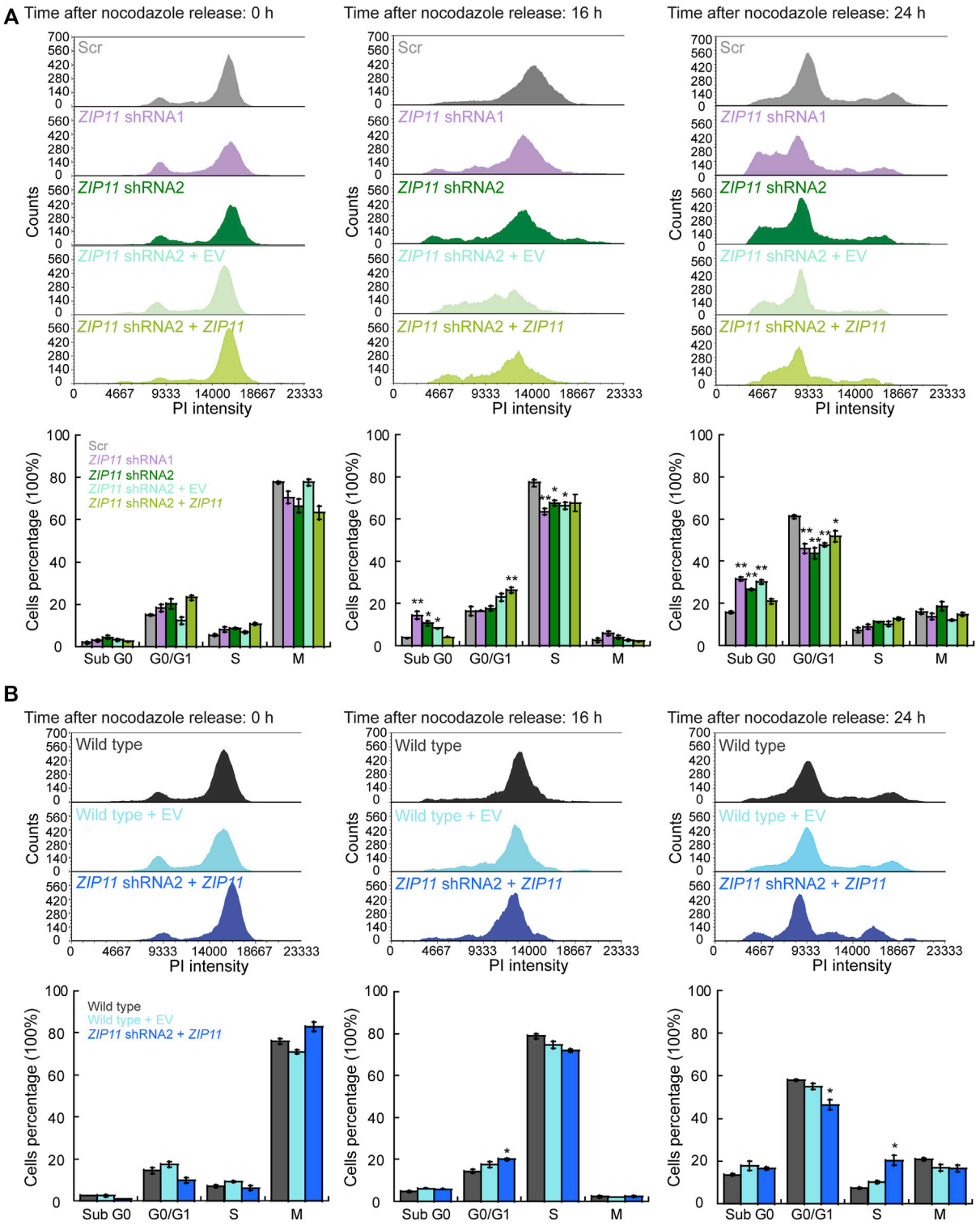

FIGURE 9 | Knockdown of ZIP11 alters cell cycle progression. Representative histograms of cell cycle progression (top panels) and percentage of cells in each cell cycle phase (bottom panel). **(A)** HeLa cells transduced with Scr, *ZIP11* shRNA1 or shRNA2 and reconstituted with an empty vector or *ZIP11* gene. **(B)** Wild type HeLa cells transduced with an empty vector or overexpressing *ZIP11*. Plots show cells arrested in mitosis with nocodazole at the time of release (0 h), and after 16 and 24 h post-release. The data are representative of three independent biological experiments. $^{*}p < 0.05$; $^{**}p < 0.01$.

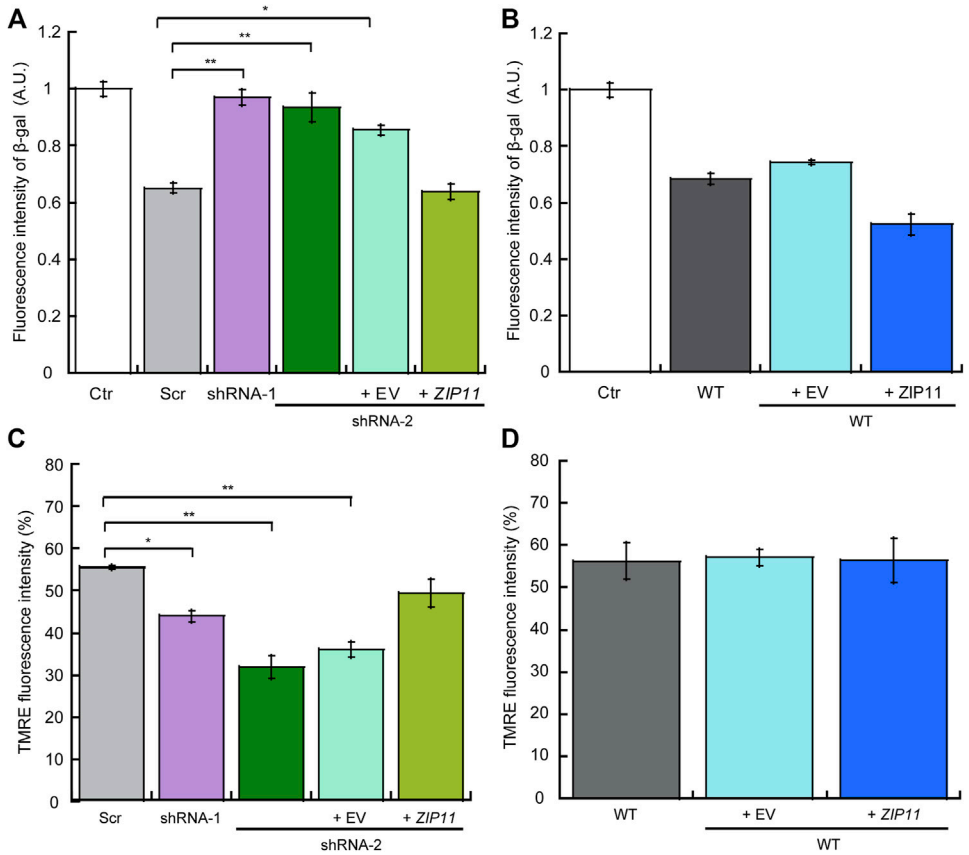

FIGURE 10 | Knockdown of ZIP11 induces a senescent state which correlates with decreased mitochondrial potential in HeLa cells. Detection of cellular senescence *via* activation of β-galactosidase hydrolysis, a marker for senescent cells, in Scr, *ZIP11* KD cells and reconstituted with exogenous *ZIP11* **(A)** or wild type cells over expressing the transporter **(B)**. WT HeLa cells treated with 5 mM Palbociclib were used as a positive control for senescence (Ctr). Data was normalized to Palbociclib treated cells. Mitochondrial membrane potential was measured by staining cells KD for ZIP11, reconstituted **(C)** or overexpressing **(D)** the exogenous gene with 200 nM TMRE and the percentage of fluorescence intensity of three independent biological replicates was plotted. Data show means ± SE of three independent biological replicates imaged. $^{*}p < 0.05$, $^{**}p < 0.01$ relative to control.

transporters, ZIPs and ZNTs, we detected no significant changes on their gene expression, which suggested that ZIP11 KD cells fail to compensate for the nuclear metal stress induced by ZIP11 malfunction. In the context of cancer patients, altered levels of Zn have been considered an indicator of tumor burden and disease progression (Prasad and Kucuk, 2002; Prasad et al., 2009). Zn defects promote the expression of the tumor suppressor p53 and affect the DNA binding capacity of several transcription factors, including p53, the nuclear factor κB (NFκB), and AP-1 in various models of cancer (Ho and Ames, 2002; Yan et al., 2008; Ho and Song, 2009). Zn is also proposed to repress tumor growth by decreasing angiogenesis, and by promoting the expression of inflammatory cytokines and apoptotic genes in cancer cells (Boehm et al., 1998; Prasad et al., 2009). Studies in murine models demonstrated that Zn treatment increases resistance against tumor growth and decreases the occurrence of spontaneous lung tumors in mice undergoing anti-carcinogenic therapies (Singh et al., 1992; Satoh et al., 1993). Consistent with these findings, Zn deficiency in rats enhances the proliferation and expression of cell cycle markers and promotes development of tumors derived from esophageal cells stimulated with the tumorigenic agent N-nitrosomethylbezylamine. This effect can be reduced by dietary Zn supplementation by inducing apoptosis (Wangu et al., 1996). Although existing evidence supports an anti-cancer role for Zn, there is still lack of understanding of the direct and indirect mechanisms by which Zn impacts cancer cells biology.

ZIP11 KD cells not only accumulated nuclear Zn and failed to proliferate, but also showed a decrease in migration and invasive properties, as well as a reduction in mitochondrial membrane potential, and increased β-gal activity, which supports the hypothesis of a potential senescent state (Passos et al., 2006; Passos and von Zglinicki, 2012; Gudmundsrud et al., 2021). These phenotypes were reverted by reintroducing the WT transporter into the *ZIP11* KD cells. Consistent with these data, enhanced proliferation, migration, and invasive features were detected in WT HeLa cells overexpressing ZIP11. Interestingly, the levels of nuclear Zn in cells overexpressing the transporter were similar to those in WT control cells. This phenotype can be partially explained by the fact that no free Zn is found in the nucleus,

and that nuclear Zn-binding proteins may have higher affinity to the ion and require the metal for proper function. Therefore, it is plausible that these proteins will not release the Zn even if the transporter expression increase. Importantly, confocal microscopy analyses showed elevated levels of ZIP11 in cytosolic vesicles, and some partially associated to Golgi. It is plausible that additional components of such vesicles contribute to the enhanced carcinogenic phenotype observed in cells overexpressing the transporters. The nature of such vesicles, their constituents and biological relevance remain to be characterized. Taken together, these data indicate that ZIP11 is essential for the proliferation and development of carcinogenic properties of the cervical cancer model, HeLa cells. This transporter may play a relevant role in the regulation of gene expression in the HeLa cell cancer model, which is in agreement with the correlation of a deleterious effect observed in cervical cancer patients that present elevated levels of ZIP11.

It is well known that senescence is a biological process that occurs in response to various stress stimuli under normal and pathological conditions. For instance, senescence can occur as a consequence of oncogene activation, chromatin and nuclear alterations, and oxidative stress (Kuilman et al., 2010). Senescence was also proposed to be a process that prevents cell replication when DNA damage occurs, and it is an efficient way to prevent cancer development and tumor progression (Campisi, 2001a; Campisi, 2001b). Interestingly, Zn has been shown to have a positive effect on DNA repair, which would prevent cancer development derived from DNA damage (Reviewed by (Yildiz et al., 2019)). Senescence is also known to suppress cancer by stopping the growth of pre-malignant cells, and it has been shown to be an important component for wound healing as well (Demaria et al., 2014). Experiments using a murine model in which senescent cells can be visualized and removed showed that senescent fibroblasts and endothelial cells appear very early in response to a cutaneous wound and promote the healing of the wound *via* the platelet-derived growth factor AA pathway (Demaria et al., 2014). From our observations in *ZIP11* KD HeLa cells, we proposed that the potential senescent phenotype resulting from nuclear Zn dysbalance impairs malignant cell mobilization. This rationale may also apply to the phenotype observed in the migratory properties of the model presented here. In conclusion, we propose a novel mechanism whereby elevated levels of Zn in the nuclei of cells lacking *ZIP11* is a contributing stress factor that impairs cell growth and other events associated with cancer cell biology (migration and invasion) by inducing a senescent state. This work highlights the importance of ZIP11, an understudied metal transporter, in cancer development and progression, and provides a foundation for future mechanistic and drug development studies that may target ZIP11 in patients affected by this disease.

DATA AVAILABILITY STATEMENT

The datasets presented in this study can be found in online repositories. The names of the repository/repositories and accession number(s) can be found in the article/ **Supplementary Material**. RNA-seq datasets are available at GEO. The accession number is: GSE198411

AUTHOR CONTRIBUTIONS

TP-B conceived and designed the research; MO-F, JK, AC, CS, CM, HR, AM, JN, and TP-B performed experiments and compiled data; MO-F, JK, SS, CM, VM, AM, JN, LC, and TP-B analyzed data; TP-B and LC prepared figures and tables; TP-B drafted the manuscript; all authors edited and revised the manuscript; all authors approved the final version of the manuscript.

FUNDING

This work was funded by Wesleyan University institutional funds and by NIH grant R01AR077578 to TP-B.

ACKNOWLEDGMENTS

The authors are thankful to Anthony N. Imbalzano, Jose Argüello and Jeffrey Gilarde for their critical comments and technical assistance on this manuscript.

SUPPLEMENTARY MATERIAL

The Supplementary Material for this article can be found online at: https://www.frontiersin.org/articles/10.3389/fcell.2022.895433/full#supplementary-material

REFERENCES

Angireddy, R., Chowdhury, A. R., Zielonka, J., Ruthel, G., Kalyanaraman, B., and Avadhani, N. G. (2020). Alcohol-induced CYP2E1, Mitochondrial Dynamics and Retrograde Signaling in Human Hepatic 3D Organoids. *Free Radic. Biol. Med.* 159, 1–14. doi:10.1016/j.freeradbiomed.2020.06.030

Antala, S., and Dempski, R. E. (2012). The Human ZIP4 Transporter Has Two Distinct Binding Affinities and Mediates Transport of Multiple Transition Metals. *Biochemistry* 51, 963–973. doi:10.1021/bi201553p

Audic, S., and Claverie, J.-M. (1997). The Significance of Digital Gene Expression Profiles. *Genome Res.* 7, 986–995. doi:10.1101/gr.7.10.986

Barresi, V., Valenti, G., Spampinato, G., Musso, N., Castorina, S., Rizzarelli, E., et al. (2018). Transcriptome Analysis Reveals an Altered Expression Profile of Zinc Transporters in Colorectal Cancer. *J. Cell Biochem.* 119, 9707–9719. doi:10.1002/jcb.27285

Bendl, J., Stourac, J., Salanda, O., Pavelka, A., Wieben, E. D., Zendulka, J., et al. (2014). PredictSNP: Robust and Accurate Consensus Classifier for Prediction of Disease-Related Mutations. *PLoS Comput. Biol.* 10, e1003440. doi:10.1371/journal.pcbi.1003440

Bin, B.-H., Fukada, T., Hosaka, T., Yamasaki, S., Ohashi, W., Hojyo, S., et al. (2011). Biochemical Characterization of Human ZIP13 Protein. *J. Biol. Chem.* 286, 40255–40265. doi:10.1074/jbc.m111.256784

Boehm, T., O'Reilly, M. S. M., Keough, K., Shiloach, J., Shapiro, R., and Folkman, J. (1998). Zinc-binding of Endostatin Is Essential for its Antiangiogenic Activity. *Biochem. biophysical Res. Commun.* 252, 190–194. doi:10.1006/bbrc.1998.9617

Bradford, M. M. (1976). A Rapid and Sensitive Method for the Quantitation of Microgram Quantities of Protein Utilizing the Principle of Protein-Dye Binding. *Anal. Biochem.* 72, 248–254. doi:10.1016/0003-2697(76)90527-3

Broun, E. R., Greist, A., Tricot, G., and Hoffman, R. (1990). Excessive Zinc Ingestion. *Jama* 264, 1441–1443. doi:10.1001/jama.1990.03450110087033

Campisi, J. (2001). Cellular Senescence as a Tumor-Suppressor Mechanism. *Trends Cell Biol.* 11, S27–S31. doi:10.1016/s0962-8924(01)82148-6

Campisi, J. (2001). Cellular Senescence, Aging and Cancer. *TheScientificWorldJournal* 1, 65. doi:10.1100/tsw.2001.23.106

Chapman, J., Fielder, E., and Passos, J. F. (2019). Mitochondrial Dysfunction and Cell Senescence: Deciphering a Complex Relationship. *FEBS Lett.* 593, 1566–1579. doi:10.1002/1873-3468.13498

Chowanadisai, W., Graham, D. M., Keen, C. L., Rucker, R. B., and Messerli, M. A. (2013). Neurulation and Neurite Extension Require the Zinc Transporter ZIP12 (Slc39a12). *Proc. Natl. Acad. Sci. U.S.A.* 110, 9903–9908. doi:10.1073/pnas.1222142110

Chowdhury, A. R., Zielonka, J., Kalyanaraman, B., Hartley, R. C., Murphy, M. P., and Avadhani, N. G. (2020). Mitochondria-targeted Paraquat and Metformin Mediate ROS Production to Induce Multiple Pathways of Retrograde Signaling: A Dose-dependent Phenomenon. *Redox Biol.* 36, 101606. doi:10.1016/j.redox.2020.101606

Collins, F. S., Guyer, M. S., and Chakravarti, A. (1997). Variations on a Theme: Cataloging Human DNA Sequence Variation. *Science* 278, 1580–1581. doi:10.1126/science.278.5343.1580

Colvin, R. A., Bush, A. I., Volitakis, I., Fontaine, C. P., Thomas, D., Kikuchi, K., et al. (2008). Insights into Zn2+homeostasis in Neurons from Experimental and Modeling Studies. *Am. J. Physiology-Cell Physiology* 294, C726–C742. doi:10.1152/ajpcell.00541.2007

Demaria, M., Ohtani, N., Youssef, S. A., Rodier, F., Toussaint, W., Mitchell, J. R., et al. (2014). An Essential Role for Senescent Cells in Optimal Wound Healing through Secretion of PDGF-AA. *Dev. cell* 31, 722–733. doi:10.1016/j.devcel.2014.11.012

Dempski, R. E. (2012). The Cation Selectivity of the ZIP Transporters. *Curr. Top. Membr.* 69, 221–245. doi:10.1016/b978-0-12-394390-3.00009-4

Devirgiliis, C., Zalewski, P. D., Perozzi, G., and Murgia, C. (2007). Zinc Fluxes and Zinc Transporter Genes in Chronic Diseases. *Mutat. Research/Fundamental Mol. Mech. Mutagen.* 622, 84–93. doi:10.1016/j.mrfmmm.2007.01.013

Dufner-Beattie, J., Langmade, S. J., Wang, F., Eide, D., and Andrews, G. K. (2003). Structure, Function, and Regulation of a Subfamily of Mouse Zinc Transporter Genes. *J. Biol. Chem.* 278, 50142–50150. doi:10.1074/jbc.m304163200

Dufner-Beattie, J., Wang, F., Kuo, Y.-M., Gitschier, J., Eide, D., and Andrews, G. K. (2003). The Acrodermatitis Enteropathica Gene ZIP4 Encodes a Tissue-specific, Zinc-Regulated Zinc Transporter in Mice. *J. Biol. Chem.* 278, 33474–33481. doi:10.1074/jbc.m305000200

Eide, D. J. (2006). Zinc Transporters and the Cellular Trafficking of Zinc. *Biochimica Biophysica Acta (BBA) - Mol. Cell Res.* 1763, 711–722. doi:10.1016/j.bbamcr.2006.03.005

Fischer, P. W., Giroux, A., and L'Abbé, M. R. (1981). The Effect of Dietary Zinc on Intestinal Copper Absorption. *Am. J. Clin. Nutr.* 34, 1670–1675. doi:10.1093/ajcn/34.9.1670

Fujishiro, H., Yano, Y., Takada, Y., Tanihara, M., and Himeno, S. (2012). Roles of ZIP8, ZIP14, and DMT1 in Transport of Cadmium and Manganese in Mouse Kidney Proximal Tubule Cells. *Metallomics* 4, 700–708. doi:10.1039/c2mt20024d

Gaither, L. A., and Eide, D. J. (2001). Eukaryotic Zinc Transporters and Their Regulation. *Biometals* 14, 251–270. doi:10.1023/a:1012988914300

Gaither, L. A., and Eide, D. J. (2000). Functional Expression of the Human hZIP2 Zinc Transporter. *J. Biol. Chem.* 275, 5560–5564. doi:10.1074/jbc.275.8.5560

Gaither, L. A., and Eide, D. J. (2001). The Human ZIP1 Transporter Mediates Zinc Uptake in Human K562 Erythroleukemia Cells. *J. Biol. Chem.* 276, 22258–22264. doi:10.1074/jbc.m101772200

Gao, J., Zhao, N., Knutson, M. D., and Enns, C. A. (2008). The Hereditary Hemochromatosis Protein, HFE, Inhibits Iron Uptake via Down-Regulation of Zip14 in HepG2 Cells. *J. Biol. Chem.* 283, 21462–21468. doi:10.1074/jbc.m803150200

Girijashanker, K., He, L., Soleimani, M., Reed, J. M., Li, H., Liu, Z., et al. (2008). Slc39a14 Gene Encodes ZIP14, a Metal/bicarbonate Symporter: Similarities to the ZIP8 Transporter. *Mol. Pharmacol.* 73, 1413–1423. doi:10.1124/mol.107.043588

Gordon, S. J. V., Fenker, D. E., Vest, K. E., and Padilla-Benavides, T. (2019). Manganese Influx and Expression of ZIP8 Is Essential in Primary Myoblasts and Contributes to Activation of SOD_2. *Metallomics* 11 (6), 1140–1153. doi:10.1039/c8mt00348c

Gordon, S. J. V., Xiao, Y., Paskavitz, A. L., Navarro-Tito, N., Navea, J. G., and Padilla-Benavides, T. (2019). Atomic Absorbance Spectroscopy to Measure Intracellular Zinc Pools in Mammalian Cells. *J. Vis. Exp.* 1, 1. doi:10.3791/59519

Gudmundsrud, R., Skjånes, T. H., Gilmour, B. C., Caponio, D., Lautrup, S., and Fang, E. F. (2021). Crosstalk Among DNA Damage, Mitochondrial Dysfunction, Impaired Mitophagy, Stem Cell Attrition, and Senescence in the Accelerated Ageing Disorder Werner Syndrome. *Cytogenet Genome Res.* 161, 297–304. doi:10.1159/000516386

Haase, H., and Rink, L. (2014). Zinc Signals and Immune Function. *Biofactors* 40, 27–40. doi:10.1002/biof.1114

Hambidge, M. (2000). Human Zinc Deficiency. *J. Nutr.* 130, 1344S–1349S. doi:10.1093/jn/130.5.1344s

Ho, E., and Ames, B. N. (2002). Low Intracellular Zinc Induces Oxidative DNA Damage, Disrupts P53, NFκB, and AP1 DNA Binding, and Affects DNA Repair in a Rat Glioma Cell Line. *Proc. Natl. Acad. Sci. U.S.A.* 99, 16770–16775. doi:10.1073/pnas.222679399

Ho, E., and Song, Y. (2009). Zinc and Prostatic Cancer. *Curr. Opin. Clin. Nutr. Metabolic Care* 12, 640–645. doi:10.1097/mco.0b013e32833106ee

Hojyo, S., Fukada, T., Shimoda, S., Ohashi, W., Bin, B.-H., Koseki, H., et al. (2011). The Zinc Transporter SLC39A14/ZIP14 Controls G-Protein Coupled Receptor-Mediated Signaling Required for Systemic Growth. *PloS one* 6, e18059. doi:10.1371/journal.pone.0018059

Hu, J. (2021). Toward Unzipping the ZIP Metal Transporters: Structure, Evolution, and Implications on Drug Discovery against Cancer. *Febs J.* 288, 5805–5825. doi:10.1111/febs.15658

Huang, L., and Kirschke, C. P. (2007). A Di-leucine Sorting Signal in ZIP1 (SLC39A1) Mediates Endocytosis of the Protein. *FEBS J.* 274, 3986–3997. doi:10.1111/j.1742-4658.2007.05933.x

Itzhak, D. N., Tyanova, S., Cox, J., and Borner, G. H. (2016). Global, Quantitative and Dynamic Mapping of Protein Subcellular Localization. *eLife* 5, 1. doi:10.7554/eLife.16950

Jenkitkasemwong, S., Wang, C.-Y., Coffey, R., Zhang, W., Chan, A., Biel, T., et al. (2015). SLC39A14 Is Required for the Development of Hepatocellular Iron Overload in Murine Models of Hereditary Hemochromatosis. *Cell metab.* 22, 138–150. doi:10.1016/j.cmet.2015.05.002

Jenkitkasemwong, S., Wang, C.-Y., Mackenzie, B., and Knutson, M. D. (2012). Physiologic Implications of Metal-Ion Transport by ZIP14 and ZIP8. *Biometals* 25, 643–655. doi:10.1007/s10534-012-9526-x

Jeong, J., and Eide, D. J. (2013). The SLC39 Family of Zinc Transporters. *Mol. aspects Med.* 34, 612–619. doi:10.1016/j.mam.2012.05.011

Kaida, A., Sawai, N., Sakaguchi, K., and Miura, M. (2011). Fluorescence Kinetics in HeLa Cells after Treatment with Cell Cycle Arrest Inducers Visualized with Fucci (Fluorescent Ubiquitination-Based Cell Cycle Indicator). *Cell. Biol. Int.* 35, 359–363. doi:10.1042/cbi20100643

Kambe, T., Hashimoto, A., and Fujimoto, S. (2014). Current Understanding of ZIP and ZnT Zinc Transporters in Human Health and Diseases. *Cell. Mol. Life Sci.* 71, 3281–3295. doi:10.1007/s00018-014-1617-0

Kambe, T., Tsuji, T., Hashimoto, A., and Itsumura, N. (2015). The Physiological, Biochemical, and Molecular Roles of Zinc Transporters in Zinc Homeostasis and Metabolism. *Physiol. Rev.* 95, 749–784. doi:10.1152/physrev.00035.2014

Kamphans, T., Sabri P Fau - Zhu, N., Zhu N Fau - Heinrich, V., Heinrich V Fau - Mundlos, S., Mundlos S Fau - Robinson, P. N., Robinson Pn Fau - Parkhomchuk, D., et al. (2013). Filtering for Compound Heterozygous Sequence Variants in Non-consanguineous Pedigrees. *Plos One* 8 (8), e70151. doi:10.1371/journal.pone.0070151

Kang, X., Chen, R., Zhang, J., Li, G., Dai, P.-G., Chen, C., et al. (2015). Expression Profile Analysis of Zinc Transporters (ZIP4, ZIP9, ZIP11, ZnT9) in Gliomas and Their Correlation with IDH1 Mutation Status. *Asian Pac. J. Cancer Prev.* 16, 3355–3360. doi:10.7314/apjcp.2015.16.8.3355

Kelleher, S. L., and Lönnerdal, B. (2003). Zn Transporter Levels and Localization Change throughout Lactation in Rat Mammary Gland and Are Regulated by Zn in Mammary Cells. *J. Nutr.* 133, 3378–3385. doi:10.1093/jn/133.11.3378

Kelleher, S. L., Velasquez, V., Croxford, T. P., McCormick, N. H., Lopez, V., and MacDavid, J. (2012). Mapping the Zinc-Transporting System in Mammary Cells: Molecular Analysis Reveals a Phenotype-dependent Zinc-Transporting Network during Lactation. *J. Cell. Physiol.* 227, 1761–1770. doi:10.1002/jcp.22900

Kim, D., Langmead, B., and Salzberg, S. L. (2015). HISAT: a Fast Spliced Aligner with Low Memory Requirements. *Nat. Methods* 12, 357–360. doi:10.1038/nmeth.3317

Kim, D., Xiao, Y., Karchere-Sun, R., Richmond, E., Ricker, H. M., Leonardi, A., et al. (2020). Atmospheric Processing of Anthropogenic Combustion Particles: Effects of Acid Media and Solar Flux on the Iron Mobility from Fly Ash. *ACS Earth Space Chem.* 4, 750–761. doi:10.1021/acsearthspacechem.0c00057

Krezel, A., and Maret, W. (2006). Zinc-buffering Capacity of a Eukaryotic Cell at Physiological pZn. *J. Biol. Inorg. Chem.* 11, 1049–1062. doi:10.1007/s00775-006-0150-5

Kuilman, T., Michaloglou, C., Mooi, W. J., and Peeper, D. S. (2010). The Essence of Senescence: Figure 1. *Genes Dev.* 24, 2463–2479. doi:10.1101/gad.1971610

Lacombe, M.-L., Lamarche, F., De Wever, O., Padilla-Benavides, T., Carlson, A., Khan, I., et al. (2021). The Mitochondrially-Localized Nucleoside Diphosphate Kinase D (NME4) Is a Novel Metastasis Suppressor. *BMC Biol.* 19, 228. doi:10.1186/s12915-021-01155-5

Langmead, B., and Salzberg, S. L. (2012). Fast Gapped-Read Alignment with Bowtie 2. *Nat. Methods* 9, 357–359. doi:10.1038/nmeth.1923

Li, B., and Dewey, C. N. (2011). RSEM: Accurate Transcript Quantification from RNA-Seq Data with or without a Reference Genome. *BMC Bioinforma.* 12, 323. doi:10.1186/1471-2105-12-323

Lichten, L. A., and Cousins, R. J. (2009). Mammalian Zinc Transporters: Nutritional and Physiologic Regulation. *Annu. Rev. Nutr.* 29, 153–176. doi:10.1146/annurev-nutr-033009-083312

Lichten, L. A., Ryu, M.-S., Guo, L., Embury, J., and Cousins, R. J. (2011). MTF-1-mediated Repression of the Zinc Transporter Zip10 Is Alleviated by Zinc Restriction. *PloS one* 6, e21526. doi:10.1371/journal.pone.0021526

Lin, W., Chai, J., Love, J., and Fu, D. (2010). Selective Electrodiffusion of Zinc Ions in a Zrt-, Irt-like Protein, ZIPB*. *J. Biol. Chem.* 285, 39013–39020. doi:10.1074/jbc.m110.180620

Liu, Z., Li, H., Soleimani, M., Girijashanker, K., Reed, J. M., He, L., et al. (2008). Cd2+ versus Zn2+ Uptake by the ZIP8 HCO3--dependent Symporter: Kinetics, Electrogenicity and Trafficking. *Biochem. biophysical Res. Commun.* 365, 814–820. doi:10.1016/j.bbrc.2007.11.067

Liuzzi, J. P., Aydemir, F., Nam, H., Knutson, M. D., and Cousins, R. J. (2006). Zip14 (Slc39a14) Mediates Non-transferrin-bound Iron Uptake into Cells. *Proc. Natl. Acad. Sci. U.S.A.* 103, 13612–13617. doi:10.1073/pnas.0606424103

Liuzzi, J. P., Bobo, J. A., Lichten, L. A., Samuelson, D. A., and Cousins, R. J. (2004). Responsive Transporter Genes within the Murine Intestinal-Pancreatic axis Form a Basis of Zinc Homeostasis. *Proc. Natl. Acad. Sci. U.S.A.* 101, 14355–14360. doi:10.1073/pnas.0406216101

Livak, K. J., and Schmittgen, T. D. (2001). Analysis of Relative Gene Expression Data Using Real-Time Quantitative PCR and the 2−ΔΔCT Method. *Methods* 25, 402–408. doi:10.1006/meth.2001.1262

Love, M. I., Huber, W., and Anders, S. (2014). Moderated Estimation of Fold Change and Dispersion for RNA-Seq Data with DESeq2. *Genome Biol.* 15, 550. doi:10.1186/s13059-014-0550-8

Mao, X., Kim, B.-E., Wang, F., Eide, D. J., and Petris, M. J. (2007). A Histidine-Rich Cluster Mediates the Ubiquitination and Degradation of the Human Zinc Transporter, hZIP4, and Protects against Zinc Cytotoxicity. *J. Biol. Chem.* 282, 6992–7000. doi:10.1074/jbc.m610552200

Maret, W., and Sandstead, H. H. (2006). Zinc Requirements and the Risks and Benefits of Zinc Supplementation. *J. Trace Elem. Med. Biol.* 20, 3–18. doi:10.1016/j.jtemb.2006.01.006

Martin, A. B., Aydemir, T. B., Guthrie, G. J., Samuelson, D. A., Chang, S.-M., and Cousins, R. J. (2013). Gastric and Colonic Zinc Transporter ZIP11 (Slc39a11) in Mice Responds to Dietary Zinc and Exhibits Nuclear Localization. *J. Nutr.* 143, 1882–1888. doi:10.3945/jn.113.184457

Noren Hooten, N., and Evans, M. K. (2017). Techniques to Induce and Quantify Cellular Senescence. *J. Vis. Exp.* 1, 55533. doi:10.3791/55533

Ogiso, T., Ogawa, N., and Miura, T. (1979). Inhibitory Effect of High Dietary Zinc on Copper Absorption in Rats. II. Binding of Copper and Zinc to Cytosol Proteins in the Intestinal Mucosa. *Chem. Pharm. Bull.* 27, 515–521. doi:10.1248/cpb.27.515

Olea-Flores, M., Zuñiga-Eulogio, M., Tacuba-Saavedra, A., Bueno-Salgado, M., Sánchez-Carvajal, A., Vargas-Santiago, Y., et al. (2019). Leptin Promotes Expression of EMT-Related Transcription Factors and Invasion in a Src and FAK-dependent Pathway in MCF10A Mammary Epithelial Cells. *Cells* 8, 1133. doi:10.3390/cells8101133

Outten, C. E., and O'Halloran, a. T. V. (2001). Femtomolar Sensitivity of Metalloregulatory Proteins Controlling Zinc Homeostasis. *Science* 292, 2488–2492. doi:10.1126/science.1060331

Palmiter, R. D., and Findley, S. D. (1995). Cloning and Functional Characterization of a Mammalian Zinc Transporter that Confers Resistance to Zinc. *EMBO J.* 14, 639–649. doi:10.1002/j.1460-2075.1995.tb07042.x

Paskavitz, A. L., Quintana, J., Cangussu, D., Tavera-Montañez, C., Xiao, Y., Ortiz-Miranda, S., et al. (2018). Differential Expression of Zinc Transporters Accompanies the Differentiation of C2C12 Myoblasts. *J. Trace Elem. Med. Biol.* 49, 27–34. doi:10.1016/j.jtemb.2018.04.024

Passos, J. F., and von Zglinicki, T. (2012). Mitochondrial Dysfunction and Cell Senescence - Skin Deep into Mammalian Aging. *Aging* 4, 74–75. doi:10.18632/aging.100432

Passos, J. F., Zglinicki, T. v., and Saretzki, G. (2006). Mitochondrial Dysfunction and Cell Senescence: Cause or Consequence? *Rejuvenation Res.* 9, 64–68. doi:10.1089/rej.2006.9.64

Pertea, M., Pertea, G. M., Antonescu, C. M., Chang, T.-C., Mendell, J. T., and Salzberg, S. L. (2015). StringTie Enables Improved Reconstruction of a Transcriptome from RNA-Seq Reads. *Nat. Biotechnol.* 33, 290–295. doi:10.1038/nbt.3122

Pinilla-Tenas, J. J., Sparkman, B. K., Shawki, A., Illing, A. C., Mitchell, C. J., Zhao, N., et al. (2011). Zip14 Is a Complex Broad-Scope Metal-Ion Transporter Whose Functional Properties Support Roles in the Cellular Uptake of Zinc and Nontransferrin-Bound Iron. *Am. J. Physiology-Cell PhysiologyCell physiology* 301, C862–C871. doi:10.1152/ajpcell.00479.2010

Pospelova, T. V., Demidenko, Z. N., Bukreeva, E. I., Pospelov, V. A., Gudkov, A. V., and Blagosklonny, M. V. (2009). Pseudo-DNA Damage Response in Senescent Cells. *Cell Cycle* 8, 4112–4118. doi:10.4161/cc.8.24.10215

Prasad, A. S., Beck, F. W. J., Snell, D. C., and Kucuk, O. (2009). Zinc in Cancer Prevention. *Nutr. cancer* 61, 879–887. doi:10.1080/01635580903285122

Prasad, A. S., and Kucuk, O. (2002). Zinc in Cancer Prevention. *Cancer Metastasis Rev.* 21, 291–295. doi:10.1023/a:1021215111729

Qin, Y., Dittmer, P. J., Park, J. G., Jansen, K. B., and Palmer, A. E. (2011). Measuring Steady-State and Dynamic Endoplasmic Reticulum and Golgi Zn 2+ with Genetically Encoded Sensors. *Proc. Natl. Acad. Sci. U.S.A.* 108, 7351–7356. doi:10.1073/pnas.1015686108

Rafi, M. A., Coppola S Fau - Liu, S. L., Liu Sl Fau - Rao, H. Z., Rao Hz Fau - Wenger, D. A., and Wenger, D. A. (2003). Disease-causing Mutations in Cis with the Common Arylsulfatase A Pseudodeficiency Allele Compound the Difficulties in Accurately Identifying Patients and Carriers of Metachromatic Leukodystrophy. *Mol. Genet. Metab.* 79 (2), 83–90. doi:10.1016/s1096-7192(03)00076-3

Risch, N., and Merikangas, K. (1996). The Future of Genetic Studies of Complex Human Diseases. *Science* 273, 1516–1517. doi:10.1126/science.273.5281.1516

Rost, B., Yachdav, G., and Liu, J. (2004). The PredictProtein Server. *Nucleic Acids Res.* 32, W321–W326. doi:10.1093/nar/gkh377

Sandstead, H. H. (2013). Human Zinc Deficiency: Discovery to Initial Translation. *Adv. Nutr.* 4, 76–81. doi:10.3945/an.112.003186

Satoh, M., Kondo, Y., Mita, M., Nakagawa, I., Naganuma, A., and Imura, N. (1993). Prevention of Carcinogenicity of Anticancer Drugs by Metallothionein Induction. *Cancer Res.* 53, 4767–4768.

Schindelin, J., Arganda-Carreras, I., Frise, E., Kaynig, V., Longair, M., Pietzsch, T., et al. (2012). Fiji: an Open-Source Platform for Biological-Image Analysis. *Nat. Methods* 9, 676–682. doi:10.1038/nmeth.2019

Sensi, S. L., Canzoniero, L. M. T., Yu, S. P., Ying, H. S., Koh, J.-Y., Kerchner, G. A., et al. (1997). Measurement of Intracellular Free Zinc in Living Cortical Neurons: Routes of Entry. *J. Neurosci.* 17, 9554–9564. doi:10.1523/jneurosci.17-24-09554.1997

Singh, K. P., Zaidi, S. I. A., Raisuddin, S., Saxena, A. K., Murthy, R. C., and Ray, P. K. (1992). Effect of Zinc on Immune Functions and Host Resistance against Infection and Tumor Challenge. *Immunopharmacol. Immunotoxicol.* 14, 813–840. doi:10.3109/08923979209009237

Suzuki, K., Bose, P., Leong-Quong, R. Y., Fujita, D. J., and Riabowol, K. (2010). REAP: A Two Minute Cell Fractionation Method. *BMC Res. Notes* 3, 294. doi:10.1186/1756-0500-3-294

Takeda, A., and Tamano, H. (2009). Insight into Zinc Signaling from Dietary Zinc Deficiency. *Brain Res. Rev.* 62, 33–44. doi:10.1016/j.brainresrev.2009.09.003

Tavera-Montañez, C., Hainer, S. J., Cangussu, D., Gordon, S. J. V., Xiao, Y., Reyes-Gutierrez, P., et al. (2019). The Classic Metal-Sensing Transcription Factor MTF1 Promotes Myogenesis in Response to Copper. *Faseb J.* 33, 14556–14574. doi:10.1096/fj.201901606R

Taylor, K. M., Hiscox, S., Nicholson, R. I., Hogstrand, C., and Kille, P. (2012). Protein Kinase CK2 Triggers Cytosolic Zinc Signaling Pathways by Phosphorylation of Zinc Channel ZIP7. *Sci. Signal* 5, ra11. doi:10.1126/scisignal.2002585

Taylor, K. M. (2000). LIV-1 Breast Cancer Protein Belongs to New Family of Histidine-Rich Membrane Proteins with Potential to Control Intracellular Zn 2+ Homeostasis. *IUBMB Life (International Union Biochem. Mol. Biol. Life)* 49, 249–253. doi:10.1080/15216540050033087

Taylor, K. M., Morgan, H. E., Johnson, A., and Nicholson, R. I. (2005). Structure-function Analysis of a Novel Member of the LIV-1 Subfamily of Zinc Transporters, ZIP14. *FEBS Lett.* 579, 427–432. doi:10.1016/j.febslet.2004.12.006

Taylor, K. M., and Nicholson, R. I. (2003). The LZT Proteins; the LIV-1 Subfamily of Zinc Transporters. *Biochimica Biophysica Acta (BBA) - Biomembr.* 1611, 16–30. doi:10.1016/s0005-2736(03)00048-8

Thiers, R. E., and Vallee, B. L. (1957). Distribution of Metals in Subcellular Fractions of Rat Liver. *J. Biol. Chem.* 226, 911–920. doi:10.1016/s0021-9258(18)70877-6

Trapnell, C., Williams, B. A., Pertea, G., Mortazavi, A., Kwan, G., van Baren, M. J., et al. (2010). Transcript Assembly and Quantification by RNA-Seq Reveals Unannotated Transcripts and Isoform Switching during Cell Differentiation. *Nat. Biotechnol.* 28, 511–515. doi:10.1038/nbt.1621

Vallee, B. L., and Falchuk, K. H. (1993). The Biochemical Basis of Zinc Physiology. *Physiol. Rev.* 73, 79–118. doi:10.1152/physrev.1993.73.1.79

Vinkenborg, J. L., Nicolson, T. J., Bellomo, E. A., Koay, M. S., Rutter, G. A., and Merkx, M. (2009). Genetically Encoded FRET Sensors to Monitor Intracellular Zn2+ Homeostasis. *Nat. Methods* 6, 737–740. doi:10.1038/nmeth.1368

Wang, F., Kim, B.-E., Petris, M. J., and Eide, D. J. (2004). The Mammalian Zip5 Protein Is a Zinc Transporter that Localizes to the Basolateral Surface of Polarized Cells. *J. Biol. Chem.* 279, 51433–51441. doi:10.1074/jbc.m408361200

Wangu, Q.-S., Sabourin, C. L. K., Wang, H., and Stoner, G. D. (1996). Overexpression of Cyclin D1 and Cyclin E in N-Nitrosomethylbezylamine-Induced Rat Esophageal Tumorigenesis. *Carcinogenesis* 17, 1583–1588. doi:10.1093/carcin/17.8.1583

Weaver, B. P., Dufner-Beattie, J., Kambe, T., and Andrews, G. K. (2007). Novel Zinc-Responsive Post-transcriptional Mechanisms Reciprocally Regulate Expression of the Mouse Slc39a4 and Slc39a5 Zinc Transporters (Zip4 and Zip5). *Biol. Chem.* 388, 1301–1312. doi:10.1515/bc.2007.149

Wu, F. Y. H., and Wu, C. W. (1987). Zinc in DNA Replication and Transcription. *Annu. Rev. Nutr.* 7, 251–272. doi:10.1146/annurev.nu.07.070187.001343

Wu, L., Chaffee, K. G., Parker, A. S., Sicotte, H., and Petersen, G. M. (2015). Zinc Transporter Genes and Urological Cancers: Integrated Analysis Suggests a Role for ZIP11 in Bladder Cancer. *Tumor Biol.* 36, 7431–7437. doi:10.1007/s13277-015-3459-2

Yan, M., Song, Y., Wong, C. P., Hardin, K., and Ho, E. (2008). Zinc Deficiency Alters DNA Damage Response Genes in Normal Human Prostate Epithelial Cells. *J. Nutr.* 138, 667–673. doi:10.1093/jn/138.4.667

Yildiz, A., Kaya, Y., and Tanriverdi, O. (2019). Effect of the Interaction between Selenium and Zinc on DNA Repair in Association with Cancer Prevention. *J. Cancer Prev.* 24, 146–154. doi:10.15430/jcp.2019.24.3.146

Yu, Y., Wu, A., Zhang, Z., Yan, G., Zhang, F., Zhang, L., et al. (2013). Characterization of the GufA Subfamily Member SLC39A11/Zip11 as a Zinc Transporter. *J. Nutr. Biochem.* 24, 1697–1708. doi:10.1016/j.jnutbio.2013.02.010

Zhang, T., Liu, J., Fellner, M., Zhang, C., Sui, D., and Hu, J. (2017). Crystal Structures of a ZIP Zinc Transporter Reveal a Binuclear Metal Center in the Transport Pathway. *Sci. Adv.* 3, e1700344. doi:10.1126/sciadv.1700344

Zhu, B., Huo, R., Zhi, Q., Zhan, M., Chen, X., and Hua, Z.-C. (2021). Increased Expression of Zinc Transporter ZIP4, ZIP11, ZnT1, and ZnT6 Predicts Poor Prognosis in Pancreatic Cancer. *J. Trace Elem. Med. Biol.* 65, 126734. doi:10.1016/j.jtemb.2021.126734

Conflict of Interest: The authors declare that the research was conducted in the absence of any commercial or financial relationships that could be construed as a potential conflict of interest.

The reviewer SC declared a shared affiliation with the author LAC to the handling editor at the time of review.

Supplementary Material

ZIP11 regulates nuclear zinc homeostasis in HeLa cells and is required for proliferation and establishment of the carcinogenic phenotype.

Monserrat Olea-Flores[1,2], Julia Kan[1], Alyssa Carlson[1,3], Sabriya A. Syed[1], Cat McCann[1], Varsha Mondal[1], Cecily Szady[4], Heather M. Ricker[4], Amy McQueen[1], Juan G. Navea[4], Leslie A. Caromile[5], Teresita Padilla-Benavides[1]*

[1] Department of Molecular Biology and Biochemistry, Wesleyan University, Middletown, CT, 06459, USA

[2] Department of Biochemistry and Molecular Biotechnology, University of Massachusetts Chan Medical School, Worcester, MA, 01605, USA

[3] Current affiliation: Tisch Multiple Sclerosis Research Center of New York, New York, NY, 10019, USA

[4] Department of Chemistry, Skidmore College, Saratoga Springs, NY, USA

[5] Center for Vascular Biology, Department of Cell Biology, UCONN Health-Center, Farmington, Connecticut 06030-3501, United States

*Correspondence: T.P.-B. tpadillabena@wesleyan.edu

SUPPLEMENTARY FIGURES

SUPPLEMENTARY FIGURE 1

TGCA-UCEC	Uterine Corpus Endometrial Carcinoma
TCGA-SKCM	Skin Cutaneous Melanoma
TGCA-STAD	Stomach Adenocarcinoma
TGCA-COAD	Colon Adenocarcinoma
TGCA-LUAD	Lung Adenocarcinoma
TCGA-READ	Rectum Adenocarcinoma
TGCA-MESO	Mesothelioma
TGCA-ESCA	Esophageal Carcinoma
TCGA-CESC	Cervical Squamous Cell Carcinoma and Endovervical Adenocarcinoma
CPTAC-2	CPTAC-Breast, Colon, Ovary
CPTAC-3	CPTAC-Brain, Head and Neck, Kidney, Lung, Pancreas, Uterus
TGCA-THYM	Thymoma
TCGA-OV	Ovarian Serous Cystadenocarcinoma
TGCA-LUSC	Lung Squamous Cell Carcinoma
TGCA-KIRC	Kidney Renal Clear Cell Carcinoma
TCGA-GBM	Glioblastoma Multiforme
TCGA-BLCA	Bladder Urothelial Carcinoma
TCGA-HNSC	Head and NEck Squamous Cell Carcinoma
TCGA-LIHC	Liver Hepatocelullar Carcinoma
TCGA-BRCA	Breast Invasive Carcinoma
MMRF-COMMPASS	Plasma Cell Tumors

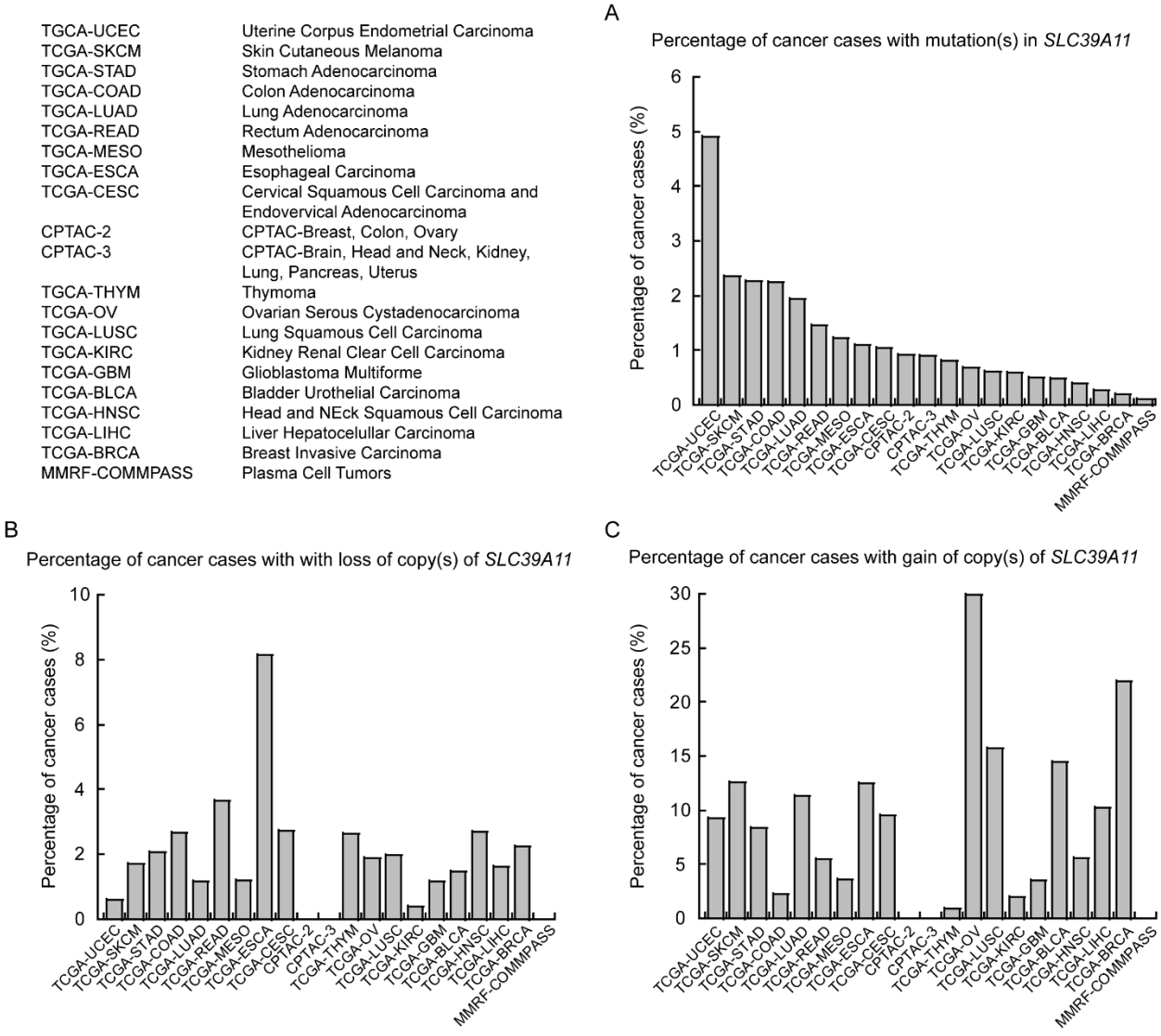

Supplementary Figure 1. Analyses of ZIP11 expression and mutation rate in patients obtained from TCGA database. (A) Incidence of mutations for ZIP11 gene occurs in cancer patients. Percentage of patients with loss **(B)** or gain **(C)** of function of the *ZIP11* gene.

SUPPLEMENTARY FIGURE 2

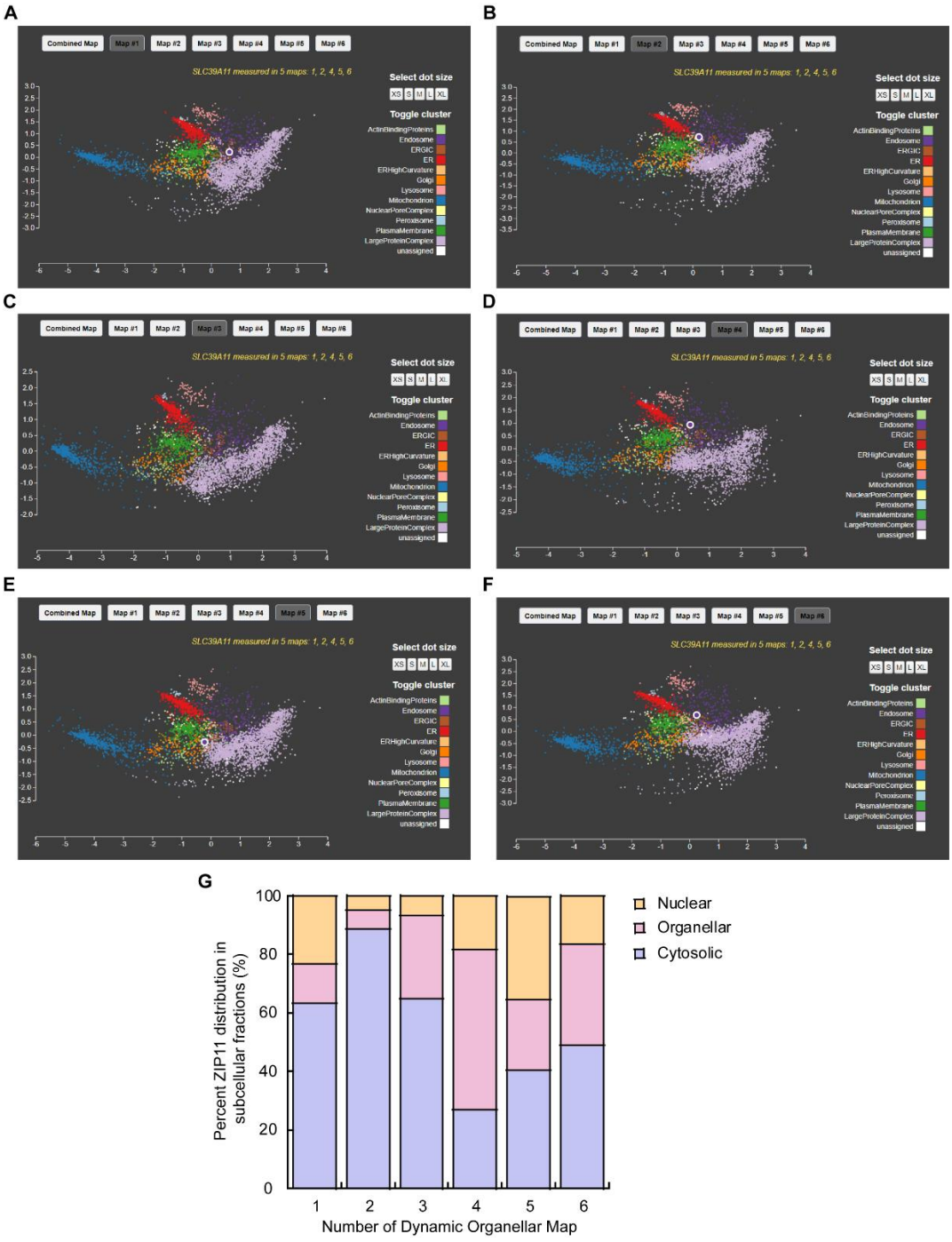

Supplementary Figure 2. Subcellular distribution of ZIP11 in HeLa cells determined by principal component analyses. A-F. Principal components analysis of six Dynamic Organellar Maps of ZIP11 generated by the interactive HeLa Spatial Proteome (http://mapofthecell.biochem.mpg.de/index.html [1]). The large white circle with a purple center on the Dynamic Organellar Maps indicates the cellular localization of ZIP11. **G.** The accompanying bar graphs also generated by the interactive HeLa Spatial Proteome, indicate the percent distribution of ZIP11 in the nucleus, cytosol, and organelles of the HeLa cells per Dynamic Organellar Map and the total percent for each map.

SUPPLEMENTARY FIGURE 3

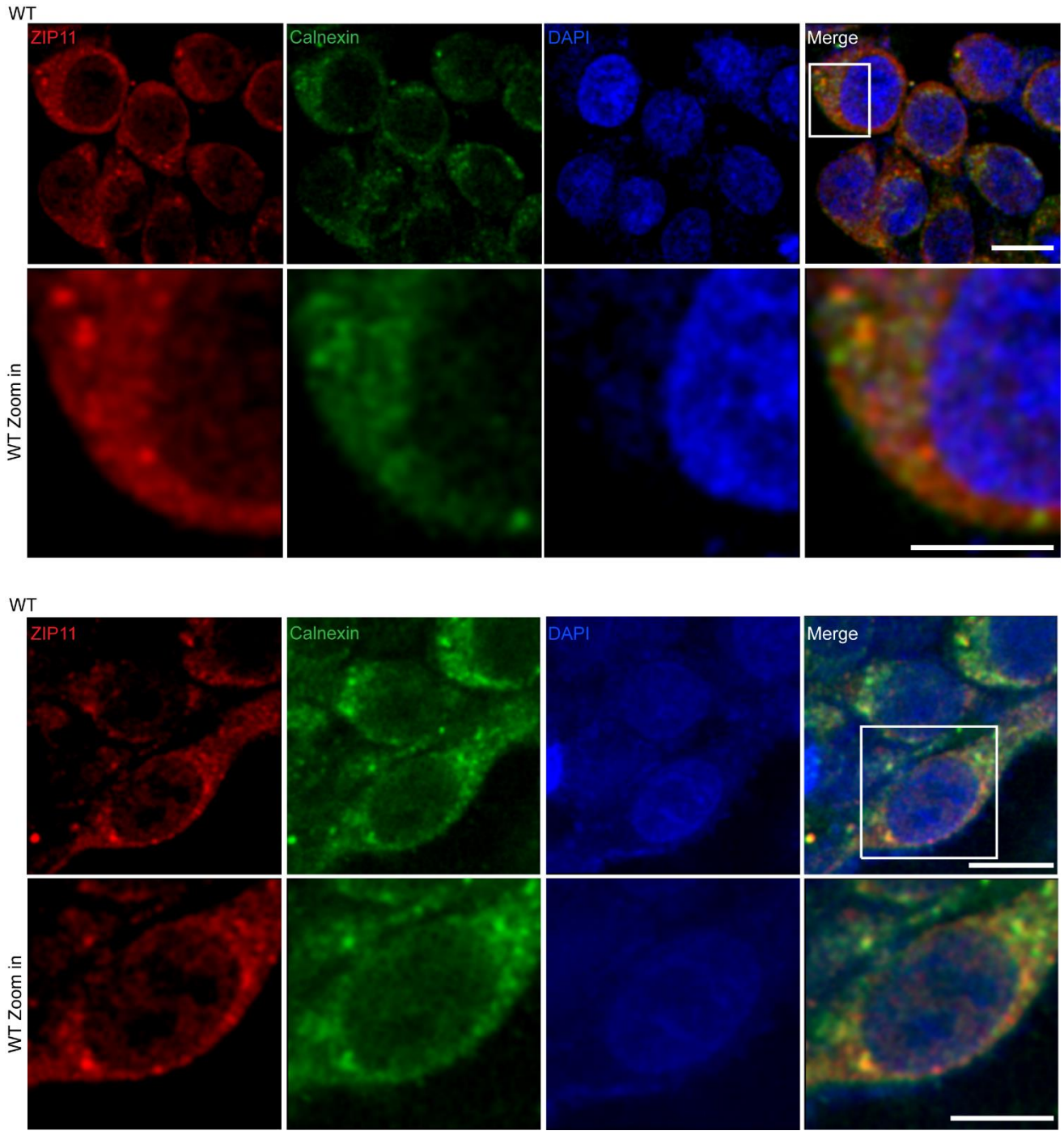

Supplementary Figure 3. ZIP11 and ER components do not colocalize in HeLa cells. Representative confocal images of two independent immunostainings showing a perinuclear and cytosolic punctuated pattern of expression of ZIP11 (red) in wild type HeLa cells. The anti-Calnexin (green) antibody was used as a marker of endoplasmic reticulum and nuclei was stained with DAPI (blue). White boxes are the zoomed-in areas presented for each of the replicates. Bar = 10 µm for low magnification images and 5 µm for zoom-in images.

SUPPLEMENTARY FIGURE 4

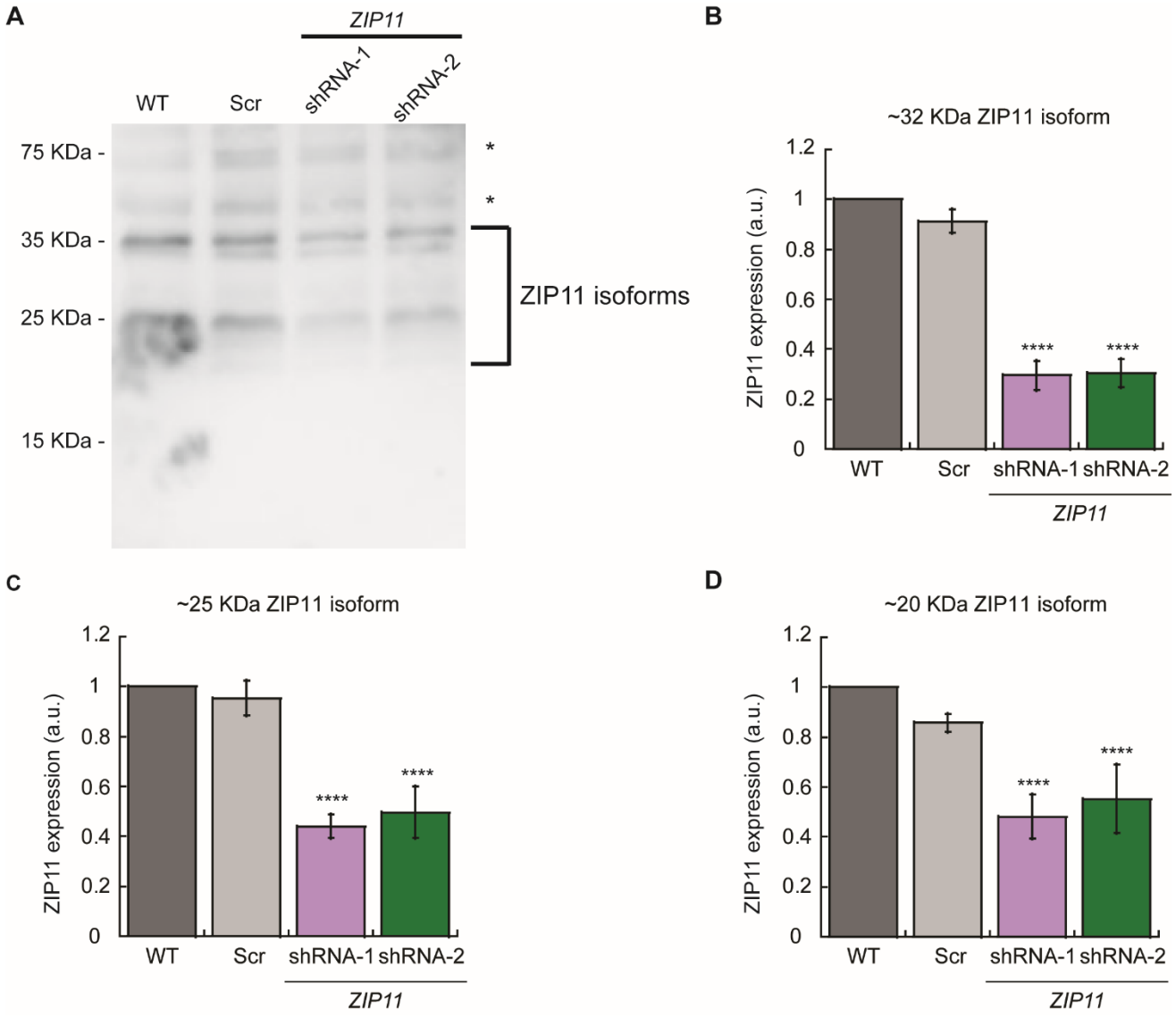

Supplementary Figure 3. ZIP11 isoforms in human cells. A. Full membrane of the representative immunoblot of *ZIP11* expression in HeLa proliferating cells shown in Fig. 2B. Several ZIP11 isoforms can be detected by the ZIP11 antibody used in this study. These isoforms are also KD by the shRNAs used for this study. Quantification of *ZIP11* levels of the protein levels ~32 KDa (**B**), ~25 KDa (**C**) and ~20 KDa (**D**) isoforms of ZIP11 in HeLa proliferating cells. Asterisks represent potential unspecific high molecular weight proteins or potential dimers of ZIP11. For all samples, data are the mean ± SE of three independent biological replicates. ****P < 0.0001.

SUPPLEMENTARY FIGURE 5

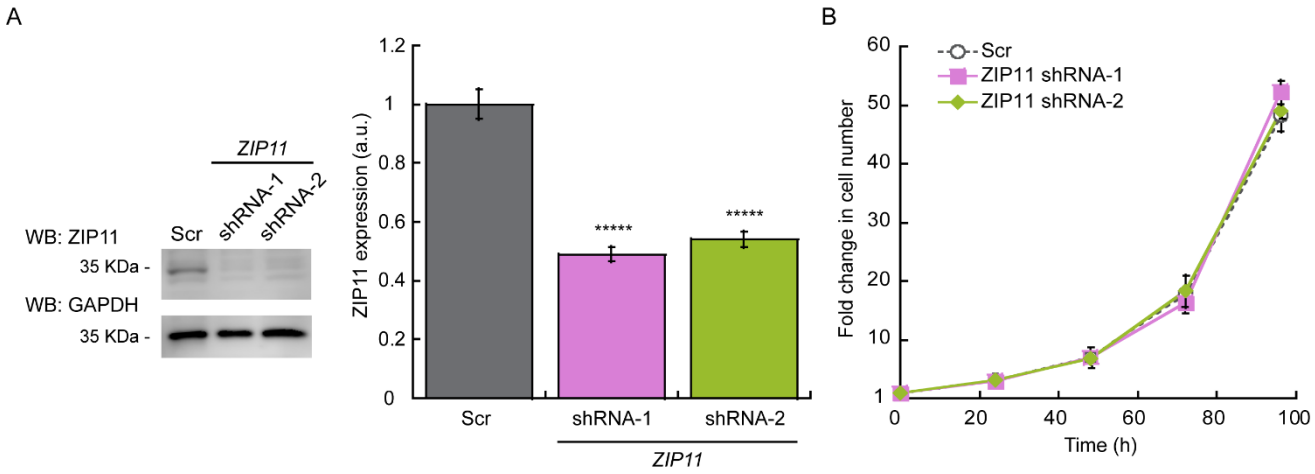

Supplementary Figure 5. ZIP11 KD does not affect the proliferation of HEK293T cells. A. Representative immunoblot (left) and quantification (right) of *ZIP11* levels in HEK293T proliferating cells. Immunoblots against GAPDH was used as loading control. Samples were compared to the corresponding Scr control. **C.** Cell counting assay of proliferating HEK293T cells transduced with scrambled shRNA (shRNA Scr), or *ZIP11* shRNAs. For all samples, data are the mean ± SE of three independent biological replicates. For all samples, data are the mean ± SE of three independent biological replicates. *****P < 0.00001.

SUPPLEMENTARY FIGURE 6

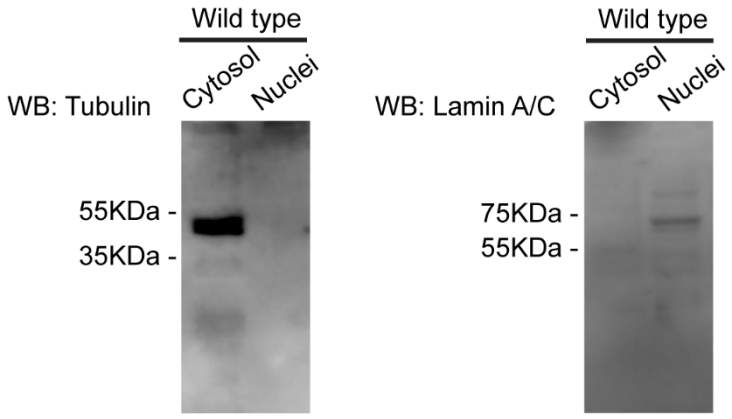

Supplemental Figure 6. Purity of subcellular fractions used in metal determinations.
Representative western blot showing the purity of the subcellular fractions of wild type HeLa cells isolated using the REAP protocol [2; 3; 4]. Tubulin and Lamin A/C were used as controls to show the separation of cytoplasmic and nuclear fractions respectively.

SUPPLEMENTARY FIGURE 7

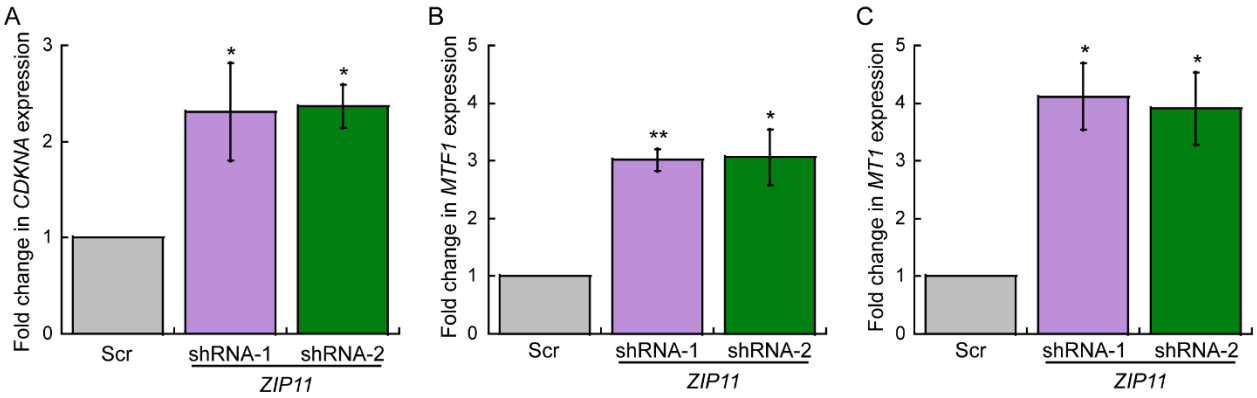

Supplemental Figure 7. Changes in the expression of senescence and metalloprotective genes dependent on *ZIP11* knockdown in HeLa cells. Steady state mRNA levels determined by qRT-PCR of representative up-regulated senescence gene [**(A)** *CDKNA* (p21)] and metalloprotective genes, *MTF1* and *MT1* genes (**B** and **C**, respectively). Data are the mean ± SE for three independent experiments. * $P < 0.05$, ** $P < 0.01$.

SUPPLEMENTARY FIGURE 8

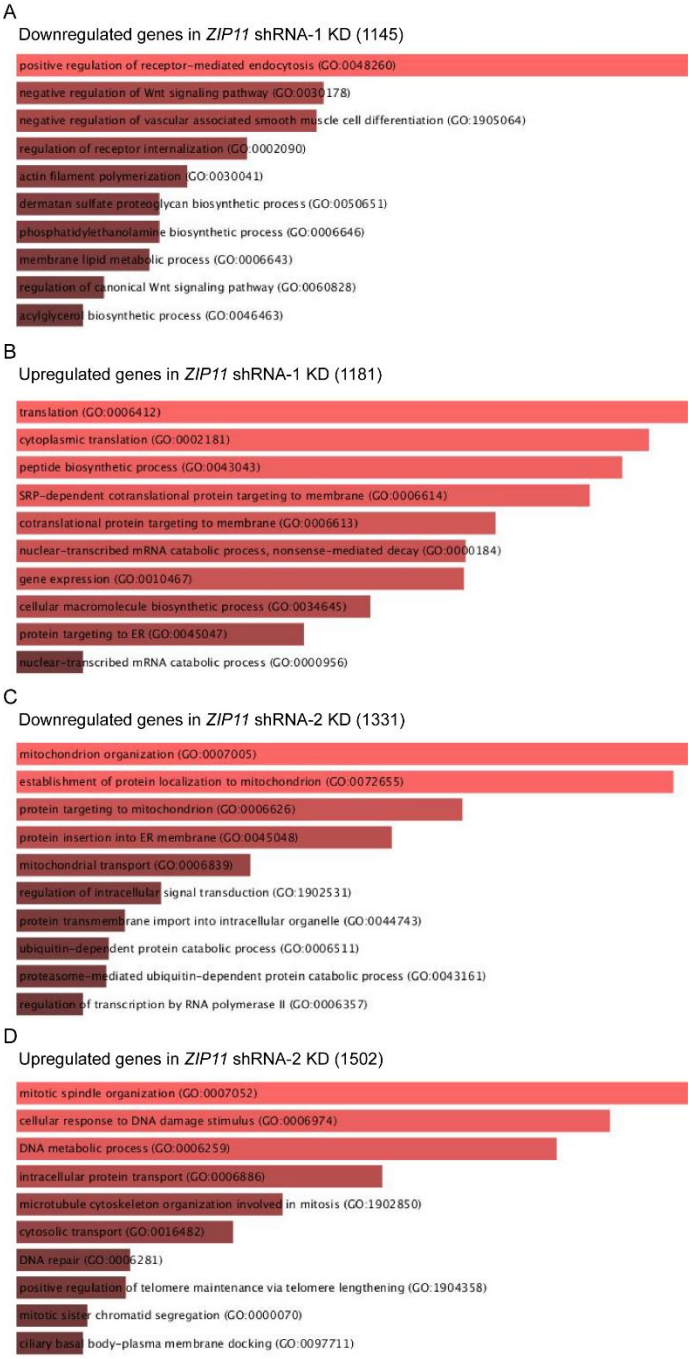

Supplemental Figure 8. GO term analyses representative of the DEG for individual *ZIP11* shRNA. GO term analysis of down-regulated (A) or up-regulated (B) genes for *ZIP11* shRNA-1 and down-regulated (C) or up-regulated (D) genes for *ZIP11* shRNA-2 in HeLa cells. Cut-off was set at 2.0 of the -log(adjusted P value). See Supp. Table 4 for the complete list of genes.

SUPPLEMENTARY TABLES

Supplementary table 1. Plasmids used in this study

Plasmid name	Specific information	Source	Use
Scr shRNA	MISSION® pLKO.1-puro Non-Target shRNA Control Plasmid DNA	Sigma-Aldrich SHC016	Control for shRNA KD
ZIP11 shRNA-1	5'- GAAGCCCAGATCAGTGGTAAT-3'	Sigma-Aldrich TRCN0000038367	KD *ZIP11* CDS
ZIP11 shRNA-2	5'-TCCTGATTGACTCTGATTATA-3'	Sigma-Aldrich TRCN0000434903	KD *ZIP11* UTR
pLV[Exp]-EGFP/Neo-EF1A>hSLC39A11[NM_001352692.2]	Human SLC39A11 ORF. Sequence available upon request	Vector Builder	Phenotype reconstitution
pLV[Exp]-EGFP/Neo-EF1A>empty vector	Empty vector	Vector Builder	Phenotype reconstitution

Supplementary table 2. Primers used in this study

Primer name	Forward sequence	Reverse sequence
CDKN2C	5'-AGACGCTTTCCGCATCAC-3'	5'-CTGAGCGGCATTAGCCCA-3'
CDK20	5'-CGGGCAAGAACGATATTG-3'	5'-TGGGTCAATTCCTTCTCT-3'
MOAP1	5'-GTCGATGAATGTCTGCAG-3'	5'-CGCCTAGACCAAGTCATT-3'
PPP2CA	5'-CCTCACGTTGGTGTCTAG-3'	5'-GTTCATGGCAATACTGTAC-3'
CDKN1A (p21)	5'-GACACCACTGGAGGGTGACT-3'	5'-CAGGTCCACATGGTCTTCCT-3'
MTF1	5'-ACCAAGAACAAATTCAGCAAGC-3'	5'-ACACTGAGGCCAATCTGCTG-3'
MT1	5'-CTCCTTGCCTCGAAATGGAC-3'	5'-GCATTTGCACTCTTTGCATTTG-3'
GAPDH	5'-GTCTCCTCTGACTTCAACAGCG-3'	5'-ACCACCCTGTTGCTGTAGCCAA-3'

Supplementary table 3. Comparison of Survival Curves

Log-rank (Mantel-Cox) Test	
Chi square	0.9845
df	1
P value	0.3211
P value summary	ns
Are the survival curves sig different?	No
Gehan-Breslow-Wilcoxon Test	
Chi square	0.0005788
df	1
P value	0.9808
P value summary	ns
Are the survival curves sig different?	No
Median survival	
High Expression	95.30
Low Expression	Undefined
Hazard Ratio	
Ratio	1.297
95% CI of ratio	0.7762 to 2.166

Supplementary references

[1] D.N. Itzhak, S. Tyanova, J. Cox, and G.H. Borner, Global, quantitative and dynamic mapping of protein subcellular localization. eLife 5 (2016).

[2] C. Tavera-Montanez, S.J. Hainer, D. Cangussu, S.J.V. Gordon, Y. Xiao, P. Reyes-Gutierrez, A.N. Imbalzano, J.G. Navea, T.G. Fazzio, and T. Padilla-Benavides, The classic metal-sensing transcription factor MTF1 promotes myogenesis in response to copper. Faseb J 33 (2019) 14556-14574.

[3] S.J.V. Gordon, Y. Xiao, A.L. Paskavitz, N. Navarro-Tito, J.G. Navea, and T. Padilla-Benavides, Atomic Absorbance Spectroscopy to Measure Intracellular Zinc Pools in Mammalian Cells. Journal of visualized experiments : JoVE (2019).

[4] K. Suzuki, P. Bose, R.Y. Leong-Quong, D.J. Fujita, and K. Riabowol, REAP: A two minute cell fractionation method. BMC research notes 3 (2010) 294.

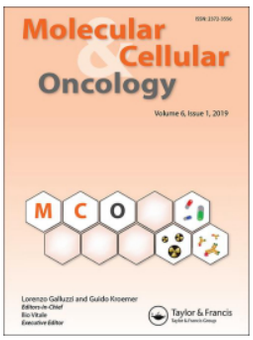

Molecular & Cellular Oncology

ISSN: (Print) (Online) Journal homepage: https://www.tandfonline.com/loi/kmco20

Therapeutic potential of targeting mirnas to prostate cancer tumors: using psma as an active target

Amir Yarahmadi, Romoye Sohan, Brenna McAllister & Leslie A. Caromile

To cite this article: Amir Yarahmadi, Romoye Sohan, Brenna McAllister & Leslie A. Caromile (2022) Therapeutic potential of targeting mirnas to prostate cancer tumors: using psma as an active target, Molecular & Cellular Oncology, 9:1, 2136476, DOI: 10.1080/23723556.2022.2136476

To link to this article: https://doi.org/10.1080/23723556.2022.2136476

Published online: 24 Oct 2022.

MOLECULAR & CELLULAR ONCOLOGY
2022, VOL. 9, NO. 1, e2136476 (10 pages)
https://doi.org/10.1080/23723556.2022.2136476

Taylor & Francis
Taylor & Francis Group

REVIEW

Therapeutic potential of targeting mirnas to prostate cancer tumors: using psma as an active target

Amir Yarahmadi[a], Romoye Sohan[b], Brenna McAllister[b], and Leslie A. Caromile[b]

[a]Vascular and Endovascular Surgery Research Center, Mashhad University of Medical Sciences, Mashhad, Iran; [b]Center for Vascular Biology, University of Connecticut Health Center, Farmington, CT, USA

ABSTRACT

Prostate cancer (PC) is a commonly diagnosed malignancy in men and is associated with high mortality rates. Current treatments for PC include surgery, chemotherapy, and radiation therapy. However, recent advances in targeted delivery systems have yielded promising new approaches to PC treatment. As PC epithelial cells express high levels of prostate-specific membrane antigen (PSMA) on the cell surface, new drug conjugates focused on PSMA targeting have been developed. microRNAs (miRNAs) are small noncoding RNAs that regulate posttranscriptional gene expression in cells and show excellent possibilities for use in developing new therapeutics for PC. PSMA-targeted therapies based on a miRNA payload and that selectively target PC cells enhances therapeutic efficacy without eliciting damage to normal surrounding tissue. This review discusses the rationale for utilizing miRNAs to target PSMA, revealing their potential in therapeutic approaches to PC treatment. Different delivery systems for miRNAs and challenges to miRNA therapy are also explored.

ARTICLE HISTORY
Received 27 August 2022
Revised 6 October 2022
Accepted 10 October 2022

KEYWORDS
PSMA; prostate cancer; miRNA; therapy; targeted delivery

Introduction

Prostate cancer (PC) is one of the leading causes of mortality in male cancer patients worldwide.[1] Effective PC management remains an ongoing challenge, with androgen deprivation therapy (ADT) the current standard PC treatment.[2] Although this course of treatment improves the survival and quality of life for individuals with PC, most men eventually progress to metastatic castration-resistant PC (mCRPC).[3] Advanced PC (including castration-sensitive and castration-resistant disease) is commonly managed with androgen axis – targeted therapies, such as abiraterone acetate and enzalutamide, docetaxel-based chemotherapy, or radium Ra-223 dichloride.[4] Unfortunately, only approximately 50% of patients with advanced disease respond favorably to these therapies, with the other 50% developing resistance and exhibiting survival rates of only 5% – 30%.[2] There are many reasons for treatment failure: Factors such as a mutation in the androgen receptor (AR) drug-binding domain, tumor heterogeneity, and vascular permeability all negatively affect efficient drug delivery to tumor sites. Moreover, many currently used drugs exhibit limited specificity and often produce deleterious effects on healthy peripheral tissues.[5,6] Therefore, targeted drug delivery holds immense potential to improve cancer treatment by selectively providing effective therapies at tumor sites. Ideally, these therapies not only specifically recognize tumors but also target survival pathways that the tumor has leveraged to achieve drug resistance.

PC cells within prostate tumors express many tumor-associated antigens that can be potentially targeted for cancer diagnosis, treatment, and selective drug delivery.[7,8] Prostate-specific membrane antigen (PSMA), a type II transmembrane protein found predominantly on the surface of prostate epithelial cells, is among these,,[9–11] PSMA is expressed on the epithelium of nearly all PCs, and its increased expression correlates with progression to castration resistance and metastatic disease.[12–14] The *cytoplasmic domain* of PSMA contains a motif that signals the internalization of PSMA via clathrin-coated pits,[15,16] and clinical technologies utilize this pathway to enhance the delivery of radiopharmaceuticals into the tumor, with ^{17}Ga-PSMA-11 PET/CT and ^{177}Lu-PSMA-617[18–20] leading the way. Studies with both antibody-drug conjugates (ADCs) and small-molecule drug conjugates (SMDCs) have demonstrated encouraging results.[21–27] thus highlighting the continued interest in PSMA in biomedical, translational medicine, and pharmaceutical fields.[28]

microRNAs (miRNAs) are conserved 21–25-nucleotide-long noncoding molecules that play essential roles in regulating gene expression and participate in various biological processes,[29] including roles in cancer [30,31] by functioning as a tumor suppressor [32] or as an onco-miRNA that represses the expression tumor suppressor genes such as p53.[32] Each miRNA has the potential to target many genes. By using a single microRNA to silence multiple genes, several signaling pathways can be simultaneously regulated, which may minimize compensatory mechanisms that cause therapeutic resistance. Therefore, manipulating cellular miRNA levels with modified oligonucleotides that mimic or inhibit miRNA function has led to the extensive research and development of miRNAs as therapeutics.[33] Loss-of-function approaches have led to superior research results, as they reveal processes dependent on physiological miRNA levels; in contrast, exogenous miRNA added to the system can lead to repressed activity of targeted mRNAs in nonphysiological contexts since miRNA – target

CONTACT Leslie A. Caromile caromile@uchc.edu Center for Vascular Biology, University of Connecticut Health Center, Farmington, CT, USA

interaction is highly concentration dependent. The expression of many miRNAs is tissue-specific and altered in different diseases, including PC. These alterations can significantly affect tumor cell growth and survival.[34,35] Furthermore, miRNAs are considered valuable diagnostic biomarkers and potential therapeutic targets in cancer;[36] for example, miRNA-15a, miRNA-21, miRNA-34a, miRNA-153, and miRNA-17 have been connected with PC pathogenesis.[37,38] Therefore, miRNAs that perturb human disease pathways are potentially powerful candidates for therapeutic intervention against various pathological conditions, including PC.

Although the understanding of miRNA biology has grown exponentially since its discovery in 1993 by Lee and colleagues,[39] a more comprehensive assessment of the strengths and limitations of miRNA-based approached for PC therapy is still necessary. In this review, we discuss potential therapeutic strategies of targeting PSMA to deliver specific miRNA payloads exclusively to PC tumors as well as provide insight into various delivery systems for miRNAs and the challenges to using these systems for therapy.

miRNA biogenesis and mechanisms of action

miRNA biogenesis is a complex process that begins with nuclear transcription mediated by RNA polymerase II forming a primary transcript known as primary miRNA (pri-miRNA).[40] Pri-miRNAs contain a unique hairpin stem–loop structure and a single-stranded sequence of differing lengths that can potentially harbor hundreds of kilobases.[41] The nuclear complex contains the ribonuclease III enzyme Drosha as well as a double-stranded RNA (dsRNA)-binding protein (DiGeorge syndrome critical region 8 protein (DGCR8)), which facilitate Drosha removal of approximately 11 bp from each side of the hairpin stem of a pri-miRNA, resulting in precursor miRNA (pre-miRNA).[41,42] A pre-miRNA is an approximately 70-nucleotide stem–loop structure that is transported from the nucleus to the cytoplasm by exportin-5 (×PO5), a Ran-GTP-dependent dsRNA-binding protein.[43] Once in the cytoplasm, the pre-miRNA is processed by the ribonuclease III enzyme Dicer to form a mature, 22-nucleotide miRNA duplex.[44] The mature miRNA is then incorporated into the miRNA-induced silencing complex (RISC),[45,46] through which it regulates gene expression through translational repression mediated by mRNA deregulation (Figure 1).[45]

miRnas in PC progression

miRNAs play crucial roles in critical cellular processes such as cell proliferation, differentiation, cell cycle progression, apoptosis, angiogenesis, the epithelial-mesenchymal transition (EMT), and metastasis during cancer progression.[47] Hao et al. showed that miRNA-101 inhibited PC cell proliferation by inhibiting cyclooxygenase-2 (COX-2) gene expression, inhibiting the activation of the COX-2/PGE2/EGFR pathway, which mediates cell proliferation during inflammation.[48] COX-2 is an inducible isozyme of COX, a key enzyme in

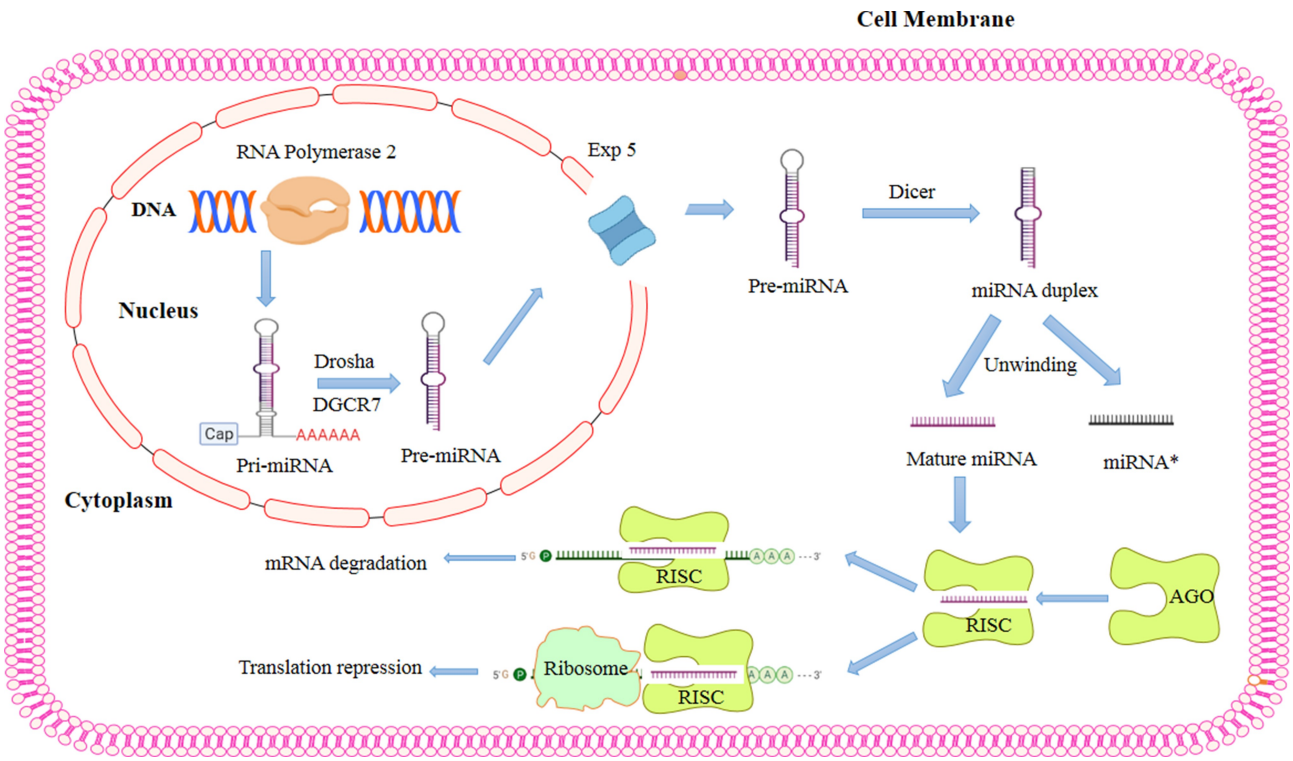

Figure 1. miRNA biogenesis and mechanisms of action in posttranscriptional gene regulation. miRNA biogenesis begins with miRNA transcription from DNA via the action of RNA polymerase II to generate primary hairpin miRNA (pri-miRNA). Then, pri-miRNA is cleaved by the RNase III drosha and its binding partner DiGeorge syndrome critical region gene 8 (DGCR8), which recognizes the hairpin structures in pri-miRNA and processes them to form precursor miRNA (pre-miRNA). The resulting pre-miRNA is exported to the cytoplasm by Exportin-5, a Ran-GTP-dependent dsRNA-binding protein. In the cytoplasm, another RNase III enzyme, dicer, further processes pre-miRNA, cleaving its hairpin and thus producing a mature miRNA duplex. Then, one strand is loaded into an argonaute (AGO) family member to form the miRNA-induced silencing complex (RISC) that recognizes the mRNA target via sequence complementarity, resulting in mRNA degradation or translation inhibition.

converting arachidonic acid to prostaglandins and other eicosanoids. COX-2 is highly expressed in several human cancers and cancer cell lines, including PC tumor cells, and activates the PGE2/EGFR pathway, leading to cell proliferation via extracellular signal-regulated kinase 2 (ERK2) activation.[49,50] A study by Zhu et al. demonstrated that miRNA-136 suppressed PC cell proliferation and invasion by targeting mitogen-activated protein kinase 4 (MAP2K4a) *in vitro* [51]. MAP2K4a can increase androgen receptor expression/activation and promote PC tumor progression via noncanonical activation of AKT.[51] Moreover, Wang et al. showed that miRNA-182 upregulation increased the expression of important regulators of cell cycle progression, namely c-MYC and cyclin D1, leading to uncontrolled proliferation of the LNCaP and PC3 immortalized human PC cell lines.[52] As miRNAs control the expression of cell cycle-related genes, identifying critical miRNAs involved in the cell cycle can lead to better treatment opportunities for cancers, including PC.[53] For instance, miRNA-193a functions as a tumor suppressor, and its expression is lower in PC tissues compared to that in benign prostatic hyperplasia.[54] In addition, Liu et al. demonstrated that miRNA-193a overexpression inhibited cell growth by targeting cyclin D1 and promoting G1-phase cell cycle arrest in the DU-145 immortalized human PC cell line as well as in PC3 cells.

Apoptosis is a complex process that involves many signaling pathways that can be modulated by miRNAs. Ma et al. showed that miRNA-143 decreases the proliferation and induces the apoptosis of LNCaP cells by suppressing the expression of the integral outer mitochondrial membrane protein BCL2, which inhibits cell death.[55] A study by Ostadrahimi et al. demonstrated that miRNA-185, miRNA-30c, and miRNA-1266 were downregulated in PC tissues compared to healthy control tissues,[56] resulting in antiapoptotic BCL2 and BCL2-XL gene upregulation and a reduced apoptosis rate.[56]

Among the crucial outcomes of cancer cell progression to metastatic phenotype acquisition is the EMT.[57] Several miRNAs have been suggested to regulate the expression of genes involved in the EMT, and a reduction in their expression leads to cancer invasion and metastasis.[58] For example, miRNA-200b targets the zinc-finger E-box-binding homeobox 1 and 2 genes (ZEB1 and ZEB2), Bim1, and E-cadherin. ZEB1/ZEB2 directly bind to the E-box in the promoter of the adhesion molecule E-cadherin, recruiting transcriptional corepressors and inducing the EMT in PC.[59–62] miRNA-200b action is crucial for cells to maintain their epithelial phenotype and prevent the EMT and tumor metastasis.[63] Yu et al. showed that administration of miRNA-200b downregulated the expression of ZEB1 and ZEB2 in PC3 cells and reversed the EMT, attenuating EMT phenotype acquisition.[63] A study by Gandellini et al. demonstrated that miRNA-205 plays a vital role in the EMT by targeting integrin-β4, laminin, and matrix metalloproteinase 2 (MMP2), which are necessary for interactions between the PC cell cytoskeleton and the extracellular matrix.[17,64,65] A decrease or loss in miRNA-205 expression results in increased cell proliferation and invasion and changes to prostate cell characteristics, moving them toward a mesenchymal phenotype.[66] The essential miRNAs involved in PC pathogenesis are summarized in Figure 2.

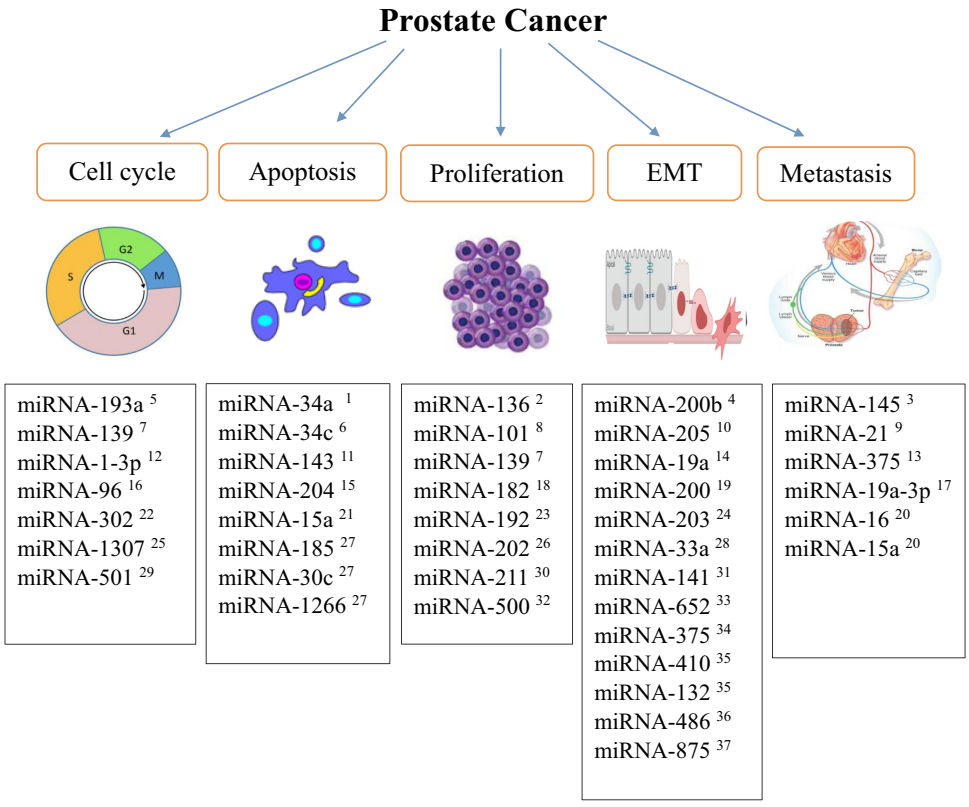

Figure 2. Summary of the important miRnas involved in PC.

Targeted systems for miRNA delivery

Primary PC results in a highly vascular tumor derived from proliferating prostatic epithelial cells.[67] Tumor vascularity significantly affects tumor growth and drug responsiveness because it influences tumor blood flow, oxygenation, and the permeability of chemotherapeutic drugs into the tumor.[68,69] Successfully targeted drug delivery systems are small (from 10 to 100 nm in diameter), remain stable in the circulation, accumulate in leaky tumor vasculature via the enhanced permeability and retention (EPR) effect, and enable targeted delivery of specific-ligand-modified drugs and drug carriers to areas with limited access.[70,71] Targeting specific cancer cells is a crucial characteristic of drug delivery systems as targeting enhances therapeutic efficacy without eliciting damage to normal surrounding tissue or causing a bystander effect.[72] Recent advances in drug delivery systems have suggested promising miRNA-based approaches for the delivery and treatment of different diseases, including PC.[73] These advances can be broadly classified into two categories: passive and active targeting approaches.

Passive targeting

Passive targeting exploits the biological characteristics of tumorous and normal tissue to deliver a drug to the target site, where it can exert a therapeutic effect. Tumor growth and metastasis depend on angiogenesis to provide an adequate supply of oxygen and nutrients to the tumor and to remove waste products.[74] However, this new tumor vasculature is often defective and leaky, hindering the delivery and effectiveness of systemically administered therapeutic cancer drugs to the tumor.[75]

Many limitations have prevented miRNAs from becoming optimal candidates for this type of delivery, including the stability of the miRNA in the circulation, its ability to accumulate in pathological sites with differing vascular permeability and nonspecific distribution, and most importantly, the fact that one miRNA has the potential to target many different mRNAs leading to a nonspecific effect.[76,77] These challenges to miRNA usage for targeted drug delivery and some possible solutions are highlighted in Table 1.

Active targeting

Active targeting affects cancer cells through direct interactions between ligands and target molecules that are overly abundant on the surface of cancer cells, allowing the carriers to distinguish targeted cells from healthy cells.[78] The drug carriers are internalized into the cell via receptor-mediated endocytosis, and then, the payload is released.[79] This active ligand-specific targeting is particularly suitable for miRNA-mediated drug delivery applications. The most common active targeting carriers for miRNAs are generated from peptides, antibodies, aptamers, and nanoparticles, which help miRNAs specifically target tumor cells.[80] In summary, active targeting is a precise mechanism for targeting tumor cells that reduces the need for a high number of miRNAs, which is required for passive targeting, and thus prevents unwanted side effects.[81]

PSMA is overly abundant on the surface of PC epithelial cells and thus has been used as a successful target for PC management.[82] Interestingly, PSMA is expressed on the surface of endothelial cells in the tumor neovasculature in many other types of cancers, including breast, lung, gastric, colorectal, pancreatic and renal cell carcinoma, and bladder cancers. Therefore, using PSMA to carry therapeutic miRNA payloads may be broadly applicable to cancers in addition to PC.[83] We discuss the most common active targeting PSMA-based carriers used for miRNA in PC.

PSMA-targeting peptides and proteins as miRNA carriers

Peptide- and protein-based carriers have been broadly used for miRNA delivery because of the ability of the positive charged amino acids to interact with negatively charged nucleotides.[84] For instance, Jin et al. developed a novel combinatorial phage biopanning procedure to identify PSMA-specific-targeting peptides as carriers for targeted drug delivery to PC cells.[85] They reported that a novel PSMA-specific-targeting peptide named GTI, on the basis of its amino acid sequence, exhibited high binding affinity and selectivity for PSMA and PSMA-positive PC cells. Specifically, GTI mediated the internalization of the apoptotic KLA peptide into PSMA-positive LNCaP cells and induced cell death. Moreover, FAM-labeled GTI displayed high and specific tumor uptake in nude mice bearing human PC xenografts. It can be employed as a PSMA-specific ligand.[85] Although this system may be an excellent tool for PC diagnosis and targeted drug delivery to PC, to date, no study on the use of this system for miRNA delivery via PSMA targeting in PC has been reported.

Anti-PSMA antibodies as miRNA carriers

Antibody-based approaches have been widely used to target tumor cells via active targeting with specific drug carriers in cancer.[86] Henry et al. used MLN2704, an antibody-chemotherapeutic conjugate consisting of a monoclonal antibody specific to PSMA conjugated to the drug maytansinoid 1 (DM1), which has microtubule-depolymerizing activity. After

Table 1. Challenges to miRNA usage for targeted drug delivery and possible solutions.

Challenges	Possible Solutions
Degradation of miRNAs by nucleases	Changing the surface charge and improving their stability
Filtration in the spleen and kidneys Destruction by macrophages while in the circulatory system	Chemical modification and/or local administration
Penetration through the cell membrane and extracellular matrix	Active targeting via specific ligands and use of cell-penetrating moieties
Poor endosomal release and intracellular localization problems	Use of conjugating peptides, lytic reactions, or miRNA sponges
Ability to target multiple mRNAs	Local administration and active targeting via specific ligands

MLN2704 binds to PSMA through its specific antibody, MLN2704-PSMA is internalized, and DM1 is released into the cells, leading to cancer cell death. The Henry et al. study demonstrated that MLN2704 showed antitumor activity in an animal model of PC, whereas an unconjugated antibody showed no antitumor activity and DM1 alone showed weak tumor-suppressing activity *in vivo* .[87] Rege et al. focused on designing and generating an amphipathic fusion peptide to destroy PC cells. Amphipathic lytic peptides exert cytotoxic effects on PC cells via depolarization of mitochondrial membranes and the induction of apoptosis.[88] This group used PSMA-targeted peptides and antibodies against PSMA to precisely deliver cytotoxic amphipathic lytic peptides to PSMA-positive LNCaP cells. The results showed that, compared to the peptides, the antibodies more efficiently targeted the PC cells. Additionally, the group compared the cytotoxic activity of fusion peptides and antibody conjugates and found that treatment with fusion peptides induced oncotic/necrotic death in LNCaP cells; moreover, treatment with the antibody conjugates caused apoptotic death in these cells.[88] Several anti-PSMA monoclonal antibodies with cytotoxic agents have been introduced for radioimmunotherapy application to target PSMA-expressing cells.[89] For example, Behe et al. used the ^{177}Lu-labeled anti-PSMA monoclonal antibody 3F11 to target PC cells in a mouse xenograft model. Their results indicated that ^{177}Lu-labeled anti-PSMA 3F11 showed high specificity and affinity for a xenograft mouse model, making it a potential candidate for radioimmunotherapeutic applications in PC.[90] However, the literature on the use of this system for miRNA delivery in PC treatment is rare.

PSMA-directed aptamers as miRNA carriers

Aptamers are short single-stranded DNA or RNA oligonucleotides with a unique three-dimensional structure that enables its selective binding to specific receptors or protein targets,[91] making them excellent drug delivery platforms.[92] Conjugation of aptamers to miRNAs is a new method to deliver miRNAs precisely to PC cells.[93] Dassie et al. developed an RNA aptamer (A9 g) that selectively inhibited PSMA enzyme activity and functioned as a smart drug for PC treatment. Because PSMA activity plays a crucial role in PC progression, this group showed that PC tumor treatment with the A9 g aptamer in a murine model significantly reduced cell migration and invasion *in vitro* and metastasis to bone *in vivo*.[94] Wu et al. showed that targeting PC with miRNA-15a and miRNA-16-1 (potent tumor suppressors in PC) through the RNA aptamer A10–3.2, which specifically targets PC cells with PSMA residing on their surface, was beneficial for the selective killing of PC cells *in vitro*.[95] Another study by Ye et al. revealed that aptamers in a compound with hyperbranched polyamidoamine (HPAA) and polyethylene glycol (PEG) and used for targeting PSMA-positive LNCaP cells via miRNA-133a-3p delivery facilitated miRNA-133a-3p delivery into LNCaP cells and showed excellent cytotoxicity in these cells. Furthermore, in an *in vivo* mouse model of PC, systemic injection of the APT-HPAA-PEG/miRNA-133a-3p compound inhibited tumor growth and prolonged animal survival.[96]

PSMA nanoparticles as miRNA carriers

Nanoparticles (NPs) are essential carriers in cancer prevention and therapy because they can be generated with unique sizes and shapes that enable them to deliver miRNAs and other chemotherapeutic agents.[97] Silica, gold, and iron oxide NPs have been primarily used for miRNA delivery in cancer treatment.[98] Luo et al. conjugated a PSMA-targeting ligand named PSMA-1 to gold NPs (AuNPs) and found that these PSMA-1-AuNPs showed greater uptake by PSMA-expressing PC3 cells compared to cells lacking PSMA receptors. As gold can increase radiotherapy sensitization, significantly enhanced radiotherapy efficacy was observed with these PSMA-targeting AuNPs.[99] Additionally Binzel et al. reported that NPs containing an anti-PSMA RNA aptamer as the targeting ligand and carrying anti-miRNA-17 or anti-miRNA-21 (two common oncogenes) suppressed miRNA oncogenic activity in PC, showing significant knockdown of miRNA-17 and miRNA-21 and upregulation of phosphatase and tensin homolog (PTEN), a negative regulator of tumor growth in both *in vitro* and *in vivo* models of PC.[100] Saniee et al. developed a docetaxel-loaded NP consisting of poly(lactic-co-glycolic acid) polyethylene glycol (PLGA-PEG) conjugated with a urea-based anti-PSMA ligand named glutamate-urea-lysine (Glu-urea-Lys) to deliver docetaxel for PC treatment. The uptake of these NPs by PSMA-positive LNCaP and PSMA-negative PC3 cells was analyzed. The results showed that docetaxel uptake was more efficient in the PSMA-positive cells when compared to the control. In addition, this group showed that compared to that of PSMA-targeted NP-carried drugs, the toxicity of untargeted NP-carried drugs was reduced by more than 70%. Finally, the NPs specifically targeting PSMA-positive PC cells showed enhanced the antitumor efficacy mediated via docetaxel.[101]

Challenges to miRNA therapy

Similar to other treatment strategies, challenges and limitations have been identified in using miRNAs in cancer treatment.[102] The first three challenges to miRNA therapy are caused by 1) nucleases quickly degrading naked miRNAs in the circulatory system,[103] 2) miRNAs quickly cleared through the kidney,[102] and 3) naked miRNAs frequently inducing immune responses and being eliminated from the circulation by macrophages, thus requiring high-dose administration, which subsequently leads to toxicity.[104,105] To address these three challenges, several different approaches have been employed to alter the miRNA surface charge through structural chemical modifications:[106] 1) locked nucleic acid (LNA) modification, 2) ribose 2′-OH group modification, 3) peptide nucleic acid (PNA) modification, and 4) backbone modification.[106]

LNA antisense oligonucleotides have been the most extensively studied miRNA structural modifications and have been demonstrated to enhance endonuclease resistance and increase biodistribution and to exhibit a lower toxicity profile than unmodified miRNA.[107] The most common groups used to as a substitution for 2′-OH are 2′-O-methyl, 2′-O-methoxyethyl, and 2′-O-fluoro groups. Substitution with these chemical groups enhanced stability, increased binding affinity, and

increased the effectiveness of miRNA inhibition *in vivo*.[108] PNAs are uncharged oligonucleotide analogs. A phosphodiester backbone replacement with PNAs produces *N*-(2-aminoethyl)-glycine units. PNA recognizes single-stranded nucleic acids with extremely high affinity and sequence selectivity. Although uncharged, PNAs increase oligonucleotide stability, making them suitable for therapeutic approaches.[109] Backbone modification is another strategy in which one of the critical atoms in an oligonucleotide is replaced to create a more stable oligonucleotide with therapeutic applications. The most widely used backbone-modified oligonucleotides are generated by replacing one oxygen atom with a sulfur atom. This modification has been shown to enhance nuclease resistance. However, modified oligonucleotides exhibit a short circulation half-life and low binding affinity.[110]

The fourth challenge in miRNA therapy is low penetration through the cell membrane and the ECM. miRNAs are hydrophilic and therefore cannot cross cell membranes, despite their negative charge.[111] Different approaches to help miRNAs cross the cell membrane include active targeting via peptides and conjugation with lipid-soluble compounds such as cholesterol.[112] For example, Fabani et al. designed anti-miRNA-122 conjugated to penetratin, a cell-penetrating peptide (also known as a protein transduction domain), enabling delivery of miRNAs through the cell membrane *in vitro*.[113]

The fifth challenge in miRNA therapy is endosomal escape and intracellular localization.[114] To enhance endosomal release, conjugating peptides and probes have been developed. For example, Xie et al. used chloroquine-containing 2-(dimethylamino)ethyl methacrylate (DMAEMA) copolymers to enhance miRNA delivery by increasing the endosomal escape rate. Their results showed that miRNA delivery efficiency was increased by using chloroquine-DMAEMA copolymers in breast cancer cells.[115]

The sixth challenge involves miRNA targeting of multiple mRNAs and the subsequent toxicity caused by off-target gene silencing. miRNAs inhibit the expression of target genes by imperfect base pairing with target mRNA, allowing a single miRNA to regulate the expression of multiple genes, acting as a potent multidrug. For example, the tumor-suppressing miRNA miR-34 can downregulate genes involved in cell proliferation (c-MYC, androgen receptor), angiogenesis (VEGF), apoptosis inhibition (BCL2), and the immune response (PD-L1), resulting in a potent antitumor response.[116,117] Localized use of miRNAs and active targeting delivery systems can reduce off-target gene silencing and the number of possible side effects.[118] Furthermore, miRNAs may face obstacles in reaching their targets due to competitors that interfere with their functions. Increasing evidence suggests that competitive endogenous RNAs (ceRNAs) can prevent the downregulation of mRNA targets by binding through their own miRNA-binding sites.[119] These ceRNAs need to be blocked before miRNA targeted therapy can exert the maximum effect. We present a summary of the most critical challenges to miRNA therapy and potential solutions to overcome these challenges through new drug delivery technologies in Table 1.

Conclusions and future perspectives

During the past decade, advancements in studies on miRNA functions and their essential roles in cancer have led to many possibilities for miRNA therapeutic applications. To date, many different strategies have been studied to find a suitable method for miRNA delivery in cancer treatment.[120] Nevertheless, the specific properties of miRNAs and various physiological obstacles remain the main limitations of *in vivo* miRNA delivery.[121] However, new opportunities and discoveries being presented by targeted miRNA research are increasing the possibility of using miRNA therapy for cancer treatment.[122] In the attempts to use miRNA in cancer treatment, PSMA is being tested as a reliable and specific target for developing a targeted delivery system with potential application in PC, one of the most common cancers worldwide.[95,96] As targeted miRNA therapy systems mediated through PSMA may increase the efficacy and prevent toxic effects on other human cells, new treatment strategies for using PSMA in PC treatment will be valuable for further studies. Furthermore, future works are needed for designing and optimizing an effective delivery system for miRNAs targeting PSMA and potential combinations of these therapies, along with other therapeutic strategies, for the long-term treatment of PC.

Acknowledgments

The authors acknowledge Kyle Guzy for editing of the manuscript as well as the financial support from NIH NCI 5R21CA256382.

Disclosure statement

No potential conflicts of interest were disclosed.

Funding

The work was supported by the National Institutes of Health [NCI 5R21CA256382]

ORCID

Amir Yarahmadi http://orcid.org/0000-0001-9397-6608
Romoye Sohan http://orcid.org/0000-0002-8262-8285
Brenna McAllister http://orcid.org/0000-0002-5567-7436
Leslie A. Caromile http://orcid.org/0000-0003-2193-5190

Data availability statement

The data that support the findings of this study are available from the corresponding author upon reasonable request.

References

1. Mohler J, Bahnson RR, Boston B, Busby JE, D'Amico A, Eastham JA, Enke CA, George D, Horwitz EM, Huben RP, et al. Prostate cancer. Journal of the National Comprehensive Cancer Network. 2010;8(2):162–200. doi:10.6004/jnccn.2010.0012.
2. Whitburn J, Rao SR, Morris EV, Tabata S, Hirayama A, Soga T, Edwards JR, Kaya Z, Palmer C, Hamdy FC, et al. Metabolic profiling of prostate cancer in skeletal microenvironments identifies

G6PD as a key mediator of growth and survival. Sci Adv. 2022;8(8): eabf9096. doi:10.1126/sciadv.abf9096.
3. Alibhai SMH, Breunis H, Feng G, Timilshina N, Hansen A, Warde P, Gregg R, Joshua A, Fleshner N, Tomlinson G, et al. Association of chemotherapy, enzalutamide, abiraterone, and radium 223 with cognitive function in older men with metastatic castration-resistant prostate cancer. JAMA Netw Open. 2021;4(7): e2114694. doi:10.1001/jamanetworkopen.2021.14694.
4. McAllister MJ, Underwood MA, Leung HY, Edwards J. A review on the interactions between the tumor microenvironment and androgen receptor signaling in prostate cancer. Transl Res. 2019;206:91–106. doi:10.1016/j.trsl.2018.11.004.
5. Pal SK, Twardowski P, Sartor O. Critical appraisal of cabazitaxel in the management of advanced prostate cancer. Clin Interv Aging. 2010;5:395–402. doi:10.2147/CIA.S14570.
6. Cereda V, Formica V, Massimiani G, Tosetto L, Roselli M. Targeting metastatic castration-resistant prostate cancer: mechanisms of progression and novel early therapeutic approaches. Expert Opin Investig Drugs. 2014;23(4):469–487. doi:10.1517/13543784.2014.885950.
7. Erdmann K, Kaulke K, Thomae C, Huebner D, Sergon M, Froehner M, Wirth MP, Fuessel S. Elevated expression of prostate cancer-associated genes is linked to down-regulation of microRnas. BMC Cancer. 2014;14(1):1–14. doi:10.1186/1471-2407-14-82.
8. Fuessel S, Sickert D, Meye A, Klenk U, Schmidt U, Schmitz M, Rost A-K, Weigle B, Kiessling A, Wirth MPet al. Multiple tumor marker analyses (PSA, hK2, PSCA, trp-p8) in primary prostate cancers using quantitative RT-PCR. Int J Oncol. 2003;23:221–228. doi:10.3892/ijo.23.1.221.
9. Caromile LA, Shapiro LH. PSMA redirects MAPK to PI3K-AKT signaling to promote prostate cancer progression. Molecular & Cellular Oncology. 2017;4:e1321168. doi:10.1080/23723556.2017.1321168.
10. Pinto JT, Suffoletto BP, Berzin TM, Qiao CH, Lin S, Tong WP, May F, Mukherjee B, Heston WD. Prostate-specific membrane antigen: a novel folate hydrolase in human prostatic carcinoma cells. Clin Cancer Res. 1996;2:1445–1451.
11. Carter RE, Feldman AR, Coyle JT. Prostate-specific membrane antigen is a hydrolase with substrate and pharmacologic characteristics of a neuropeptidase. Proc Natl Acad Sci U S A. 1996;93:749–753. doi:10.1073/pnas.93.2.749.
12. Ghosh A, Heston WD. Tumor target prostate specific membrane antigen (PSMA) and its regulation in prostate cancer. J Cell Biochem. 2004;91(3):528–539. doi:10.1002/jcb.10661.
13. Murphy GP, Su S, Jarisch J, Kenny GM. Serum levels of PSMA. The Prostate. 2000;42:318–319. doi:10.1002/(SICI)1097-0045(20000301)42:4<318:AID-PROS10>3.0.CO. 2-L [pii].
14. Bacich DJ, Pinto JT, Tong WP, Heston WD. Cloning, expression, genomic localization, and enzymatic activities of the mouse homolog of prostate-specific membrane antigen/NAALADase/folate hydrolase. Mamm Genome. 2001;12(2):117–123. doi:10.1007/s003350010240.
15. Rajasekaran AK, Anilkumar G, Christiansen JJ. Is prostate-specific membrane antigen a multifunctional protein? Am J Physiol Cell Physiol. 2005;288(5):C975–981. doi:10.1152/ajpcell.00506.2004.
16. Liu H, Rajasekaran AK, Moy P, Xia Y, Kim S, Navarro V, Rahmati R, Bander NH. Constitutive and antibody-induced internalization of prostate-specific membrane antigen. Cancer Res. 1998;58:4055–4060.
17. Li S, Luo W. Matrix metalloproteinase 2 contributes to aggressive phenotype, epithelial-mesenchymal transition and poor outcome in nasopharyngeal carcinoma. Onco Targets Ther. 2019;12:5701. doi:10.2147/OTT.S202280.
18. Chatalic KL, Heskamp S, Konijnenberg M, Molkenboer-Kuenen JDM, Franssen GM, Groningen MCCV, Schottelius M, Wester H-J, van Weerden WM, Boerman OC, et al. Towards personalized treatment of prostate cancer: pSMA I&T, a promising prostate-specific membrane antigen-targeted theranostic agent. Theranostics. 2016;6(6):849–861. doi:10.7150/thno.14744.
19. Ganguly T, Dannoon S, Hopkins MR, Murphy S, Cahaya H, Blecha JE, Jivan S, Drake CR, Barinka C, Jones EF, et al. A high-affinity [18F]-labeled phosphoramidate peptidomimetic PSMA-targeted inhibitor for PET imaging of prostate cancer. Nucl Med Biol. 2015;42(10):780–787. doi:10.1016/j.nucmedbio.2015.06.003.
20. Haberkorn U, Eder M, Kopka K, Babich JW, Eisenhut M. New strategies in prostate cancer: prostate-specific membrane antigen (psma) ligands for diagnosis and therapy. Clin Cancer Res. 2016;22(1):9–15. doi:10.1158/1078-0432.ccr-15-0820.
21. Choy CJ, Ling X, Geruntho JJ, Beyer SK, Latoche JD, Langton-Webster B, Anderson CJ, Berkman CE. 177lu-labeled phosphoramidate-based psma inhibitors: the effect of an albumin binder on biodistribution and therapeutic efficacy in prostate tumor-bearing mice. Theranostics. 2017;7(7):1928–1939. doi:10.7150/thno.18719.
22. Ling X, Latoche JD, Choy CJ, Kurland BF, Laymon CM, Wu Y, Salamacha N, Shen D, Geruntho JJ, Rigatti LH, et al. Preclinical dosimetry, imaging, and targeted radionuclide therapy studies of lu-177-labeled albumin-binding, psma-targeted CTT1403. Mol Imaging Biol. 2019;22(2):274–284. doi:10.1007/s11307-019-01404-8.
23. Nedrow-Byers JR, Moore AL, Ganguly T, Hopkins MR, Fulton MD, Benny PD, Berkman CE. PSMA-targeted SPECT agents: mode of binding effect on in vitro performance. The Prostate. 2013;73(4):355–362. doi:10.1002/pros.22575.
24. Nedrow-Byers JR, Jabbes M, Jewett C, Ganguly T, He H, Liu T, Benny P, Bryan JN, Berkman CE. A phosphoramidate-based prostate-specific membrane antigen-targeted SPECT agent. The Prostate. 2012;72(8):904–912. doi:10.1002/pros.21493.
25. Liu T, Wu LY, Kazak M, Berkman CE. Cell-surface labeling and internalization by a fluorescent inhibitor of prostate-specific membrane antigen. The Prostate. 2008;68:955–964. doi:10.1002/pros.20753.
26. Choy CJ, Geruntho JJ, Davis AL, Berkman CE. Tunable pH-sensitive linker for controlled release. Bioconjug Chem. 2016;27:824–830. doi:10.1021/acs.bioconjchem.6b00027.
27. Choy CJ, Ley CR, Davis AL, Backer BS, Geruntho JJ, Clowers BH, Berkman CE. Second-generation tunable ph-sensitive phosphoramidate-based linkers for controlled release. Bioconjug Chem. 2016;27(9):2206–2213. doi:10.1021/acs.bioconjchem.6b00422.
28. Dassie JP, et al. Targeted inhibition of prostate cancer metastases with an RNA aptamer to prostate-specific membrane antigen.
29. Romero-Cordoba SL, Salido-Guadarrama I, Rodriguez-Dorantes M, Hidalgo-Miranda A. miRNA biogenesis: biological impact in the development of cancer. Cancer Biology & Therapy. 2014;15:1444–1455. doi:10.4161/15384047.2014.955442.
30. Volinia S, Calin GA, Liu C-G, Ambs S, Cimmino A, Petrocca F, Visone R, Iorio M, Roldo C, Ferracin M, et al. A microRNA expression signature of human solid tumors defines cancer gene targets. Proceedings of the National Academy of Sciences. 2006;103(7):2257–2261. doi:10.1073/pnas.0510565103.
31. Borralho PM, Simões AES, Gomes SE, Lima RT, Carvalho T, Ferreira DMS, Vasconcelos MH, Castro RE, Rodrigues CMP. miR-143 overexpression impairs growth of human colon carcinoma xenografts in mice with induction of apoptosis and inhibition of proliferation. PloS One. 2011;6(8):e23787. doi:10.1371/journal.pone.0023787.
32. Gambari R, Brognara E, Spandidos DA, Fabbri E. Targeting oncomiRnas and mimicking tumor suppressor miRnas: new trends in the development of miRNA therapeutic strategies in oncology. Int J Oncol. 2016;49(1):5–32. doi:10.3892/ijo.2016.3503.
33. Garzon R, Marcucci G, Croce CM. Targeting microRnas in cancer: rationale, strategies and challenges. Nat Rev Drug Discov. 2010;9(10):775–789. doi:10.1038/nrd3179.
34. Yarahmadi A, Shahrokhi SZ, Mostafavi-Pour Z, Azarpira N. MicroRnas in diabetic nephropathy: from molecular mechanisms

to new therapeutic targets of treatment. Biochem Pharmacol. 2021;189:114301. doi:10.1016/j.bcp.2020.114301.
35. Wang H, Jiang Y, Peng H, Chen Y, Zhu P, Huang Y. Recent progress in microRNA delivery for cancer therapy by non-viral synthetic vectors. Adv Drug Deliv Rev. 2015;81:142–160. doi:10.1016/j.addr.2014.10.031.
36. Bader A, Brown D, Stoudemire J, Lammers P. Developing therapeutic microRnas for cancer. Gene Ther. 2011;18:1121–1126. doi:10.1038/gt.2011.79.
37. Sharma N, Baruah MM. The microRNA signatures: aberrantly expressed miRnas in prostate cancer. Clin Transl Oncol. 2019;21:126–144. doi:10.1007/s12094-018-1910-8.
38. Chen W-Y, Liu S-Y, Chang Y-S, Juan Yin J, Yeh H-L, Mouhieddine TH, Hadadeh O, Abou-Kheir W, Liu Y-N. MicroRNA-34a regulates WNT/TCF7 signaling and inhibits bone metastasis in ras-activated prostate cancer. Oncotarget. 2015;6(1):441. doi:10.18632/oncotarget.2690.
39. Lee RC, Feinbaum RL, Ambros V. The C. elegans heterochronic gene lin-4 encodes small RNAs with antisense complementarity to lin-14. Cell. 1993;75:843–854. doi:10.1016/0092-8674(93)90529-y.
40. Lee Y, Kim M, Han J, Yeom K-H, Lee S, Baek SH, Kim VN. MicroRNA genes are transcribed by RNA polymerase II. Embo J. 2004;23(20):4051–4060. doi:10.1038/sj.emboj.7600385.
41. Han J, Lee Y, Yeom K-H, Kim Y-K, Jin H, Kim VN. The drosha-DGCR8 complex in primary microRNA processing. Genes & Development. 2004;18(24):3016–3027. doi:10.1101/gad.1262504.
42. Guo Z, Li B, Tian P, Li D, Zhang Y, Li Q, Fan T, Yue J, Guo Y. DGCR8 expression is altered in children with congenital heart defects. Clinica Chimica Acta. 2019;495:25–28. doi:10.1016/j.cca.2019.03.1619.
43. Zeng Y, Cullen BR. Structural requirements for pre-microRNA binding and nuclear export by exportin 5. Nucleic Acids Res. 2004;32(16):4776–4785. doi:10.1093/nar/gkh824.
44. Flores-Jasso CF, Arenas-Huertero C, Reyes JL, Contreras-Cubas C, Covarrubias A, Vaca L. First step in pre-miRnas processing by human dicer. Acta Pharmacol Sin. 2009;30(8):1177–1185. doi:10.1038/aps.2009.108.
45. Yoda M, Kawamata T, Paroo Z, Ye X, Iwasaki S, Liu Q, Tomari Y. ATP-dependent human RISC assembly pathways. Nature Structural & Molecular Biology. 2010;17(1):17–23. doi:10.1038/nsmb.1733.
46. Meijer HA, Smith EM, Bushell M. Regulation of miRNA strand selection: follow the leader? Biochem Soc Trans. 2014;42:1135–1140. doi:10.1042/BST20140142.
47. Cochetti G. Role of miRNAs in prostate cancer: Do we really know everything? Urologic oncology: seminars and original investigations. 2020 Jul;38(7):623–635. doi:10.1016/jurolonc.2020.03.007. PubMed ID: 32284256.
48. Hao Y, Gu X, Zhao Y, Greene S, Sha W, Smoot DT, Califano J, Wu T-C, Pang X. Enforced expression of miR-101 inhibits prostate cancer cell growth by modulating the COX-2 pathway in vivo. Cancer Prevention Research. 2011;4(7):1073–1083. doi:10.1158/1940-6207.CAPR-10-0333.
49. Zhu Y, Shao S, Pan H, Cheng Z, Rui X. MicroRNA-136 inhibits prostate cancer cell proliferation and invasion by directly targeting mitogen-activated protein kinase kinase 4. Mol Med Rep. 2018;17:4803–4810. doi:10.3892/mmr.2018.8417.
50. Liu C-Y, Su S-H, Chang T-H, Hsieh M-L, Chang Y-H, Pang JST, Chuang C-K. Promoter gene methylation regulates clooxygenase-2 expression in androgen-dependent and independent prostate cancer cells. World J Oncol. 2022;13(3):107–116. doi:10.14740/wjon1478.
51. Shen T, Wang W, Zhou W, Coleman I, Cai Q, Dong B, Ittmann MM, Creighton CJ, Bian Y, Meng Y, et al. MAPK4 promotes prostate cancer by concerted activation of androgen receptor and AKT. J Clin Invest. 2021;131(4). doi:10.1172/JCI135465.
52. Ji X, Lu Y, Tian H, Meng X, Wei M, Cho WC. Chemoresistance mechanisms of breast cancer and their countermeasures. Biomedicine & Pharmacotherapy. 2019;114:108800. doi:10.1016/j.biopha.2019.108800.
53. Yu Z, Baserga R, Chen L, Wang C, Lisanti MP, Pestell RG. microRNA, cell cycle, and human breast cancer. Am J Pathol. 2010;176(3):1058–1064. doi:10.2353/ajpath.2010.090664.
54. Liu Y, Xu X, Xu X, Li S, Liang Z, Hu Z, Wu J, Zhu Y, Jin X, Wang X, et al. MicroRna-193a-3p inhibits cell proliferation in prostate cancer by targeting cyclin D1. Oncol Lett. 2017;14:5121–5128. doi:10.3892/ol.2017.6865.
55. Ma Z, Luo Y, Qiu M. miR-143 induces the apoptosis of prostate cancer LNCap cells by suppressing Bcl-2 expression. Medical Science Monitor: international Medical Journal of Experimental and Clinical Research. 2017;23:359. doi:10.12659/MSM.899719.
56. Ostadrahimi S, Fayaz S, Parvizhamidi M, Abedi-valugerdi M, Hassan M, Kadivar M, Teimoori-toolabi L, Asgari M, Shahrokh H, Abolhasani M, et al. Downregulation of miR-1266-5P, miR-185-5P and miR-30c-2 in prostatic cancer tissue and cell lines. Oncol Lett. 2018;15:8157–8164. doi:10.3892/ol.2018.8336.
57. Derynck R, Weinberg RA. EMT and cancer: more than meets the eye. Dev Cell. 2019;49:313–316. doi:10.1016/j.devcel.2019.04.026.
58. Zaravinos A. The regulatory role of microRnas in EMT and cancer. J Oncol. 2015;2015. doi:10.1155/2015/865816.
59. Zhang P, Sun Y, Ma L. ZEB1: at the crossroads of epithelial-mesenchymal transition, metastasis and therapy resistance. Cell Cycle. 2015;14:481–487. doi:10.1080/15384101.2015.1006048.
60. Li H. The EMT regulator ZEB2 is a novel dependency of human and murine acute myeloid leukemia. Blood, the Journal of the American Society of Hematology. 2017;129(4):497–508. doi:10.1182/blood-2016-05-714493.
61. Fardi M, Alivand M, Baradaran B, Farshdousti Hagh M, Solali S. The crucial role of ZEB2: from development to epithelial-to-mesenchymal transition and cancer complexity. J Cell Physiol. 2019;234:14783–14799. doi:10.1002/jcp.28277.
62. Sommariva M, Gagliano N. E-cadherin in pancreatic ductal adenocarcinoma: a multifaceted actor during EMT. Cells. 2020;9:1040. doi:10.3390/cells9041040.
63. Yu J, LU Y, CUI DI, LI E, ZHU Y, ZHAO Y, ZHAO F, XIA S. miR-200b suppresses cell proliferation, migration and enhances chemosensitivity in prostate cancer by regulating Bmi-1. Oncol Rep. 2014;31(2):910–918. doi:10.3892/or.2013.2897.
64. Scott LE, Weinberg SH, Lemmon CA. Mechanochemical signaling of the extracellular matrix in epithelial-mesenchymal transition. Frontiers in Cell and Developmental Biology. 2019;7:135. doi:10.3389/fcell.2019.00135.
65. Giannelli G, Bergamini C, Fransvea E, Sgarra C, Antonaci S. Laminin-5 with transforming growth factor-β1 induces epithelial to mesenchymal transition in hepatocellular carcinoma. Gastroenterology. 2005;129:1375–1383. doi:10.1053/j.gastro.2005.09.055.
66. Gandellini P, Profumo V, Casamichele A, Fenderico N, Borrelli S, Petrovich G, Santilli G, Callari M, Colecchia M, Pozzi S, et al. miR-205 regulates basement membrane deposition in human prostate: implications for cancer development. Cell Death & Differentiation. 2012;19(11):1750–1760. doi:10.1038/cdd.2012.56.
67. Bostwick DG. The pathology of early prostate cancer. CA Cancer J Clin. 1989;39(6):376–393. doi:10.3322/canjclin.39.6.376.
68. Hasan J, Byers R, Jayson GC. Intra-tumoural microvessel density in human solid tumours. Br J Cancer. 2002;86(10):1566–1577. doi:10.1038/sj.bjc.6600315.
69. Sharma S, Sharma MC, Sarkar C. Morphology of angiogenesis in human cancer: a conceptual overview, histoprognostic perspective and significance of neoangiogenesis. Histopathology. 2005;46:481–489. doi:10.1111/j.1365-2559.2005.02142.x.
70. Torchilin V. Tumor delivery of macromolecular drugs based on the EPR effect. Adv Drug Deliv Rev. 2011;63:131–135. doi:10.1016/j.addr.2010.03.011.
71. Au J-S, Yeung BZ, Wientjes MG, Lu Z, Wientjes MG. Delivery of cancer therapeutics to extracellular and intracellular targets:

determinants, barriers, challenges and opportunities. Adv Drug Deliv Rev. 2016;97:280–301. doi:10.1016/j.addr.2015.12.002.
72. Craig V, Tzankov A, Flori M, Schmid CA, Bader AG, Müller A. Systemic microRNA-34a delivery induces apoptosis and abrogates growth of diffuse large B-cell lymphoma in vivo. Leukemia. 2012;26(11):2421–2424. doi:10.1038/leu.2012.110.
73. Zang X, Zhang X, Zhao X, Hu H, Qiao M, Deng Y, Chen D. Targeted delivery of miRNA 155 to tumor associated macrophages for tumor immunotherapy. Mol Pharm. 2019;16(4):1714–1722. doi:10.1021/acs.molpharmaceut.9b00065.
74. Folkman J. Angiogenesis in cancer, vascular, rheumatoid and other disease. Nat Med. 1995;1(1):27–31. doi:10.1038/nm0195-27.
75. Carmeliet P, Jain RK. Angiogenesis in cancer and other diseases. Nature. 2000;407:249–257. doi:10.1038/35025220.
76. Zhang L, Liao Y, Tang L. MicroRNA-34 family: a potential tumor suppressor and therapeutic candidate in cancer. Journal of Experimental & Clinical Cancer Research. 2019;38:1–13.
77. Jain RK. Barriers to drug delivery in solid tumors. Sci Am. 1994;271 (1):58–65. doi:10.1038/scientificamerican0794-58.
78. Bertrand N, Wu J, Xu X, Kamaly N, Farokhzad OC. Cancer nanotechnology: the impact of passive and active targeting in the era of modern cancer biology. Adv Drug Deliv Rev. 2014;66:2–25. doi:10.1016/j.addr.2013.11.009.
79. Farokhzad OC, Langer R. Impact of nanotechnology on drug delivery. ACS Nano. 2009;3:16–20. doi:10.1021/nn900002m.
80. Bae YH. Drug targeting and tumor heterogeneity. J Control Release. 2009;133(1). doi:10.1016/j.jconrel.2008.09.074.
81. Hayes J, Peruzzi PP, Lawler S. MicroRnas in cancer: biomarkers, functions and therapy. Trends Mol Med. 2014;20:460–469. doi:10.1016/j.molmed.2014.06.005.
82. Caromile LA, Dortche K, Rahman MM, Grant CL, Stoddard C, Ferrer FA, Shapiro LH. PSMA redirects cell survival signaling from the MAPK to the PI3K-AKT pathways to promote the progression of prostate cancer. Sci Signal. 2017;10(470). doi:10.1126/scisignal.aag3326.
83. Nguyen DP, Xiong PL, Liu H, Pan S, Leconet W, Navarro V, Guo M, Moy J, Kim S, Ramirez-Fort MK, et al. Induction of PSMA and internalization of an anti-PSMA mAb in the vascular compartment. Mol Cancer Res. 2016;14(11):1045–1053. doi:10.1158/1541-7786.MCR-16-0193.
84. Singh S, Grossniklaus HE, Kang SJ, Edelhauser HF, Ambati BK, Kompella UB. Intravenous transferrin, RGD peptide and dual-targeted nanoparticles enhance anti-VEGF intraceptor gene delivery to laser-induced CNV. Gene Ther. 2009;16(5):645–659. doi:10.1038/gt.2008.185.
85. Jin W, Qin B, Chen Z, Liu H, Barve A, Cheng K. Discovery of PSMA-specific peptide ligands for targeted drug delivery. Int J Pharm. 2016;513(1–2):138–147. doi:10.1016/j.ijpharm.2016.08.048.
86. Zhao Z, Ukidve A, Kim J, Mitragotri S. Targeting strategies for tissue-specific drug delivery. Cell. 2020;181:151–167. doi:10.1016/j.cell.2020.02.001.
87. Henry MD, Wen S, Silva MD, Chandra S, Milton M, Worland PJ. A prostate-specific membrane antigen-targeted monoclonal antibody–chemotherapeutic conjugate designed for the treatment of prostate cancer. Cancer Res. 2004;64(21):7995–8001. doi:10.1158/0008-5472.CAN-04-1722.
88. Rege K, Patel SJ, Megeed Z, Yarmush ML. Amphipathic peptide-based fusion peptides and immunoconjugates for the targeted ablation of prostate cancer cells. Cancer Res. 2007;67:6368–6375. doi:10.1158/0008-5472.CAN-06-3658.
89. Tykvart J, Navrátil V, Sedlák F, Corey E, Colombatti M, Fracasso G, Koukolík F, Bařinka C, Šácha P, Konvalinka J. Comparative analysis of monoclonal antibodies against prostate-specific membrane antigen (PSMA). The Prostate. 2014;74 (16):1674–1690. doi:10.1002/pros.22887.
90. Behe M, Alt K, Deininger F, Bühler P, Wetterauer U, Weber WA, Elsässer-Beile U, Wolf P. In vivo testing of 177lu-labelled anti-PSMA antibody as a new radioimmunotherapeutic agent against prostate cancer. In Vivo. 2011;25:55–59.
91. Keefe AD, Pai S, Ellington A. Aptamers as therapeutics. *Nature reviews Drug discovery*. 2010;9:537–550. doi:10.1038/nrd3141.
92. Kruspe S, Mittelberger F, Szameit K, Hahn U. Aptamers as drug delivery vehicles. ChemMedchem. 2014;9:1998–2011. doi:10.1002/cmdc.201402163.
93. Esposito CL, Cerchia L, Catuogno S, De Vita G, Dassie JP, Santamaria G, Swiderski P, Condorelli G, Giangrande PH, de Franciscis V et al. Multifunctional aptamer-miRNA conjugates for targeted cancer therapy. Molecular Therapy. 2014;22 (6):1151–1163. doi:10.1038/mt.2014.5.
94. Dassie JP, Hernandez LI, Thomas GS, Long ME, Rockey WM, Howell CA, Chen Y, Hernandez FJ, Liu XY, Wilson ME, et al. Targeted inhibition of prostate cancer metastases with an RNA aptamer to prostate-specific membrane antigen. Molecular Therapy. 2014;22(11):1910–1922. doi:10.1038/mt.2014.117.
95. Wu X . Second-generation aptamer-conjugated PSMA-targeted delivery system for prostate cancer therapy. Int J Nanomedicine. 2011;6:1747. doi:10.2147/IJN.S23747.
96. Ye Y, Zhang L, Dai Y, Wang Z, Li C, Peng Y, Ma D, He P. PSMA-Targeting reduction-cleavable hyperbranched polyamide-amine gene delivery system to treat the bone metastases of prostate cancer. molecular Therapy. 2020;15:7173. doi:10.2147/IJN.S268398.
97. Mehlhorn H. 2016. Nanoparticles in the fight against parasites. In: Melhorn H, editor. Parasitology Research MonographsSwitzerland. 1st ed. pp. 1–14. Springer Cham: Nanoparticles - Definitions. doi: 10.1007/978-3-319-25292-6.
98. Bhattacharyya S, Kudgus RA, Bhattacharya R, Mukherjee P. Inorganic nanoparticles in cancer therapy. Pharm Res. 2011;28:237–259. doi:10.1007/s11095-010-0318-0.
99. Luo D, Wang X, Zeng S, Ramamurthy G, Burda C, Basilion JP. Prostate-specific membrane antigen targeted gold nanoparticles for prostate cancer radiotherapy: does size matter for targeted particles? Chemical Science. 2019;10(35):8119–8128. doi:10.1039/C9SC02290B.
100. Binzel DW, Shu Y, Li H, Sun M, Zhang Q, Shu D, Guo B, Guo P. Specific delivery of miRNA for high efficient inhibition of prostate cancer by RNA nanotechnology. Molecular Therapy. 2016;24 (7):1267–1277. doi:10.1038/mt.2016.85.
101. Saniee F, Shabani Ravari N, Goodarzi N, Amini M, Atyabi F, Saeedian Moghadam E, Dinarvand R. Glutamate-urea-based PSMA-targeted PLGA nanoparticles for prostate cancer delivery of docetaxel. Pharm Dev Technol. 2021;26(4):381–389. doi:10.1080/10837450.2021.1875238.
102. Chen Y, Gao D-Y, Huang L. In vivo delivery of miRnas for cancer therapy: challenges and strategies. Adv Drug Deliv Rev. 2015;81:128–141. doi:10.1016/j.addr.2014.05.009.
103. Segal M, Slack F. Challenges identifying efficacious miRNA therapeutics for cancer. Expert Opinion on Drug Discovery. 2020;15 (9):987–991. doi:10.1080/17460441.2020.1765770.
104. Cortez MA, Anfossi S, Ramapriyan R, Menon H, Atalar SC, Aliru M, Welsh J, Calin GA. Role of miRnas in immune responses and immunotherapy in cancer. Genes Chromosomes Cancer. 2019;58(4):244–253. doi:10.1002/gcc.22725.
105. Curtale G. MiRnas at the crossroads between innate immunity and cancer: focus on macrophages. Cells. 2018;7(12). doi:10.3390/cells7020012.
106. Pereira DM, Rodrigues PM, Borralho PM, Rodrigues CM. Delivering the promise of miRNA cancer therapeutics. Drug Discov Today. 2013;18:282–289. doi:10.1016/j.drudis.2012.10.002.
107. Stenvang J, Silahtaroglu AN, Lindow M, Elmen J, Kauppinen S. The utility of LNA in microRNA-based cancer diagnostics and therapeutics. Seminars in cancer biology. 2008;18(2):89–102. doi:10.1016/j.semcancer.2008.01.004.
108. Davis S, Lollo B, Freier S, Esau C. Improved targeting of miRNA with antisense oligonucleotides. Nucleic Acids Res. 2006;34:2294–2304. doi:10.1093/nar/gkl183.
109. Sharma C, Awasthi SK. Versatility of peptide nucleic acids (PNA s): role in chemical biology, drug discovery, and origins of life. Chemical Biology & Drug Design. 2017;89:16–37. doi:10.1111/cbdd.12833.

110. Lima JF, Cerqueira L, Figueiredo C, Oliveira C, Azevedo NF. Anti-miRNA oligonucleotides: a comprehensive guide for design. RNA Biol. 2018;15:338–352. doi:10.1080/15476286.2018.1445959.
111. Schachner-Nedherer A-L, Werzer O, Kornmueller K, Prassl R, Zimmer A. Biological activity of miRNA-27a using peptide-based drug delivery systems. Int J Nanomedicine. 2019;14:7795. doi:10.2147/IJN.S208446.
112. Zou L-L, Ma J-L, Wang T, Yang T-B, Liu C-B. Cell-penetrating peptide-mediated therapeutic molecule delivery into the central nervous system. Chemical Biology & Drug Design. 2013;11(2):197–208. doi:10.2174/1570159X11311020006.
113. Fabani MM, Gait MJ. miR-122 targeting with LNA/2′-O-methyl oligonucleotide mixmers, peptide nucleic acids (PNA), and PNA–peptide conjugates. Rna. 2008;14:336–346. doi:10.1261/rna.844108.
114. Orellana EA, Abdelaal AM, Rangasamy L, Tenneti S, Myoung S, Low PS, Kasinski AL. Enhancing microRNA activity through increased endosomal release mediated by nigericin. Molecular Therapy-Nucleic Acids. 2019;16:505–518. doi:10.1016/j.omtn.2019.04.003.
115. Xie Y, Yu F, Tang W, Alade BO, Peng Z-H, Wang Y, Li J, Oupický D. Chloroquine-containing DMAEMA copolymers as efficient anti-miRNA delivery vectors with improved endosomal escape and anti-migratory activity in cancer cells. Macromol Biosci. 2018;18(1). doi:10.1002/mabi.201700194.
116. Siemens H, Jackstadt R, Hünten S, Kaller M, Menssen A, Götz U, Hermeking H. miR-34 and SNAIL form a double-negative feedback loop to regulate epithelial-mesenchymal transitions. Cell Cycle. 2011;10(24):4256–4271. doi:10.4161/cc.10.24.18552.
117. Li WJ, Wang Y, Liu R, Kasinski AL, Shen H, Slack FJ, Tang DG. microRNA-34A: potent tumor suppressor, cancer stem cell inhibitor, and potential anticancer therapeutic. Front Cell Dev Biol. 2021;9:640587. doi:10.3389/fcell.2021.640587.
118. Tong A, Nemunaitis J. Modulation of miRNA activity in human cancer: a new paradigm for cancer gene therapy? Cancer Gene Ther. 2008;15:341–355. doi:10.1038/cgt.2008.8.
119. Thomson DW, Dinger ME. Endogenous microRNA sponges: evidence and controversy. Nat Rev Genet. 2016;17(5):272–283. doi:10.1038/nrg.2016.20.
120. Fernandez-Piñeiro I, Badiola I, Sanchez A. Nanocarriers for microRNA delivery in cancer medicine. Biotechnol Adv. 2017;35:350–360. doi:10.1016/j.biotechadv.2017.03.002.
121. Conde J, Artzi N. Are RNAi and miRNA therapeutics truly dead? Trends Biotechnol. 2015;33:141–144. doi:10.1016/j.tibtech.2014.12.005.
122. Ganju A, Khan S, Hafeez BB, Behrman SW, Yallapu MM, Chauhan SC, Jaggi M. miRNA nanotherapeutics for cancer. Drug Discov Today. 2017;22(2):424–432. doi:10.1016/j.drudis.2016.10.014.